COMPARISON OF THE LEAKAGE CHARACTERISTICS OF THE STRAIGHT ANNULAR AND CONVERGENT SEALS

A Thesis

by

SERAFETTIN USTUN

Submitted to the Office of Graduate Studies of
Texas A&M University
in partial fulfillment of the requirements for the degree of

MASTER OF SCIENCE

August 2012

Major Subject: Mechanical Engineering

Comparison of the Leakage Characteristics of the Straight Annular and Convergent Seals

COMPARISON OF THE LEAKAGE CHARACTERISTICS OF THE STRAIGHT ANNULAR AND CONVERGENT SEALS

A Thesis

by

SERAFETTIN USTUN

Submitted to the Office of Graduate Studies of
Texas A&M University
in partial fulfillment of the requirements for the degree of

MASTER OF SCIENCE

Approved by:

Chair of Committee,	Gerald Morrison
Committee Members,	Michael Pate
	Jerome J. Schubert
Head of Department,	Jerald Caton

August 2012

Major Subject: Mechanical Engineering

ABSTRACT

Comparison of the Leakage Characteristics of the Straight Annular and Convergent Seals. (August 2012)

Serafettin Ustun, B.E., Gazi University, Turkey;

Chair of Advisory Committee: Dr. Gerald L. Morrison

Annular seals are devices, which are used in turboMachinery systems to reduce the flow leakage, and to provide better dynamic stability to the system. Leakage flow can strongly affect cooling quality, heating balance, and efficiency of a turboMachinery system. Due to the fact that annular seals can significantly reduce the flow leakage, and provide the most cost-effective way of enhancing the aerodynamic efficiency, understanding of the flow characteristics through the annular seal configurations is an important subject.

Seals are classified in two main groups, which are contacting, and non-contacting seals. Straight annular and convergent seal configurations are characterized as non-contacting seals, and they are widely used in rotating turbocMachinery systems. The flow kinetic energy obtained from the flow pressure is dissipated by the effects of shear stresses along the free shear layers. In addition, viscosity of the flow has an impact on the dissipation rate of the flow kinetic energy.

In this research, the leakage characteristics of the straight annular, and convergent seal configurations under specified working conditions are compared to each other. This study aims to investigate which seal configuration exhibits better leakage characteristics with respect to the different seal clearances, shaft speeds, surface roughness heights, and pressure ratios.

Commercial code ANSYS Fluent ® is used to perform the flow simulations for the straight annular and convergent seal configurations. Effects of the seal clearances, shaft speeds, pressure ratios, and surface roughness heights on the leakage rate are analyzed. It was observed that the seal clearance has a significant impact on the flow leakage, and clearance control is an important subject in seal technology. Additionally, dynamic system is compared to the static system, and results showed that shaft speed less than 15,000 rpm has not considerable impacts on the leakage.

DEDICATION

To my family.

ACKNOWLEDGEMENTS

Firstly, I would like to express my special thanks to my committee chair, Dr.Gerald L. Morrison, for being a constant source of great knowledge and motivation. He has also been my academic advisor.

I am greatly thankful to Dr. Michael Pate and Dr. Jerome Schubert for being on my thesis committee and their guidance. I am also grateful to all faculty members of Mechanical Engineering Department for providing me with gaining important knowledge.

I thank my mom, dad, sister, and my aunt for their belief in me. I would also like to express my thanks to Texas A&M University as a whole for providing me with such a good education environment.

NOMENCLATURE

A	Clearance area, πdc
C	Radial clearance, m
D	Shaft diameter, m
L	Axial length of the seal, m
$\dot{M}$	Mass flow rate of leakage flow, kg/s
P_I	Tooth inlet pressure, Pa
Pr	Absolute pressure ratio, P_E/P_I
W	Shaft speed, rpm
X	Axial distance, m
μ	Dynamic viscosity, Pa/s
P_I	Fluid density at the seal inlet, kg/m^3
R_t	Shaft radius, m
Vθ	Swirl velocity, m/s
U	Axial velocity, m/s
U_{in}	Average axial velocity at the inlet, m/s
C_{ex}	Exit seal clearance, m
C_f	Friction coefficients

TABLE OF CONTENTS

Page

LIST OF FIGURES

Page

LIST OF TABLES

Page

1. INTRODUCTION

Turbo Machinery systems have been an indispensable part of life, especially in this technology era. They are used in many areas to accommodate our increasing demands. As a result of this demand, technology is directed on turbo Machinery systems to improve the efficiency of these systems and to provide longer life. Basic imperfections of turbo Machinery systems are specified as leakage and instability. Seals are the devices, which are used for decreasing the leakage in turbo Machinery system components like compressors, turbines, pumps, and for stabilizing the system. There are different type of seals, which have their own rotor dynamic and leakage characteristic. As a result, working principles of seals differ from each other. The function of a seal is to decrease the kinetic energy of the secondary flow, that is to say, to reduce linear inertia of the flow, which will increase the resistance to the flow. Consequently, this leakage rate will be significantly decreased.

Seal technology is also improved with better understanding of the flow field inside the seal and optimization of the moments and forces affecting the rotor shaft. Accurate analysis of mass flow rate through the seals is necessary for increasing turbo Machinery system efficiency. Seals are working in a section of a turbo Machinery system that has unbalanced pressure. Estimation of secondary flow rate through the seal also has an importance in terms of calculating rotor dynamic coefficients.

This thesis follows the style of the Journal of Engineering for Gas Turbines and Power.

In order to estimate the flow conditions in a seal domain, experimental and CFD methods have been applied. Seals are classified in two main groups, which are contacting and non-contacting seals. This particular study generally focuses on non-contacting seals. Complete flow constriction is possible with the usage of contacting seals, and leakage ratio can be considerably eliminated, which will highly increase the system efficiency. Due to friction, distortion is one disadvantage of these seals. That is why these seals are not applicable for high-speeds processes. In contrast to contacting seals, non-contacting ones do not have a wear problem, because there is no friction. There is a clearance in non-contacting seals between the rotating shaft and the stationary seal. As a result, it is possible to apply this type of seal to high-speed processes. Labyrinth, honeycomb, straight, and convergent seals are classified as non-contacting seals.

Annular seals have a vital role in improving turbo Machinery system performance. Labyrinth seals can be assumed to be inestimable because of their high effective leakage blocking characteristics and their being non-contacting, which will make it possible to reach high rotor speeds. But these seals also have some negative characteristics, which generally relate to the instability. Unlike labyrinth seals, pocket damper seals do not have instability problems. Pocket damper seals can significantly decrease the rotor vibration. Convergent tapered-damper seals can specify better stability. Convergent seals provides higher main stiffness coefficient because of their convergent-tapered clearance. Along with improved rotor dynamic properties,

convergent seals also have very good leakage characteristics because of surface roughness effect.

This thesis will focus on convergent seals. In terms of leakage performance, straight annular seals and convergent seals will be compared under the same boundary conditions. Simulations will be performed based on main factors, which have a direct effect on the secondary flow of the seal. These factors are seal geometry, pressure conditions, rotational speed of the rotor shaft, and surface roughness. Convergent seal configuration is shown in figure 1 below.

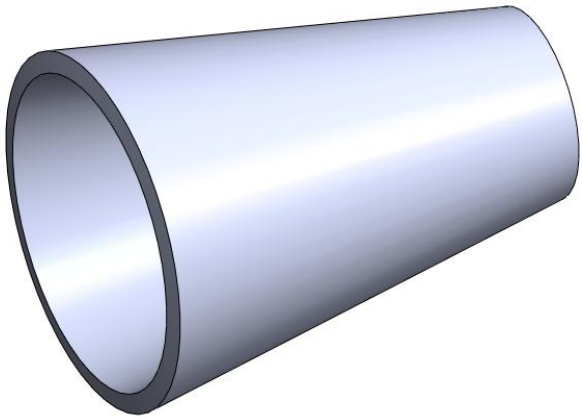

Fig. 1 Convergent seal configuration

Dissipation of the energy of the secondary flow through the convergent seal will be decreased by friction effects. When compared to labyrinth seals, the effects can be clearly seen. In labyrinth seals, there are cavities located on the seal, and flow through labyrinth seal is captured by these cavities. Vortices generated in these cavities will dissipate the energy of the flow, and by this way leakage rate will be decreased. In the geometry shown in figure 2, there are no cavities as in labyrinth seals. The main effect of dissipation is friction.

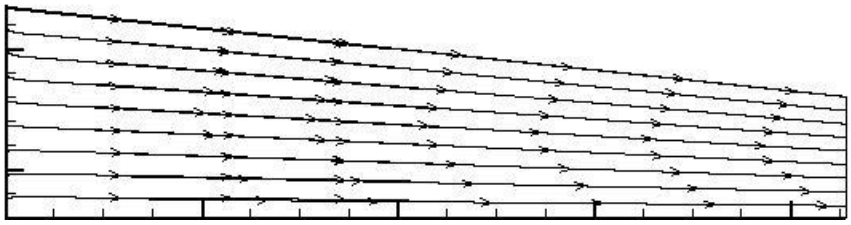

Fig. 2 Streamlines through convergent seal

Analysis performed shows that there is no vortex generated in the flow path through convergent seals. Since any vortex formation is not observed in flow domain, linear inertia of fluid particles in the flow domain will be dissipated by wall friction effects.

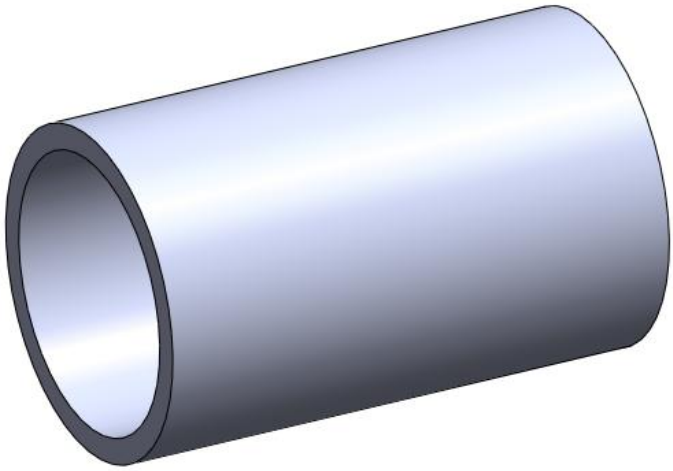

Fig. 3 Straight annular seal

Another flow domain which will be used in the analysis is shown in figure 3 This geometry is a straight smooth seal. These two seal configurations will be compared to each other in terms of leakage performance. This will be done by analyzing the forces, and moments imposed upon the rotor shaft under the different shaft speeds, surface roughness heights, seal clearance, and pressure ratios.

2. LITERATURE REVIEW

In the introduction section, the importance of turbo Machinery systems is emphasized. There is appreciable research which has contributed to the seal development. More specifically, focus of this study is on seal technology and its role in preventing leakage. This research also brings to light the important concern that studies related to the convergent seal technology are limited.

Since 1965, smooth-rotor/honeycomb stator seals have been used in many industrial applications instead of aluminum labyrinth seals because aluminum labyrinth seals have wear problems, which result in deformation of the material. Research performed in this area shows that, at the same clearances, honeycomb seals have better leakage characteristic than labyrinth seals. In addition, this research also suggest that honeycomb seals are greatly applicable for preventing instabilities in any turbo-Machinery system. In order to estimate rotor dynamic force coefficients more accurately, new studies have been performed. Ha, and Childs [1] improved the approach by using two control volume systems for honeycomb annular gas seals. As a result of this study, Kleyhans, and Childs [2] improved bulk-flow solutions in order to analyze two control volume models. Their approach uses a general transfer function model. Despite the research, new two-volume analysis cannot be analyzed deeply because of inadequate excitation frequency intervals (just 40 Hz to 70 Hz). With new test facilities and apparatus, it has been possible to evaluate the new analysis. Dynamic impedances D (jΩ) and E (jΩ) of honeycomb and smooth annular seals have been measured.

Benckert, and Wachter [3] first studied annular gas seal rotordyanmic coefficients. Their experiment only measured direct and cross-coupled stiffness coefficients. But their experiments showed that eliminating tangential fluid flow through annular seal clearance would provide great opportunity to prevent unstable cross-coupled seal forces. Childs et al. [4] performed experiments to compare rotor dynamic and leakage characteristics of different honeycomb, labyrinth, and smooth-seal configurations. His results showed that leakage performance of the honeycomb seals is the best inside this seal group. Maximum stability, which means large direct damping and small cross coupled coefficients is also observed in honeycomb seals. In these experiments, the seal length was set at 85.70 mm and radial clearance was 0.19 mm, which taken from a previous study performed by Kerr [5]. Pressure ratios were 0.4 and 0.6 and three different rotor speeds were applied. Kleyhans, and Childs [2] wrote a two control-volume annular gas seal code, called ISOTSEAL. With the application of this code, it has been possible to get an idea about stiffness coefficient, damping coefficient, and leakage characteristic. ISOTSEAL input parameters consist of seal geometry, working conditions, inlet losses, and friction coefficients for both stator and rotor.

Many analyses are also performed to observe the surface roughness effect on the flow through annular seal configurations. In order to obtain high efficient energy production from turbo engines, these turbo systems must be designed to work with high performance under extreme conditions. Nelson, and Nguyen [6] developed calculations to analyze annular seals, which have identically roughened stator and rotor surfaces. During their analysis, bulk flow model was used.

Rotor dynamic characteristics of the annular seals are also observed under the surface roughness effect. In this thesis, surface roughness effects will be analyzed in terms of leakage performance. Surface roughness will be applied both on rotor and stator surfaces. Besides the rotor dynamic analysis, damper seal configurations are also analyzed in terms of leakage, and results showed that secondary flow rate through seal is considerably decreasing by the application of surface roughness to seal surfaces. Childs, and Chang-Ho [7] tested these results In their study, Hir's [8] Bulk Flow model is used. By applying Moody's Friction Factor, wall roughness, pressure drop through seals, and turbulence effects are observed. Prior to this study, Lucas, Danaila, Bonneau, and Frene [9] proposed a turbulent flow model with surface roughness. Turbulence model is determined with algebraic equation and also surface roughness effects are observed.

Ongoing research, which is performed for better understanding of seal characteristics, provides a new friction factor model to analyze an entrance region of a duct. This model is applied to estimate the leakage and direct damping coefficients. Fleming [10-11] have performed a study to analyze the rotor dynamic coefficients of annular gas seals. In order to eliminate leakage and instability problems in turbo Machinery systems, he designed a short seal configuration. His design has a deficiency because this system was designed to analyze just one dimensional and axial flow. Because of that reason, it was not possible to accurately calculate cross-coupled coefficients. In addition, he also analyzed the rotordynamic characteristics of convergent tapered and straight seals. His result showed that convergent tapered seals have higher direct stiffness K and direct damping coefficients. Nelson [12-13] contributed to this

study by analyzing the effect of inlet swirl. Additionally, his study suggested important information about pressure effects on tangential velocity in constant and convergent tapered gas seals, which have different rotor and stator surface roughness. His solution method was similar to the model, which is developed by Childs [14-15]. While Nelson designed this model, he generally considered Hir's [8] turbulent bulk flow model. He also analyzed leakage and direct and cross-coupled rotor dynamic coefficients by applying perturbation analysis. His result supported the research performed by Fleming [10-11]. Both studies that Fleming [10-11] and Nelson [12-13] performed, showed that rotor dynamic characteristic of tapered seals are better than straight seals, because tapered seal geometry gives higher direct stiffness coefficients.

Black [16], and Jenssen, and Black [17-19] have performed a study, which shows effect of seal forces on rotor dynamic behavior of pumps. They have contributed to the development of dynamic damping and stiffness coefficients of high pressure annular seals. In addition, they accepted that friction factor is a function of axial and radial Reynolds numbers. Allaire, Gunter, Lee, and Barrett [20] improved Black's model to calculate rotor dynamic coefficients for large eccentricity and stationary systems.

There are also studies about optimization of CFD modeling to estimate the leakage and rotor dynamic coefficients of liquid annular seals. Geometry optimization in non contacting annular seals is done to eliminate instabilities in the turbo Machinery system. Ustinov [21] performed a study about journal orbits in annular seals. He tried to show that the rotor is more stable in diverging tapered seals. Smalley et al. [22] performed a study about dynamic characteristic of honeycomb seals with diverging

taper. He found that damping increases with the increment of diverging taper. Marquette, Childs, and San Andres [23] performed a study for smooth annular seals. They calculated rotor dynamic coefficients of smooth annular seals by using different pressures, eccentricities, and rotor speeds. Their study showed that the rotor dynamic coefficients of smooth annular seals are strongly dependent on eccentricity. In this thesis, rotor dynamic analysis will not be analyzed.

3. OBJECTIVES AND METHODLOGY

The objective of this thesis is to compare the performance of convergent and straight annular seals by performing leakage analysis for both under the same boundary conditions. Depending on the results obtained from these analysis, applicability and efficiency of convergent and straight annular seal configurations under the same working conditions will be discussed. In order to understand which seal configuration has better leakage characteristics, either experimental or computational methods can be applied. In this study, a CFD method will be used. These analyses will be performed based on the following steps.

1. Geometry of the convergent and straight annular seals will be created by using GAMBIT 2.4.6. Then, a mesh structure will be created by using same software. Axisymmetric flow pattern, which makes it possible to apply 2D analysis, will be used.

2. After creating the seal geometry and mesh structure, flow analysis will be performed by using commercial code FLUENT ®. Water and air will be used as working mediums in different simulations. Different boundary conditions and rotor speeds will be applied. Moreover, the surface roughness effect will also be observed. K-epsilon and standard wall function tools of FLUENT will be compared to each other.

3. Post processing will be done by using TECPLOT. Swirl shear and axial shear stress graphics will be plotted in order to understand the flow regime in the domain. Pressure contours will be analyzed as well. Beside these processes, Mach number distributions will also be created in TECPLOT

4. Depending on different seal-clearances, rotor speeds, seal configurations and surface roughness, the secondary flow rate will be calculated. According to these results, convergent and straight annular seal configurations will be compared in terms of leakage characteristics.

5. Results will be compared to the previous studies and existing analysis to evaluate the accuracy of this study. In figure 4, convergent and straight annular seal geometries are presented.

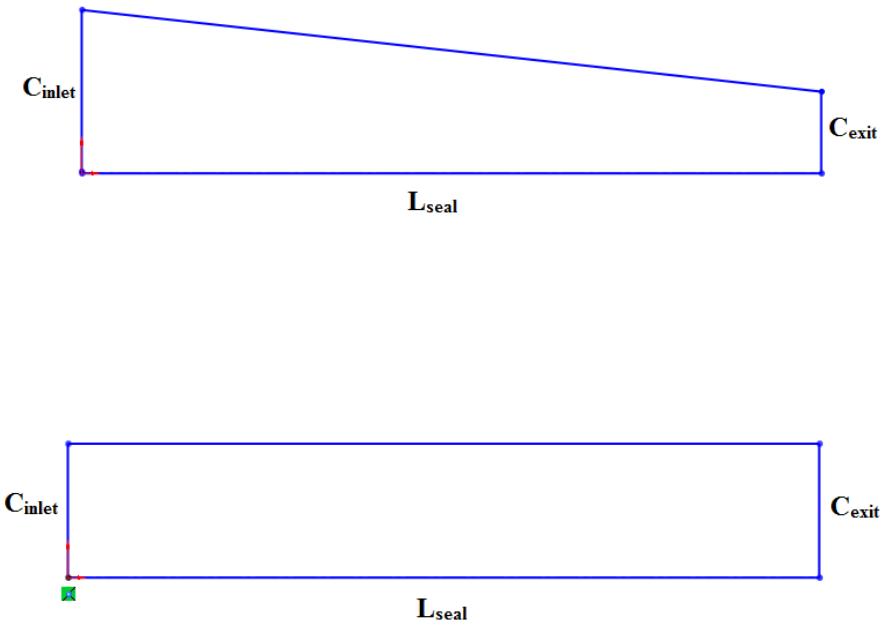

Fig. 4 Convergent and straight seals

Table 1 Geometrical parameters

Geometric Parameters	Convergent	Straight	Convergent	Straight
C_{ex} (mm)	0.1	0.1	0.2	0.2
C_{in} (mm)	0.175	0.1	0.35	0.35
L_{seal} (mm)	85.70	85.70	85.70	85.70
C_{in}/C_{ex}	1.75	1	1.75	1
D_{ROTOR} (mm)	114.72	114.72	114.72	114.72

Table 1 includes the geometrical parameters, which will be used in construction of the seal geometry and simulations. Geometric parameters and working conditions are taken from previous studies. In addition to these parameters, surface roughness effect on leakage characteristics of these seal configurations will be analyzed. These surface roughness parameters will be 0.0004 mm, 0.0008 mm and 0.0016 mm. As seen from table 1, two different seal clearances will be applied to these seal configurations. The ratio between inlet, and exit seal clearances for the convergent seal configurations is 1.75, which is taken from the previous studies.

4. COMPUTATIONAL METHOD

Experimental fluid dynamics have a vital importance on construction and application of governing equations to various fluid dynamic systems. Wind tunnel, which is one way of simulating real flow, provides very cost effective option compared to full-scale analysis. In design of many systems that directly related to flow characteristics, application of full-scale analyses is not possible. Technological improvements make it possible to use very high speed computers for computational analyses. This was the main reason that makes computation fluid dynamics (CFD) fundamental method for fluid dynamic applications. Process time for flow analyses is considerably decreased by the application of computational fluid dynamics. In addition, computational fluid analyses provides to get more comprehensive information about flow behavior. In addition, pressure and velocity distributions can be analyzed by applying CFD analysis.

In this study, computational fluid dynamic analyses are used to understand the leakage characteristics of straight annular and convergent seal configurations. The seal geometries and the mesh structures are created by using commercial code GAMBIT 2.4.6. The flow simulations are performed by using commercial code FLUENT 12.0.16., and TECHPLOT is used for post processing.

.

FLUENT 12.0.16 uses finite volume method for solving Navies-Stokes Equations. K-ε model, which is known as the most accurate tool based on experiments done by Morrison, and Al-Ghasem [24], is used to perform the simulations. More detail information about k-ε model and finite volume method will be presented in appendix.

As specified in previous section, convergent and straight annular seal geometries are created in GAMBIT ®. 2D analyses are performed by using commercial code FLUENT 12.0.16 instead of 3D. Because seal geometries make application of axisymmetric tool of FLUENT ® possible. Simulations are performed with enhanced wall treatment and standard k-ε models. In order to analyze flow through smooth surfaces, enhanced wall treatment model is applied. Y^+ adaptation is done to keep Y^+ under 5. Standard k-ε model is applied for simulations with surface roughness, because enhanced wall treatment model is not applicable for flow simulations with surface roughness effect.

Mesh refinement is done near to the rotor and the stator walls by setting successive ratio to 1.064, which makes it possible to see the effects of boundary layer. Surface roughness is applied to both the stator and the rotor surfaces. As a working material, water and air are used.

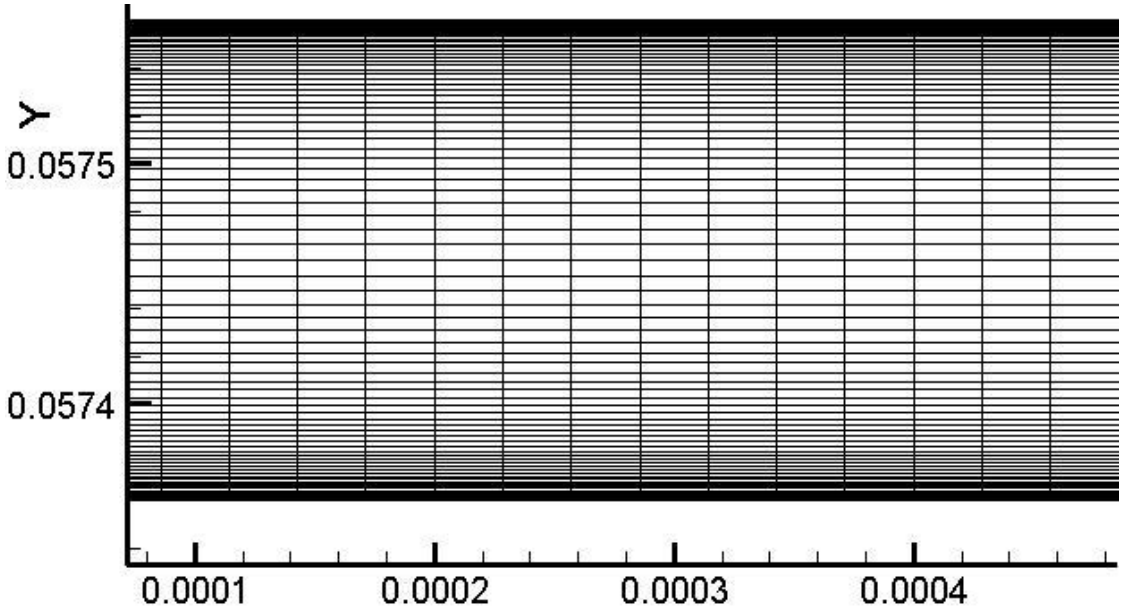

Fig. 5 Mesh structure of straight annular seal (straight annular seal, successive ratio=1.064)

In figure 5, mesh structure of straight annular seal is shown. More strict mesh structure, close to the walls, shows the effect of successive ratio. In order to understand mesh density effect, simulations with different mesh structures for both straight and convergent annular seals are performed. Secondary flow rates obtained from these simulations are compared to each other to see the effects of seal geometries with different grid numbers.

In these analyses, exit clearances for both seal configurations are kept constant, and same boundary conditions are applied to all seal configurations. In order to provide wall resolution, Y^+ is kept under 5, which is a requirement for k-ε model. Grid independent study is applied to get leakage rate, which is independent from number of nodes. Starting from 20000 nodes number, different mesh structures are applied.

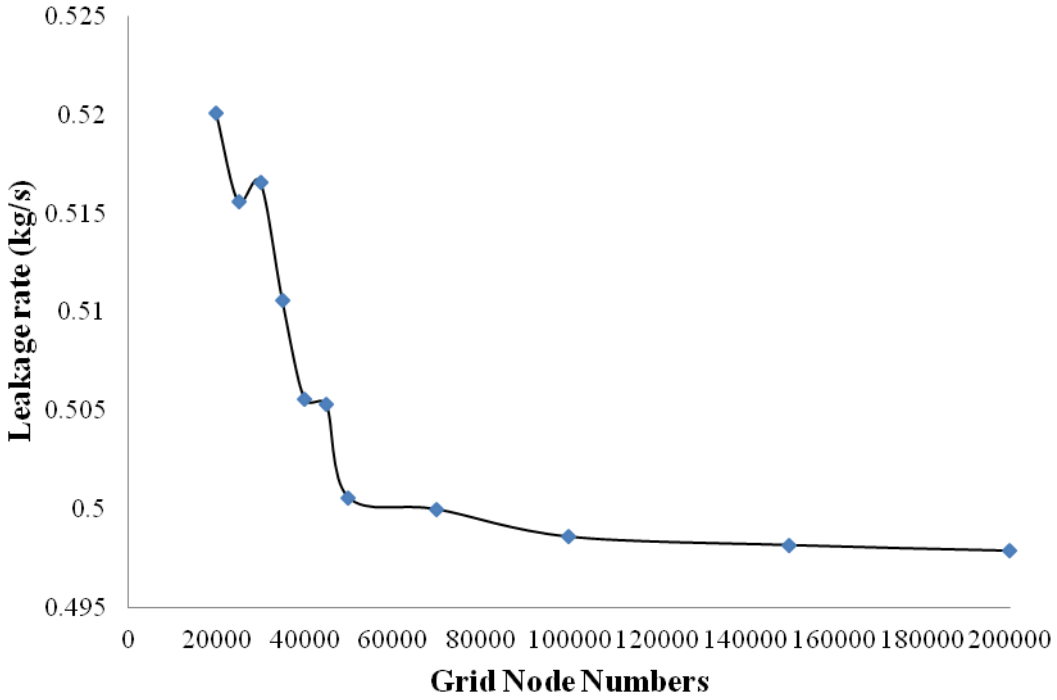

Fig. 6 Mesh structure of the straight annular seal (grid independent analysis)

Figure 6 includes the secondary flow rates compared to the mesh structures with different number of nodes. This study, as specified in previous section, is performed to get grid independent result. According to this graphic, after 55000 node numbers, leakage rates start to be stable, and the leakage rate variation is considerably small. Accuracy of these results increase by increment of grid node numbers, but it will also increase the process time. Because of that reason, optimum mesh structure should be defined. According to the figure 6, mesh structure with 55000 nodes can be applied for all simulations to understand the flow behavior.

While creating mesh structure, surface roughness heights are also taken into consideration. Commercial code FLUENT ® manual suggested that surface roughness

height must be kept smaller than distance of center point of a node, which is the closest to the wall, to wall.

Comparison of enhanced wall treatment and standard k-ε models is also performed to see how results are changing when different turbulence models are used. Results obtained from the simulations are presented in the table 2. Results show that standard k- ε, and enhanced wall treatment models give almost same leakage flow rates under same boundary conditions.

Table 2 Convergent seal mass flow rates for the standard-enhanced models

Rotor Speed(RPM)	Standard Model		Enhanced Model	
	0.28 PR	0.39 PR	0.28 PR	0.39 PR
0	0.869	0.866	0.855	0.854
5200	0.867	0.865	0.853	0.856
10200	0.864	0.861	0.849	0.813
15200	0.864	0.856	0.843	0.842
20200	0.862	0.849	0.836	0.836

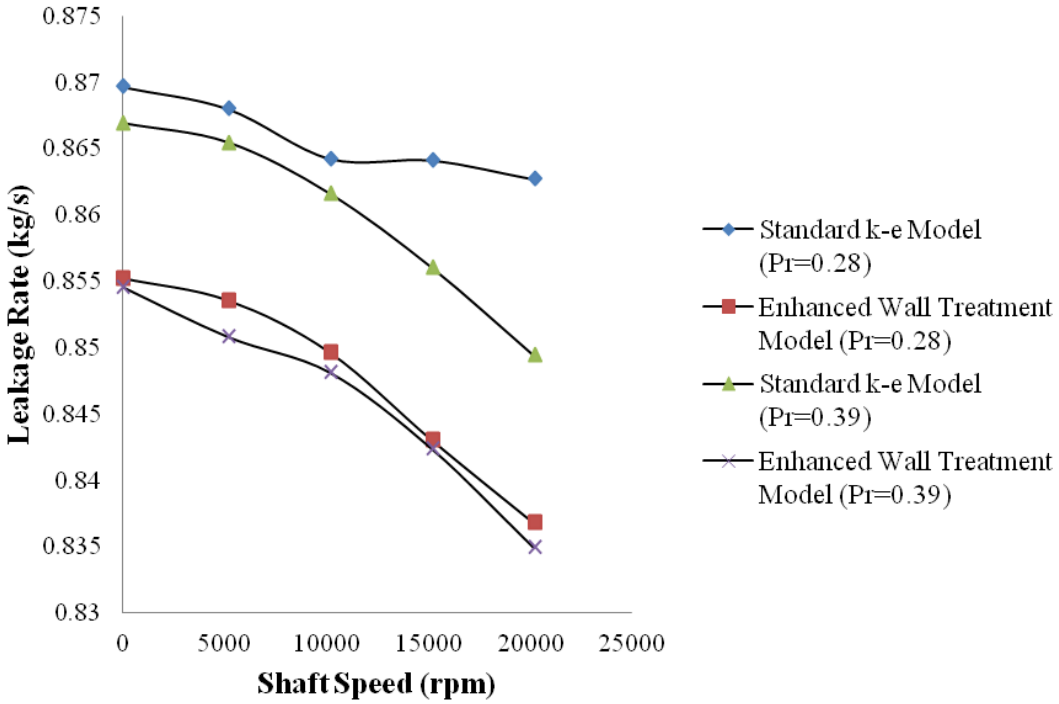

Fig. 7 Comparison of the standard k-ε and enhanced wall treatment models (convergent seal, Cex=0.1 mm)

In figure 7, results obtained from the flow simulations, which performed by using the standard k-ε, and enhanced wall treatment models, are presented. Results show that variation of the flow model has not significant impacts on the results. In table 3, comparison of the enhanced and standard flow models for the straight annular seal configurations with larger clearances are performed.

Table 3 Straight annular seal mass flow rates for the standard-enhanced models

Rotor Speed(RPM)	Standard Model		Enhanced Model	
	0.28 PR	0.39 PR	0.28 PR	0.39 PR
0	0.677	0.669	0.664	0.650
5200	0.675	0.668	0.661	0.660
10200	0.670	0.665	0.661	0.649
15200	0.667	0.659	0.648	0.638
20200	0.661	0.651	0.657	0.638

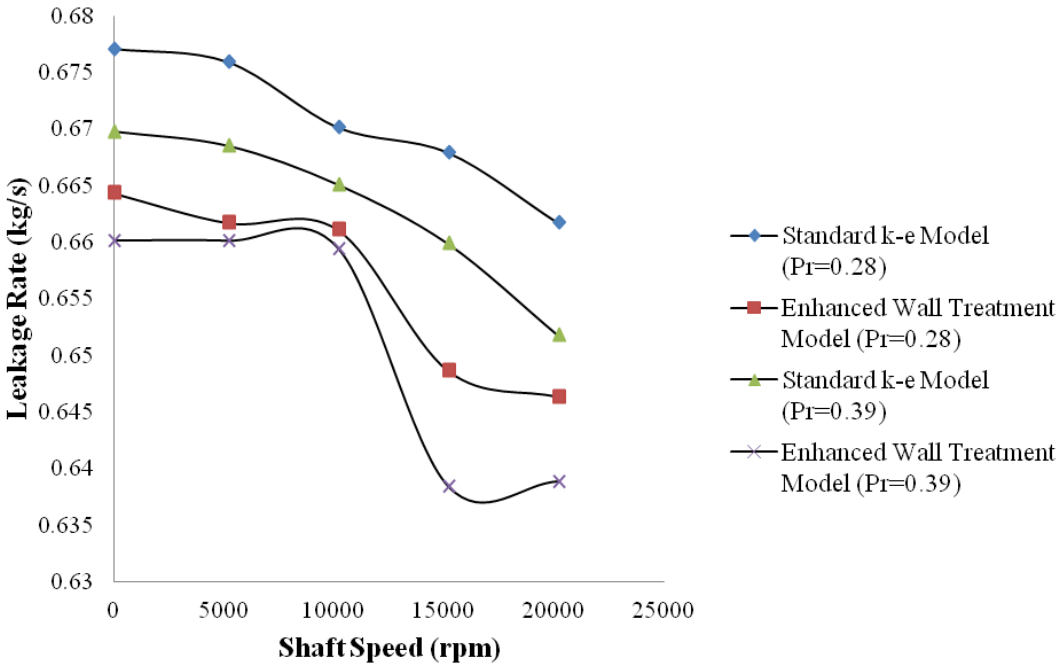

Fig. 8 Comparison of the standard k-ε and enhanced wall treatment models (straight annular seal, C_{ex}=0.1 mm)

In figures 7 and 8, results, which are obtained by using enhanced wall treatment and standard k-ε models are presented. This analysis aims to show the effects of different turbulent models on the secondary flow rate. As specified in previous section, some of the simulations are performed by using enhanced wall treatment model; others are performed with standard k-ε model. In order to perform accurate analyses, these two turbulent models are compared, and this comparison showed that there is not a big difference on the results obtained from each models.

Standard k-ε model is used to perform the simulations with surface roughness heights. Y^+ will be kept under 5 to provide wall resolution for turbulent flow model with enhanced wall function.

5. SEAL GEOMETRY

In this study, different seal geometries are analyzed to understand the flow characteristics of convergent and straight annular seal configurations. Different pressure ratios, seal clearances, rotor speeds, and surface roughness parameters are applied for flow simulations. According to these factors, secondary flow rates through these seal configurations are analyzed. Exit clearances for both convergent and annular seal configurations are kept constant and inlet and exit clearance ratio is accepted to be 1.75 for convergent seal configurations, which is taken from previous studies.

Rotational speed effects on the leakage rate are also analyzed. Simulations are performed when the rotor is stationary, and rotating as well. Different rotational speeds are applied to see how the leakage characteristics of these seal configurations are changing.

Water and air are used as working materials in the simulations. 20 atm inlet and 0 atm exit gage pressures are applied for all cases performed with water. Different pressure ratios are applied to the simulations, which are performed by using air and effects of pressure ratio are discussed

In addition, different surface roughness parameters are applied to both the stator and the rotor surfaces to understand how leakage rate is changing.

6. RESULTS AND DISCUSSIONS

In this section, leakage characteristics of convergent and straight annular seals will be compared based on the results of flow simulations. As specified in previous section, seal clearance effects, rotor speed effects, pressure ratios effects, and surface roughness effects on the leakage will be analyzed and discussed.

6.1. Effects of the Seal Clearances

Clearance control is one of the most efficient way to increase the aerodynamic performance and to develop cooling capability of a gas turbine engine. Because of different working conditions, during an aerodynamic system is operating, seal clearance between rotor and stator generally changes. As a consequence of this, secondary flow rates change. Therefore, design of a seal is very important issue in terms of keeping leakage rate considerably small. Because increment of leakage rate will decrease the efficiency of an aerodynamic system and will also affect cooling performance of a gas turbine engine negatively. In addition to these complications, seal design will also affect heat balance of aerodynamic system components.

In order to keep the leakage under control, various type of seal configurations are used. Labyrinth, convergent, and straight annular seal configurations are mostly used in rotating systems, because their manufacturing way is considerably simple. Different seal configurations are being tested to figure out which seal configuration provides the best seal clearance control performance.

Many experimental and computational studies are performed to find the most effective seal configuration. A study performed by Chupp, Hendrilciks, Lattime, and Steinetz [25] showed that honeycomb stator has better characteristics compared to the smooth labyrinth seals when higher rotor speeds are applied. Because of that reason, honeycomb seal configurations are mostly used in many industrial applications instead of labyrinth seal configurations. With the application of honeycomb seal configurations, aerodynamic losses are minimized, and very tight seal clearances can be applied.

In order to understand the effect of seal clearance on the leakage through stepped labyrinth seals, some experiments are performed. Similar observations will be performed in this study for convergent and straight annular seal configurations. After performing grid independent study, and choosing appropriate flow model, Willenborg, Schramm, Kim, and Witting [26] performed a research using different seal clearances to calculate discharge coefficient, and they compared their results to experimental data. In these analyses, k-ε model, which is representative of high Reynolds Number turbulence model, is applied. In addition, same analyses are performed with k-ω model. Between these two turbulence models, considerable difference is not observed. In their study, three sealing clearances were tested, and discharge coefficients were calculated. Results showed that increment of seal clearances cause decrement of discharge coefficient, which shows total losses in flow domain. Raise in discharge coefficient indicates decrement of secondary flow rate through labyrinth seal configurations. As clearly specified in previous section, this study showed that higher seal clearances causes increment of the leakage rate. In this study, pressure ratio effects on discharge

coefficients were also analyzed, and results showed that discharge coefficient increases when higher pressure ratios are applied.

Rhode [27] performed another research to understand the leakage characteristics of annular and labyrinth seal configurations depending on variation of seal clearance. His results showed that leakage rate through these seal configurations increases when larger seal clearances are applied, and he also observed that labyrinth seal configurations displayed 20% better working performance respectively. He suggested that higher precision of turbulent shear stress effect in labyrinth seal configurations provides better leakage characteristics.

Rhode [27] also analyzed the pressure drop and swirl velocity distribution based on the variation of seal clearance. His results showed that swirl velocity is increasing as a consequence of decrement of seal clearance. Higher swirl velocity means that higher tangential forces, which have great impact on dissipation of the flow energy, which will decrease secondary flow rate considerably. Childs, and Dressman [28] performed a study to understand the effect of swirl velocities on tangential forces, and their results showed that tangential forces are increasing while lower swirl velocity formations are observed.

In this research, same analyses will performed to understand the effect of seal clearances on the leakage through convergent and straight annular seal configurations. As specified in previous section, water and air are used as working materials for flow simulations, which are performed by using commercial code FLUENT 12.0.16.

6.1.1. Effect of Seal Clearance on the Water Leakage

In this section, results that show the effects of the seal clearance on the secondary flow rate through the convergent and straight annular seal configurations will be presented and discussed.

Table 3, which is presented in a previous section, illustrates all the geometric parameters, which are used in creating seal geometries. Comparison of seal configurations will be performed based upon these parameters. As clearly seen from this table, two different seal clearances, 0.1 mm and 0.2 mm, are applied to both convergent and straight seal configurations. Comparison of the leakage characteristics of the convergent and straight annular seals will be performed to understand which seal configuration provides higher sealing efficiency.

In these simulations, the same boundary conditions are applied to both seal configurations. Inlet gage pressure is set at 20 atm and exit pressure is set at 0 atm gage. Different rotor speeds are applied, and effects of rotational speed on the secondary flow rate through these seal configurations will be discussed in following section as well.

Pressure distribution, swirl velocity, swirl shear stress, and axial shear stress distributions are obtained. Flow is incompressible for these cases, since the working material is water.

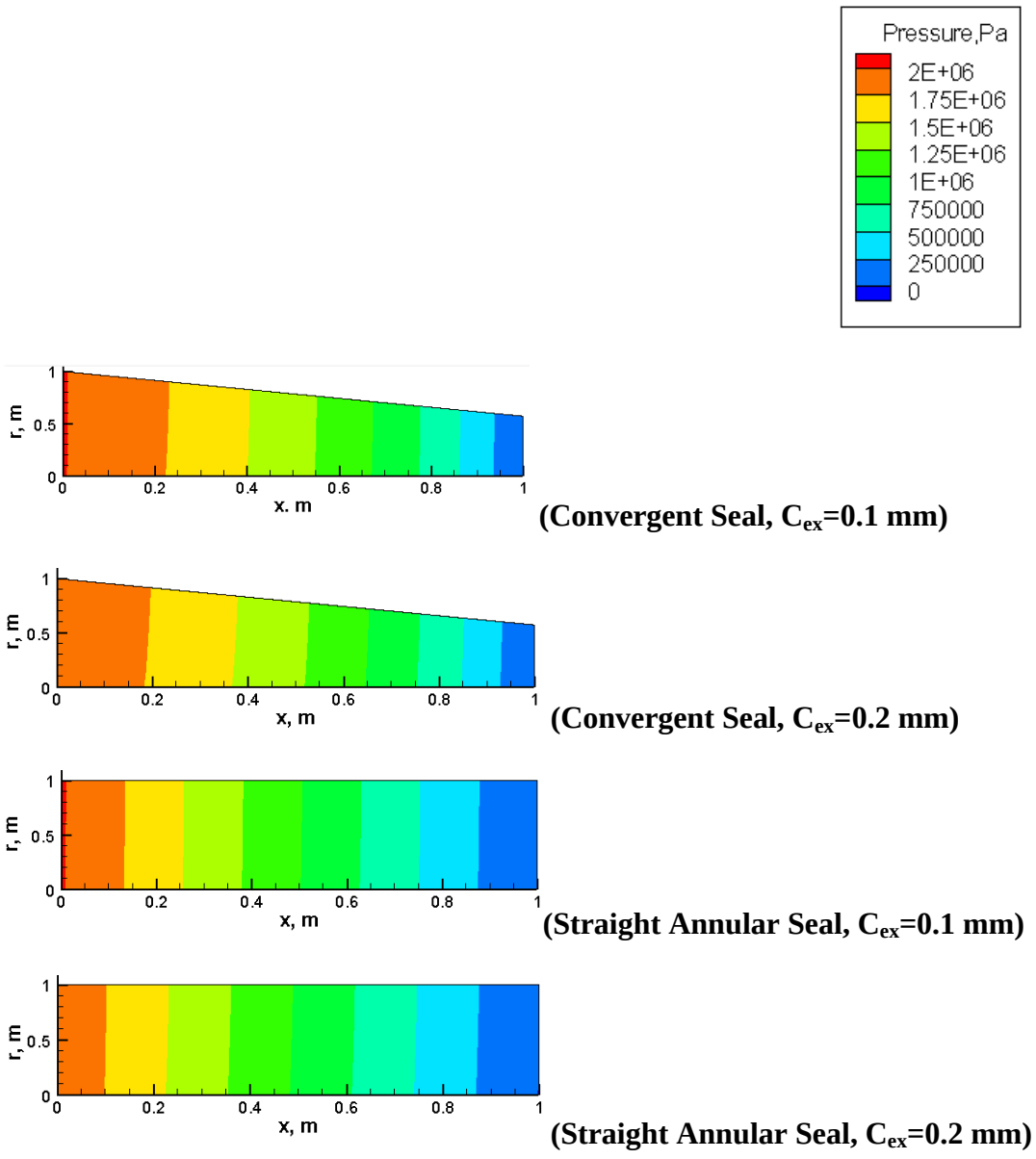

Fig. 9 Pressure contours for the convergent and straight annular seals (rotor wall, 20,200 rpm)

Figure 9 shows the pressure distributions in the four seals on the axial-radial plane. There is a small radial increase in pressure across the seal due to the centrifugal acceleration. For easier direct comparison, the axial pressure distribution on the rotor is presented in figure 10.

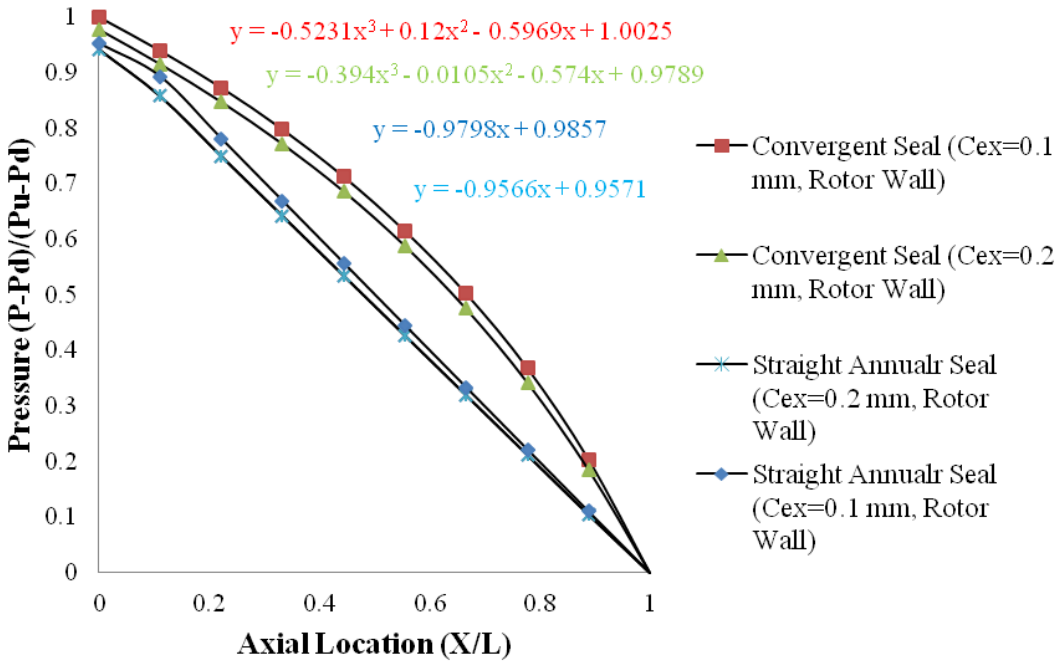

Fig. 10 Pressure distributions for the convergent and straight annular seal configurations (20, 200 rpm, water flow)

In figure 10, pressure distributions through the convergent, and straight annular seal configurations at 20,200 rpm are presented. Pressure, and axial location are non-dimensionalized by using the equations, which Rhode [27] used in his study. Rhode [27] also observed the static pressure distributions in the axial direction versus different seal clearances for the labyrinth, and annular seal conifurations. His results suggested that the

rate of pressure drop increases with the decrease of seal clearance. In addition, he observed that pressure drop in annular seal configurations is higher compared to the labyrinth seals. Higher pressure drop shows the increment of the linear inertia of the flow.

Rhode [27] created the same graphic, which shows the pressure distributions in the axial direction for the labyrinth, and annular seal configurations to investigate the shear stress effects on the bulk relative pressure. His results showed that the labyrinth seals gave higher pressure formations than annular seal configurations, which is resulted from the lower velocity profile in the labyrinth seal configurations. Rhode [27] suggested that the labyrinth seal configurations exhibit sharp decrement in the static pressure.

As specified in the previous section, 20 atm inlet gage pressure, and 0 atm exit gage pressure are applied to all the seal configurations with different rotational speeds. Figure 10 is created considering the static pressure distributions for the convergent, and straight annular seal configurations at 20,200 rpm shaft speed. It can be deduced from figure 10. that straight annular seal configurations cause linear decrement in the static pressure. Static pressure distributions at same clearances for the same seal configurations are almost same. In the following section, axial velocity distributions for these seal configurations will be analyzed to investigate the effects of the seal geometry on the axial velocity formation.

.

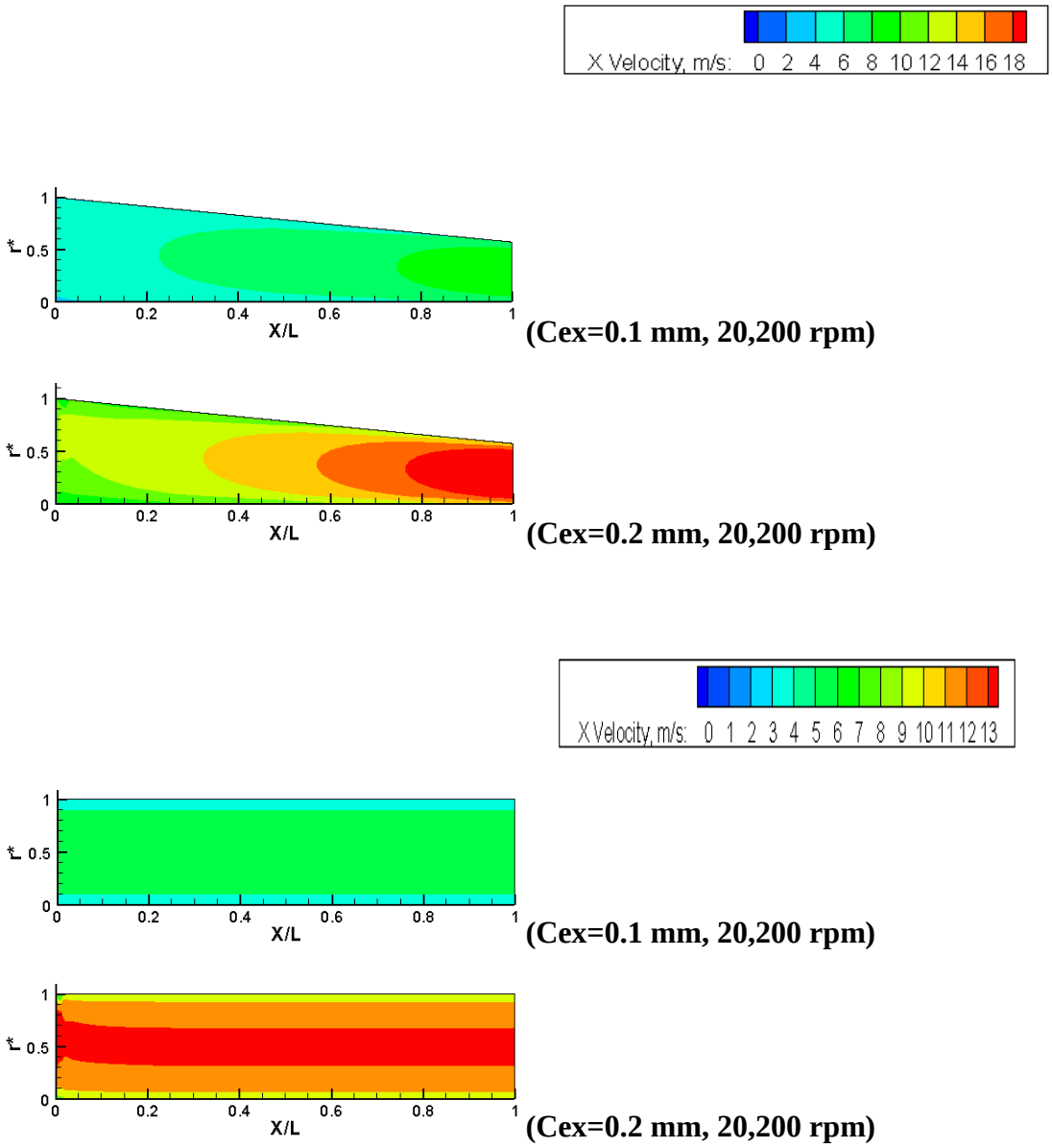

Fig. 11 Axial velocity contours for the convergent and straight annular seals (20,200 rpm, water flow, $r^*=(r-r_{rotor})/ r_{rotor}$)

In figure 11, axial velocity distributions for the convergent and straight annular seal configurations are shown. According to this figure, It can be deduced that

convergent seal configurations with 0.2 mm exit seal clearance gives the greatest axial velocity formation, which is caused by the high seal clearance.

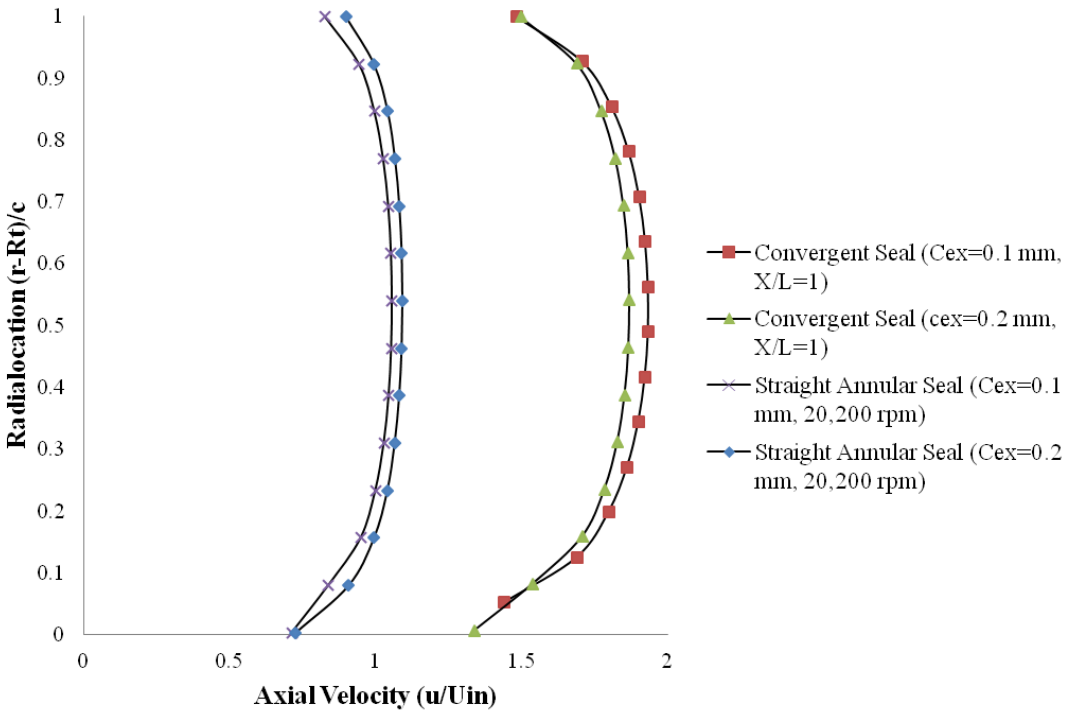

Fig. 12 Axial velocity distributions for the convergent, and straight annular seals (20,200 rpm, water flow, X/L=1)

In figure 12, axial velocity distributions at the exit for the convergent and straight annular seal configurations are shown. In order to make the axial velocity non-dimensional, bulk inlet axial velocity is calculated for each case. Average mass weighed integral of the inlet axial velocities is performed to calculate the inlet bulk axial velocity for all the seal configurations. Results show that convergent seal configurations give higher axial velocity formations.

Table 4 Bulk inlet velocities

Seal Type	Clearance(mm)	U_{in}(m/s)
Straight	0.1	4.47
Straight	0.2	11.2
Convergent	0.1	4.95
Convergent	0.2	11.3

According to figure 12, convergent seal configuration with smaller seal clearance gives higher axial velocity formation compared to the same seal configuration with 0.2 mm exit seal clearance while straight annular seal configuration with 0.2 mm seal clearance gives greater axial velocity formation than annular seal with smaller seal clearance. In addition, table 4 shows the bulk inlet velocities for the both convergent, and straight annular seal configurations. It can be deduced from this table that convergent seal configurations exhibits higher axial velocity formations compared to the straight annular seals.

Rhode [27] performed same analyses for the labyrinth, and annular seal configurations to investigate how axial velocity formations at the exit change with the variation of seal clearance. Axial velocity distributions at the exit exhibits the effects of wall shear layers. Axial velocity near the walls is significantly reduced by the effects of the shear layer. Figure 12 shows that exit velocity profiles for all the seal configurations are fully developed.

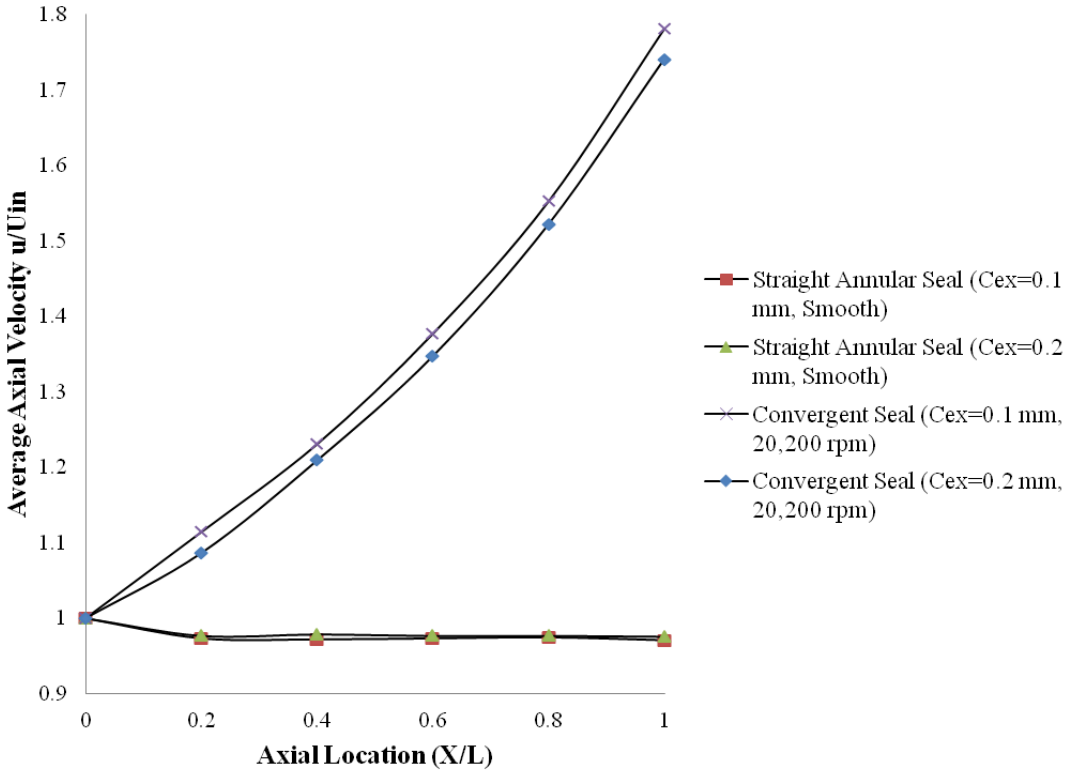

Fig. 13 Average axial velocity distributions for the convergent, and straight annular seals (20,200 rpm, water flow, X/L=0-0.2-0.4-0.6-0.8-1)

In figure 13, average axial velocity distributions for the convergent, and straight annular seal configurations are presented. A thousand data points in the radial direction are collected from the different axial locations (X/L=0-0.2-0.4-0.6-0.8-1), and then an average integral process is performed to calculate the average axial velocities at these points. In order to better understand the seal clearance effects on the axial velocity formation, these average axial velocity distributions are analyzed in figure 13. Results show that convergent seal configuration with 0.1 mm exit seal clearance gives the greatest average axial velocity formation, which is resulted from the high flow inertia. In addition, average axial velocities for the convergent seal configurations are continuously

increasing while almost uniform average axial velocity profiles are obtained for the straight annular seal configurations. This is another important effect of the seal clearance.

In the following section, pressure gradient distributions for the convergent and straight annular seal configurations will be analyzed to investigate the effects of axial wall shear stress, and shaft speeds on the axial pressure distributions. In figure 14, axial pressure gradients for the convergent and straight annular seal configurations are presented at 20,200 rpm shaft speed. This figure shows that straight annular seal configurations give constant pressure gradient distributions while axial pressure gradients for the convergent seal configurations are continuously increasing in magnitude. As specified in figure 13, constant average axial velocity distributions are observed for the straight annular seal configurations. Therefore, there is no axial acceleration, and thus pressure drop is solely due to the wall friction as is the case for the Couette flow. The axial flow acceleration in the convergent seals cause partial pressure drop . Axial Pressure gradient distributions with respect to the different shaft speed for the straight annular, and convergent seal configurations will also be analyzed in the following section.

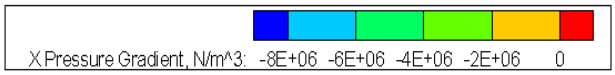

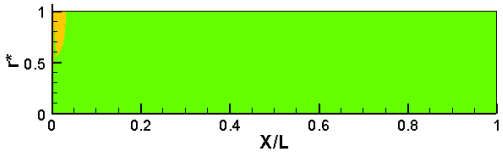

(Cex=0.1 mm, 20,200 rpm)

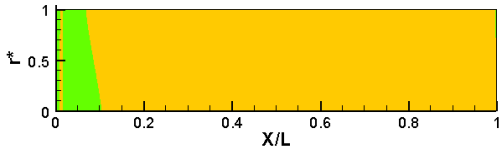

(Cex=0.2 mm, 20,200 rpm)

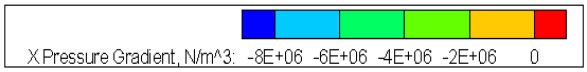

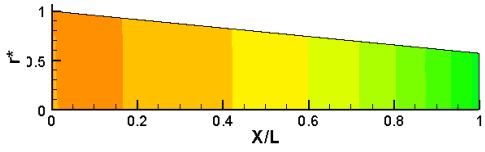

(Cex=0.1 mm, 20,200 rpm)

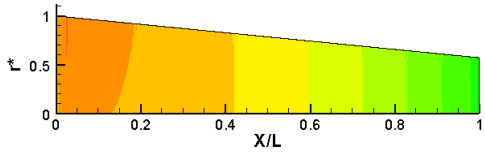

(Cex=0.2 mm, 20,200 rpm)

Fig. 14 Axial pressure gradient for the convergent and straight annular seals (20,200 rpm, water flow, C_{ex}=0.1-0.2 mm)

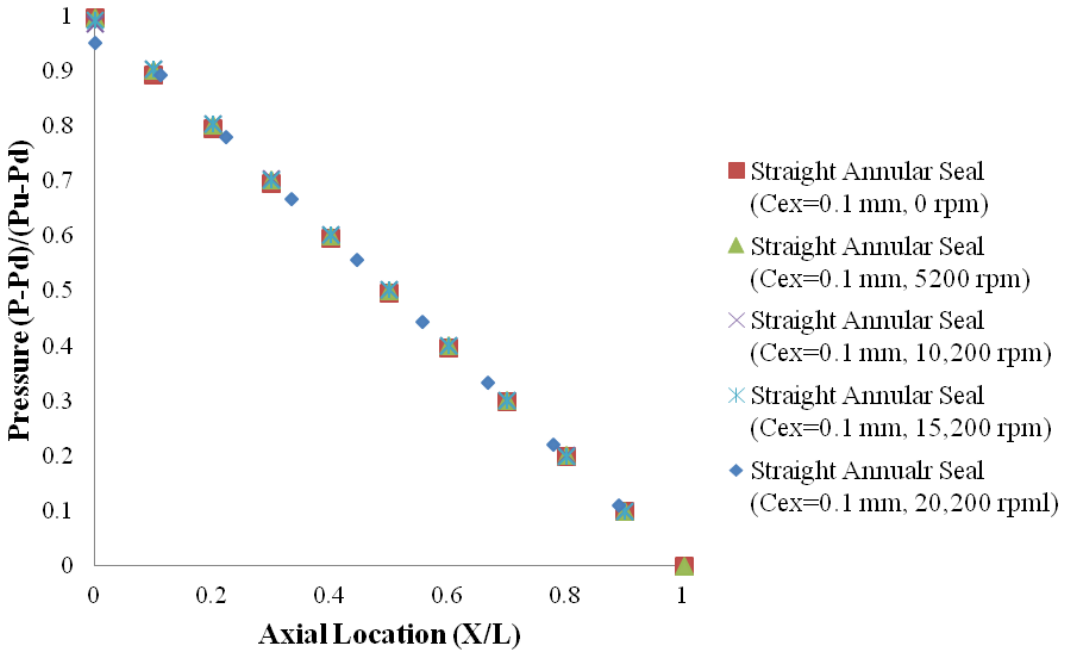

Fig. 15 Pressure distributions for the straight annular seal configurations (0-20,200 rpm, rotor wall, water flow)

Figure 15 shows that pressure distributions at the same clearances, and different shaft speeds for the straight annular seal configurations are almost same, and linear. Boundary conditions are set as 20 atm inlet, and 0 atm exit gage pressure for all cases. In the following section, axial pressure gradient distributions for the straight annular seal configurations will be analyzed.

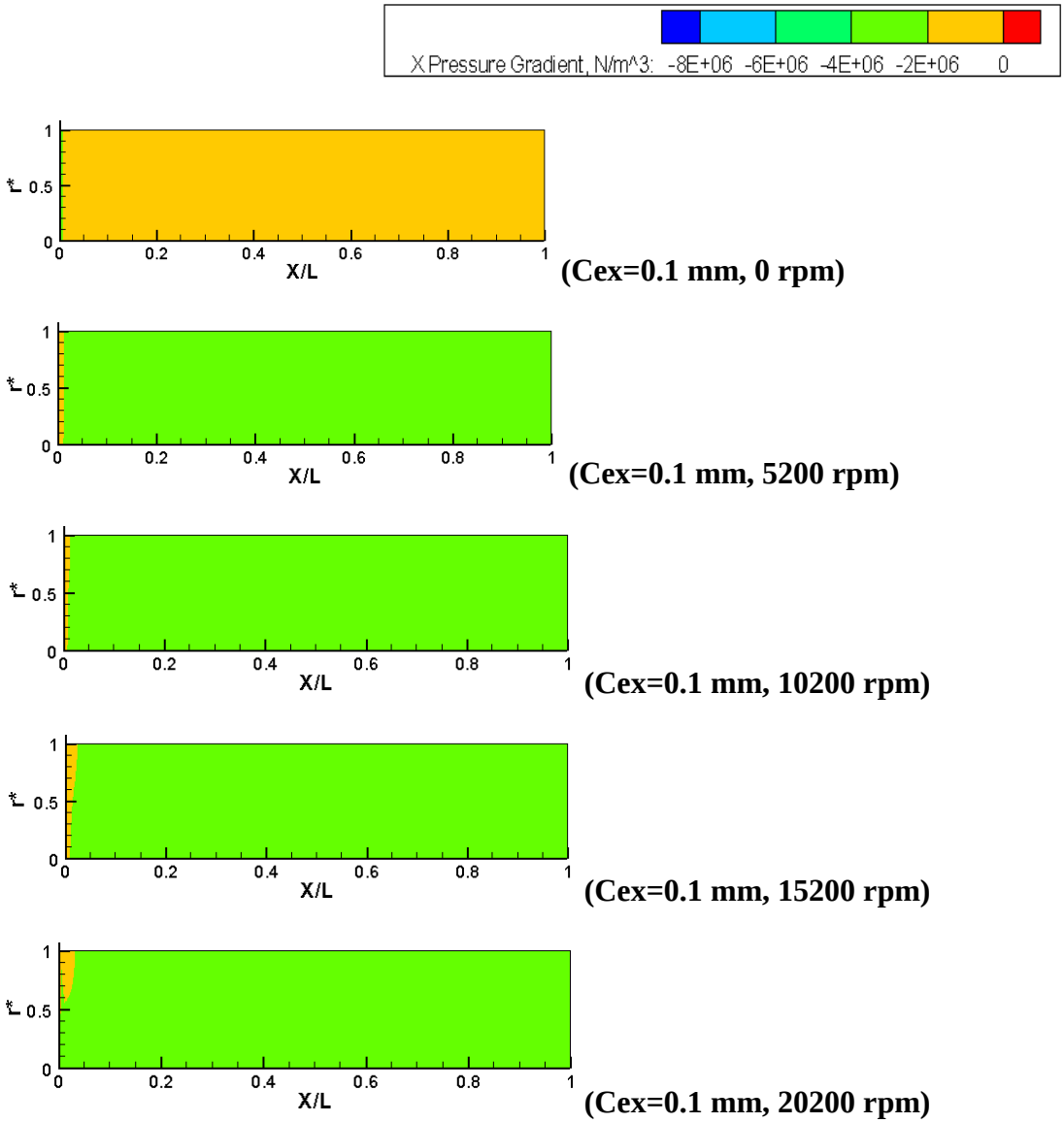

(Cex=0.1 mm, 0 rpm)

(Cex=0.1 mm, 5200 rpm)

(Cex=0.1 mm, 10200 rpm)

(Cex=0.1 mm, 15200 rpm)

(Cex=0.1 mm, 20200 rpm)

Fig. 16 Axial pressure gradient contours for the straight annular seal (0-20,200 rpm, water flow)

Figure 16 shows the pressure gradients corresponding to the different shaft speeds for the straight annular seal configurations with 0.1 mm exit seal clearances. Results show that shaft speed has not a significant effect on the pressure gradient.

Table 5 ((dp/dx)/τ_{xy})*c (straight annular seals)

rpm	c=0.1	c=0.2
0	-0.171	-0.171
5200	-0.171	-0.171
10200	-0.171	-0.171
15200	-0.172	-0.171
20200	-0.172	-0.172

The axial wall shear stress, $\tau_{xy,}$ was found to be essentially constant. Table 5 shows the variation of axial pressure gradient-to-axial wall shear stress (rotor wall) ratio evaluated at the location, (X/L=1/2), for both straight annular seal configurations with different shaft speeds. Results show that there is not a significant variation in this ratio for these cases. It can be deduced from these analyses that shaft speeds do not have apparent effects on this ratio for the straight annular seal configurations. In the following section, the same analyses will be performed for the convergent seal configurations.

CFD accuracy is such that -0.1715 should be used as the correct value (uncertainty in CFD is more than the spread (-0.1717-0.17135)). The axial velocity in the convergent tapered seals increases as the clearance decreases. This results in some of the axial pressure drop being due to the axial acceleration is established. The equations used for obtaining figure 16 are presented in the following section.

By Bernoulli equation,

$P/\rho+1/2V^2+gz=\text{constant}$ (1)

ρ is constant for incompressible flow, and friction is present, then

$(P_1-P_2)/\rho+1/2(V_1^2-V_2^2)=$ head loss due to the friction (2)

If there is no friction,

$1/\rho dp/dx+1/2\ dV^2/dx=0$ (3)

$1/\rho dp/dx+VdV/dx=0$ or $dP/dx=-\rho VdV/dx$ for $\tau_w=0$ (4)

$V=\dot{m}/(\rho A)=\dot{m}/(\rho\pi Dc)=\beta/c$ since $\dot{m}/(\rho\pi Dc)=$constant (5)

then $dV/dx==\beta(d/dx(1/c))$ but $c=C_o-mx$ (6)

$d/dx(1/(C_o-mx))=$so now know that (7)

dp/dx is due to the fluid acceleration (8)

In figure 17, axial pressure gradients-to-axial wall shear stress ratios for the convergent seal configurations with 0.1 mm exit seal clearances are presented. In the axial direction, four data point are specified on the rotor wall, and pressure gradients, and axial wall shear stresses are collected from these points. This figure shows that pressure gradient is independent of shaft speed, and is caused by the effects of axial wall shear stress and convergent seal geometry. When these results are made non-dimensional by multiplying with local seal clearances at these data points, almost linear distributions will be obtained.

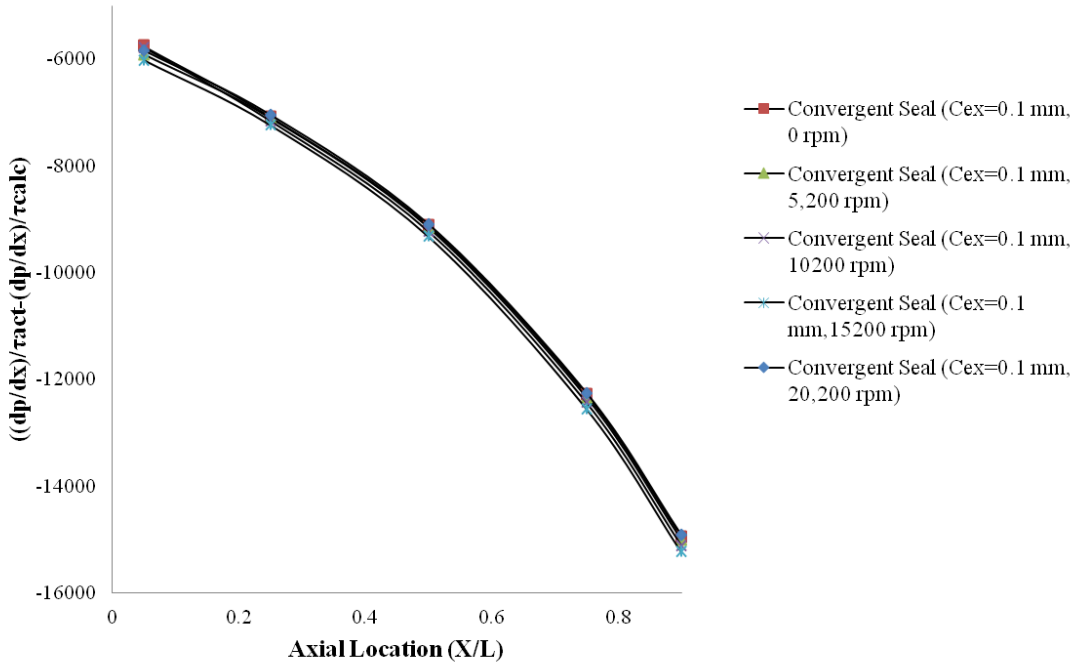

Fig. 17 $((dp/dx)/\tau_{xy})_{actual}$-$(dp/dx)/\tau_{xy})_{calculated}$) versus x for the convergent seal (C_{ex}=0.1 mm , 0-20,200 rpm, water flow)

If you non dimensionalize figure 17 by τ_{wall}/c then the ratio equals to 0.171. For the straight seal that ratio is also 0.171. This results show that this flow constant applies to the straight, and convergent seals. In addition to that, these analyses show that it is possible to model axial wall shear stress distributions by just knowing the pressure distributions. In the following section, swirl velocity distributions with respect to the different seal configurations, and shaft speeds will be analyzed.

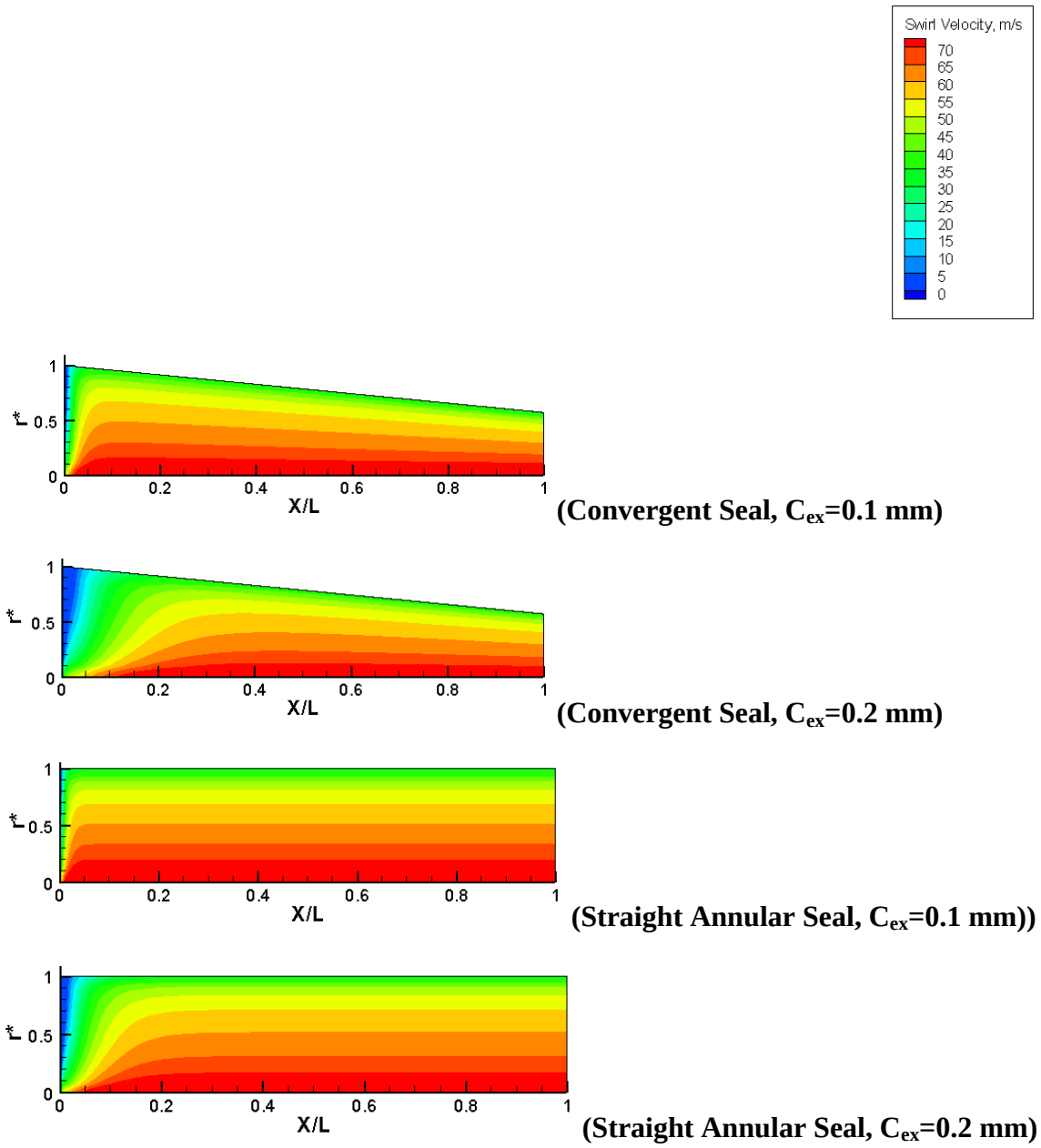

(Convergent Seal, C_{ex}=0.1 mm)

(Convergent Seal, C_{ex}=0.2 mm)

(Straight Annular Seal, C_{ex}=0.1 mm))

(Straight Annular Seal, C_{ex}=0.2 mm)

Fig. 18 Swirl velocity contours for the convergent and straight annular seals (20,200 rpm, water flow)

In figure 18, swirl velocity formations for the convergent, and straight annular seal configurations are presented. The bottom edge shown in this figure represents the

rotor shaft, which is rotating and upper edge symbolizes the stator, which is stationary when the system is working. As clearly seen from the figure 18, swirl velocity is decreasing moving away from the rotor shaft towards the casing. This figure also shows that the highest inlet swirl formation is observed for the straight annular seal configuration with 0.1 mm exit seal clearance. As seen from this figure, variation of seal configuration, and seal clearance affects the entrance region, where swirl velocity distributions vary with axial location. Results show that the increase of seal clearances cause the increase of the distance that flow starts to be fully developed.

Table 6 shows the distances, that flow starts to be fully developed, for the convergent, and straight annular seal configurations. At these points, the highest swirl velocity formations are observed for all seal configurations.

Table 6 Entrance region with seal clearance

Seal Type	Clearance(mm)	Entrance (mm)
Straight Annular	0.1	0.053
Straight Annular	0.2	0.209
Convergent	0.1	0.106
Convergent	0.2	0.421

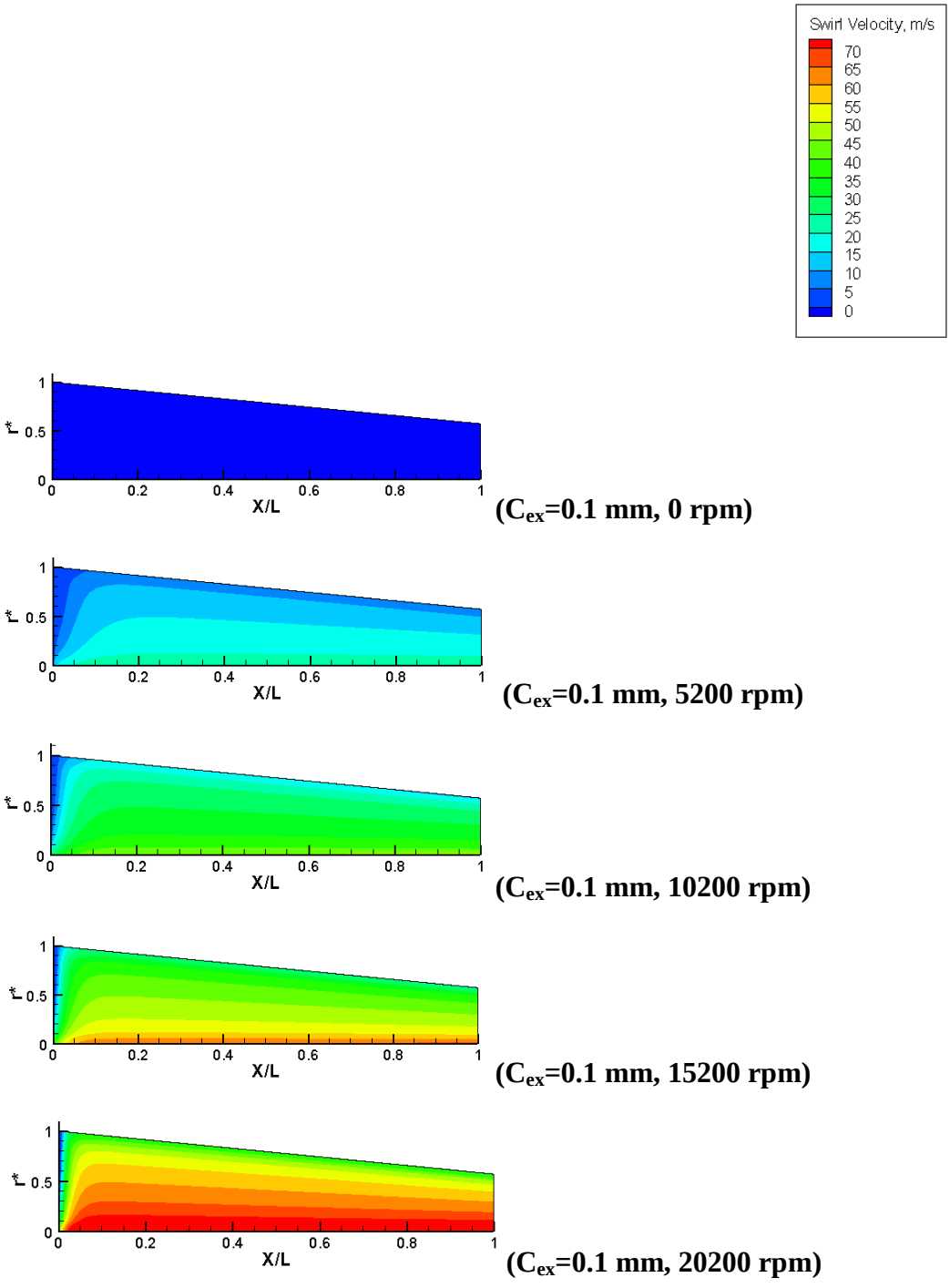

(C_{ex}=0.1 mm, 0 rpm)

(C_{ex}=0.1 mm, 5200 rpm)

(C_{ex}=0.1 mm, 10200 rpm)

(C_{ex}=0.1 mm, 15200 rpm)

(C_{ex}=0.1 mm, 20200 rpm)

Fig. 19 Swirl velocity contours for the convergent seals (C_{ex}=0.1 mm, 0-20200 rpm)

In figure 19, swirl velocity distributions for the convergent seal configuration with 0.1 mm exit seal clearances are presented. This figure shows that higher swirl velocity formations in both radial, and axial directions are observed with higher shaft speed.

Table 7 Entrance region with shaft speed

Seal Type	rpm	Entrance (mm)
Convergent	5200	0.285
Convergent	10200	0.215
Convergent	15200	0.143
Convergent	20200	0.106

Table 7 shows that the increase of shaft speed causes the flow stream to be fully developed in a shorter distance. Rhode [27] also analyzed the swirl velocity formations compared to different seal clearances for the labyrinth, and annular seal configurations. He analyzed radial and axial swirl velocity distributions to understand how the seal leakage affects swirl velocity formation for these seal configurations. His results showed that the decrease of the seal clearances provide greater swirl velocity formations in the radial and axial directions.

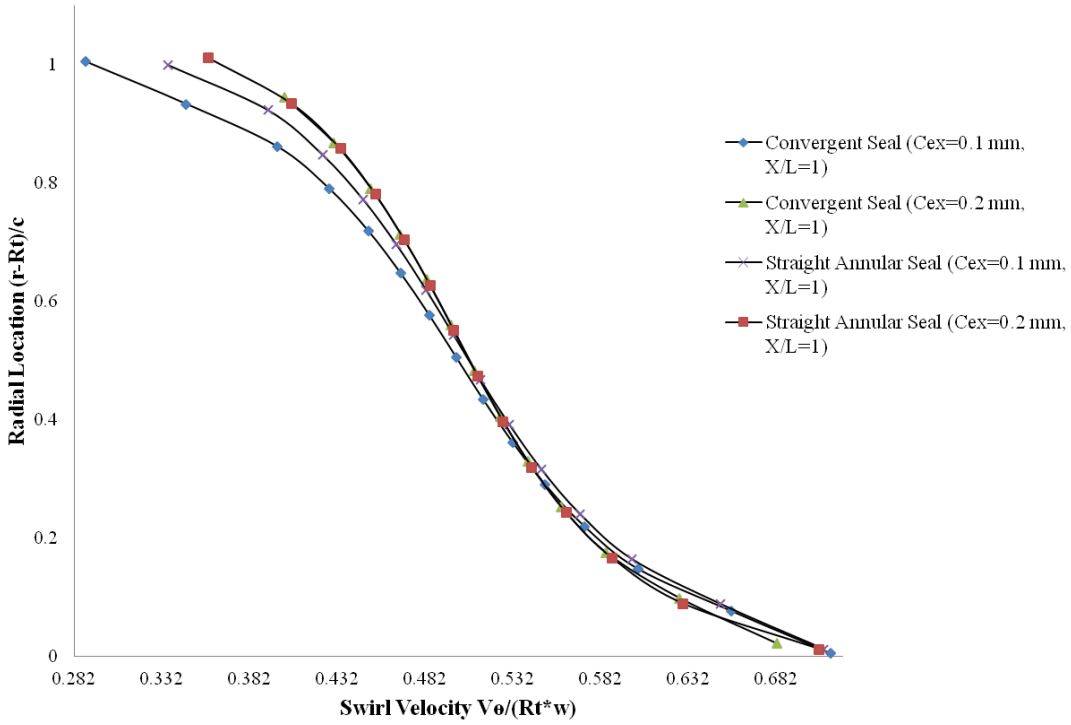

Fig. 20 Swirl velocity distributions for the convergent, and straight annular seals (water flow, X/L=1, 20,200 rpm)

In figure 20, swirl velocity distributions in the radial direction for the convergent, and straight annular seal configurations are presented. Swirl velocities are taken from the exit of the both seal configurations. Swirl velocities are made non-dimensional by using the equations presented in the study, which Rhode [27] performed. Rhode also analyzed the effects of the seal clearance on the swirl velocity formation in the radial direction for the labyrinth, and annular seal configurations at the 20,000 cpm shaft speed. He applied two different seal clearances (0.051 cm, 0.013 cm) to the flow simulations. His results showed that the labyrinth seal configurations give faster swirl formation than the annular seal configurations due to the greater circumferential stress effects along the labyrinth

seal shear layer, which is resulted from the higher turbulence intensity in the flow domain. Figure 19 shows that convergent seal configuration with 0.1 mm exit seal clearance exhibits decrease in swirl velocity near the stator wall, and other cases show not considerable variation. In addition, figure 20 presents that the average swirl velocity distributions in the axial direction for all cases are almost same. It can be deduced from this result that seal configurations with smaller seal clearances give greater swirl velocity gradients since they exhibit the same swirl velocity profiles in a shorter clearance with the seal configurations with higher seal clearances.

It can be deduced from this figure that effects of the seal clearance on the swirl velocity formations for the different seal configurations with same exit clearances are not apparent, but higher seal clearances gave greater swirl velocity formations.

Additionally, figure 20 shows that small seal clearances give greater swirl velocity gradient because they give same swirl velocity profile with larger clearances. In terms of rotor dynamic aspect, it can be deduced from these results that the decrease of the seal clearance causes the decrease of the stability of the system. In the following section, swirl velocity distributions with respect to the different shaft speeds will be analyzed as well.

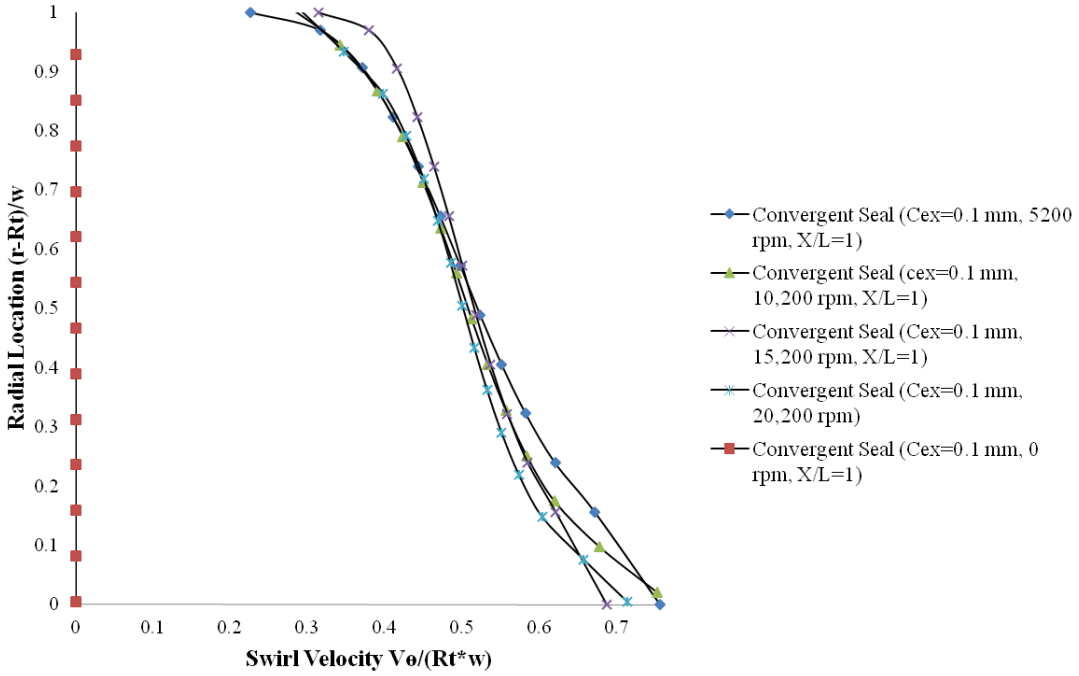

Fig. 21 Swirl velocity distributions for the convergent seals (C_{ex}=0.1 mm, water flow, X/L=1, 0-20,200 rpm)

Figure 21 shows swirl velocity distributions at the seal exit for the convergent, and straight annular seal configurations. Results show that variation of the shaft speeds does not cause considerable variations of swirl velocity profiles for different shaft speeds. On the rotor wall, there is a slight difference on the swirl velocities.

Rhode [27] also suggested that shortened residence time can be the reason of the lower swirl velocity formation in the annular seal configurations, when the fluid particles are close to the rotor wall. His results showed that increment of the seal clearance causes decrement of the swirl velocity. Lower swirl velocity profile shows that intensity of the circumferential stresses is low in the flow domain.

Rhode analyzed the exit radial local swirl velocity profiles for both labyrinth, and annular seal configurations, and his results showed that the labyrinth seal configurations provide more angular momentum diffusion in the radial direction, which is resulted from the higher turbulence generation along the free shear layers in the labyrinth seal flow domains. Friction coefficient is also analyzed to better understand the effects of the seal clearance, and shaft speed.

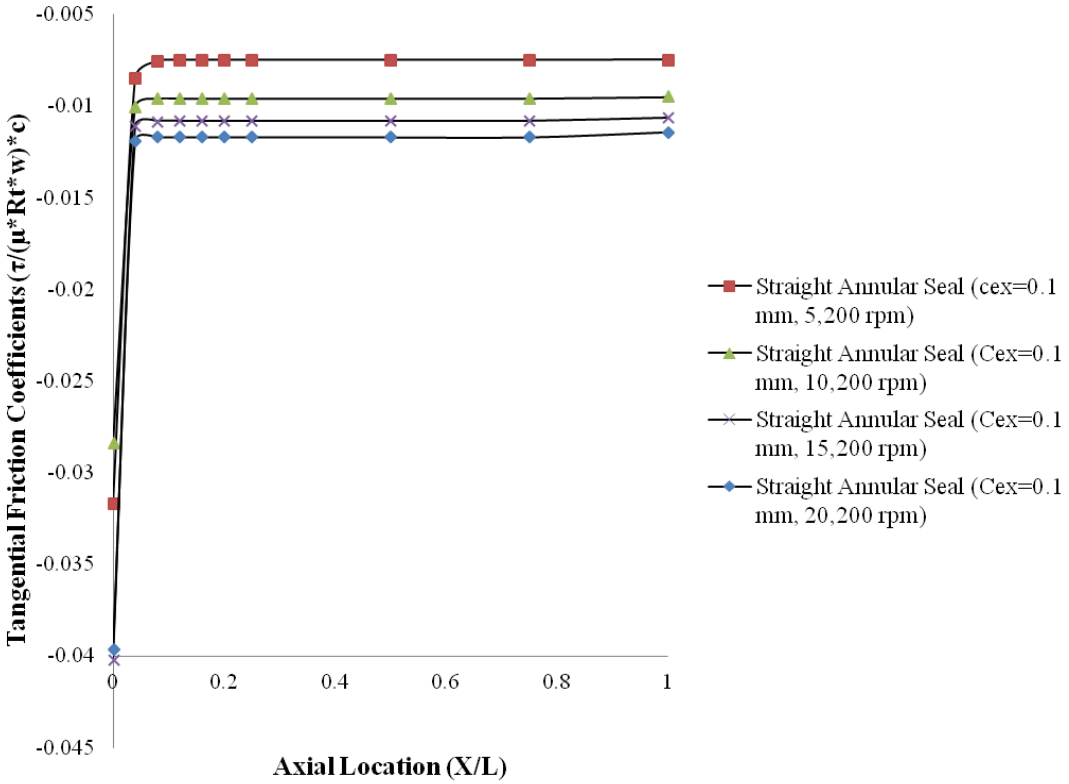

Fig. 22 Tangential friction coefficients for the straight annular seals (C_{ex}=0.1 mm, water flow, 0-20,200 rpm)

Figure 22 shows distributions of the tangential friction coefficients, on the rotor wall, with respect to the different shaft speeds for the straight annular seal configurations. Results show that friction coefficient is dependent on the shaft speed, and high shaft speeds introduce high circumferential stresses to the system, which means high friction coefficients. The increase of the shaft speed also provides high circumferential force effects, which push the flow to the stator wall. As a consequence of this, static pressure in the radial direction also increases.

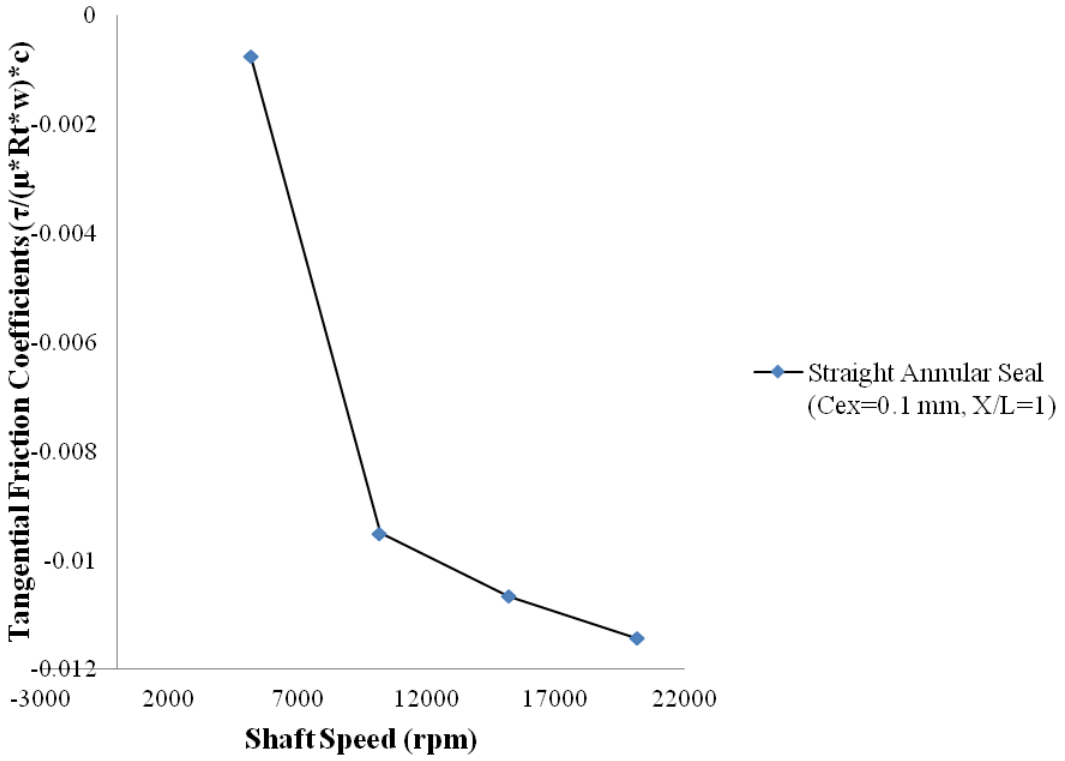

Fig. 23 Tangential friction coefficients for the straight annular seals (C_{ex}=0.1 mm, water flow, 0-20,200 rpm, X/L=1)

In figure 23, effects of the shaft speeds on the tangential friction coefficients for the straight annular seal configurations are shown in detail. Results show that increment of the shaft speed gives higher friction coefficient. Corresponding friction coefficients to the different shaft speeds for the straight annular seal configurations are presented in table 8. Same analyses are also performed for the convergent seal configurations to better understand the effects of shaft speeds on the friction coefficients. Table 8 shows that increase of the shaft speed causes higher friction coefficients. In the following section, tangential friction coefficient distributions for the convergent seal configurations will be analyzed.

Table 8 Friction coefficients (straight annular seal, C_{ex}=0.1 mm, X/L=1)

Shaf Speed(rpm)	Friction Coefficient
5200	-0.001
10200	-0.009
15200	-0.010
20200	-0.011

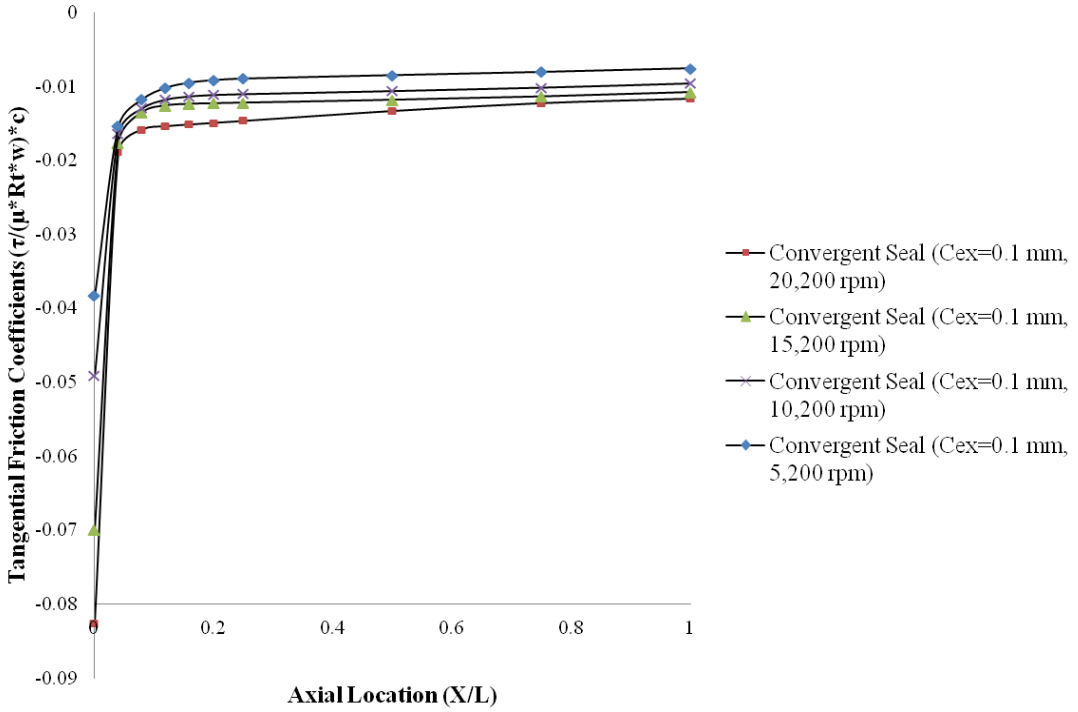

Fig. 24 Tangential friction coefficients for the convergent seal (C_{ex}=0.1 mm, water flow, 0-20,200 rpm, X/L=1, rotor wall)

Figure 24 shows that the increase of the shaft speed provides higher tangential stress formation on the rotor wall for the convergent seal configurations. Additionally, tangential friction coefficients continuously decreases along the axial direction after the entrance region due to the effects of axial flow acceleration. In figure 25, effects of shaft speed are presented in more detail.

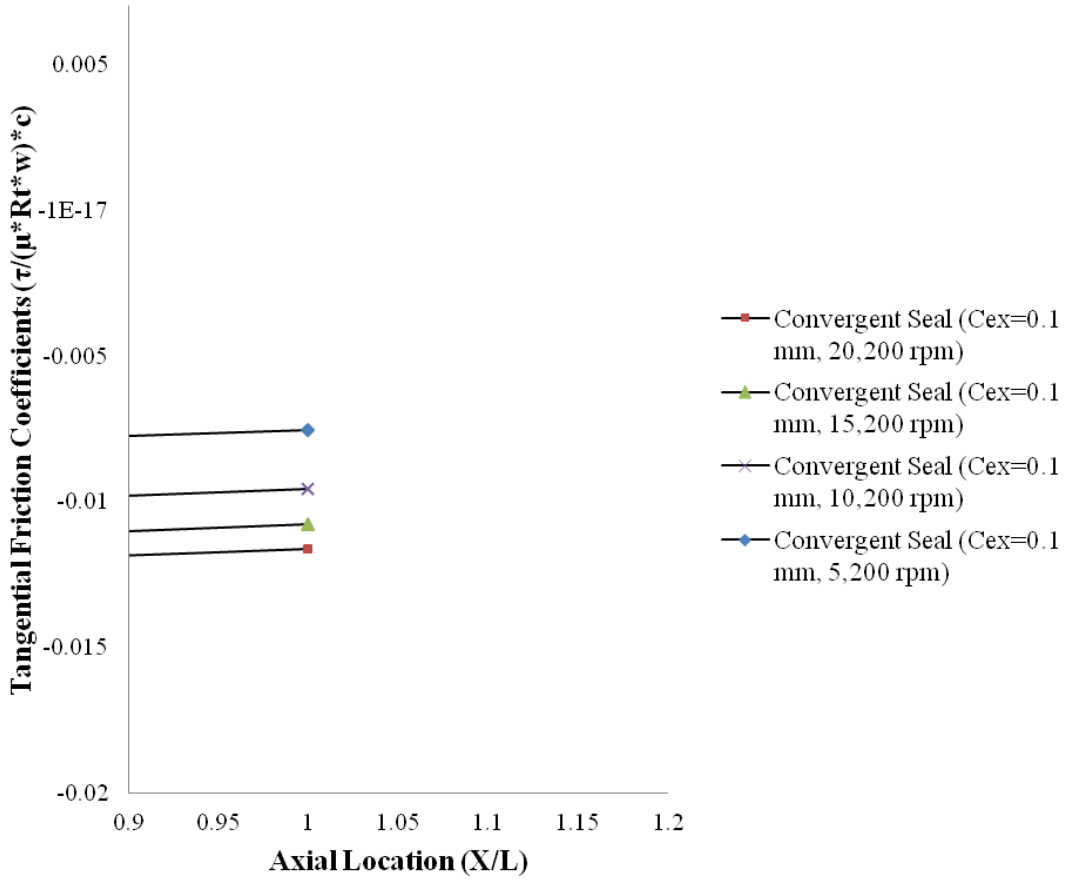

Fig. 25 Tangential friction coefficients for the convergent seal (C_{ex}=0.1 mm, water flow, 0-20,200 rpm, X/L=1)

Figure 25 shows the tangential friction coefficients at the exit plane of the convergent seal configurations. As clearly seen from this figure, the highest friction coefficient is obtained at the 20,200 rpm shaft speed. The friction coefficients become constant after the entrance region even though τ_{wall} is not constant but varying with c. Additionally, this means that τ_{wall} increases linearly with decreasing the seal clearance.

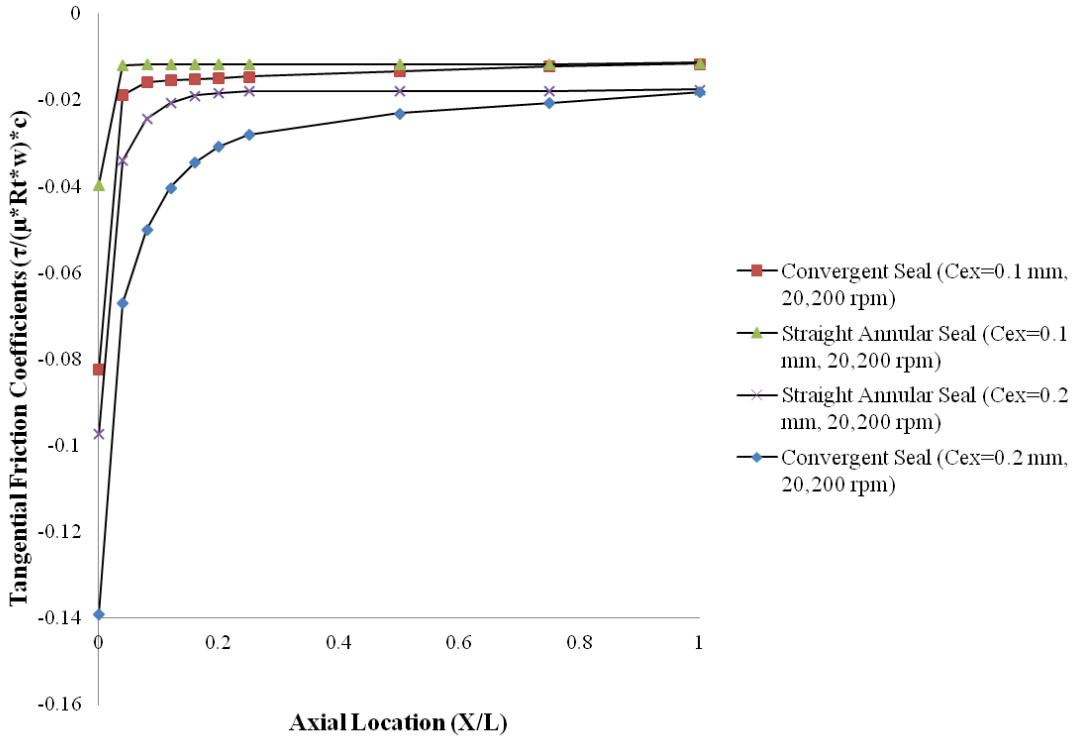

Fig. 26 Tangential friction coefficients for the convergent and straight annular seals (Cex=0.1-0.2 mm, water flow, 20,200 rpm, rotor wall)

In figure 26, the tangential friction coefficients for the convergent and straight annular seal configurations at 20,200 rpm are presented. Results show that effects of seal clearance on the friction coefficient are apparent in the entrance region. The highest friction factors are observed at the inlet for the convergent seal with 0.2 mm exit seal clearance. On the other hand, same friction coefficients are obtained at the exit for the seal configurations with same exit seal clearances. This indicates that for small convergent rates the convergent seal behaves quasi straight seal on a local level the same way a journal bearing is analyzed as being Quasi Couette flow on the local basis.

In figure 27, swirl velocity distributions at the inlet seal clearance for the convergent, and straight annular seal configurations are presented. This figure shows that low seal clearances give greater swirl velocity formations due to the higher turbulence effects on the leakage flow. It can also be deduced from this figure that swirl velocity is low at the points, which are close to the stationary wall, and maximum at the rotor wall. According to this figure, convergent seal configuration with 0.1 mm exit seal clearance gives greater swirl velocity formations than straight annular seal with 0.1 mm exit seal clearance. In terms of the seal configurations with 0.2 mm exit seal clearances, there is almost no difference between the swirl velocity distributions.

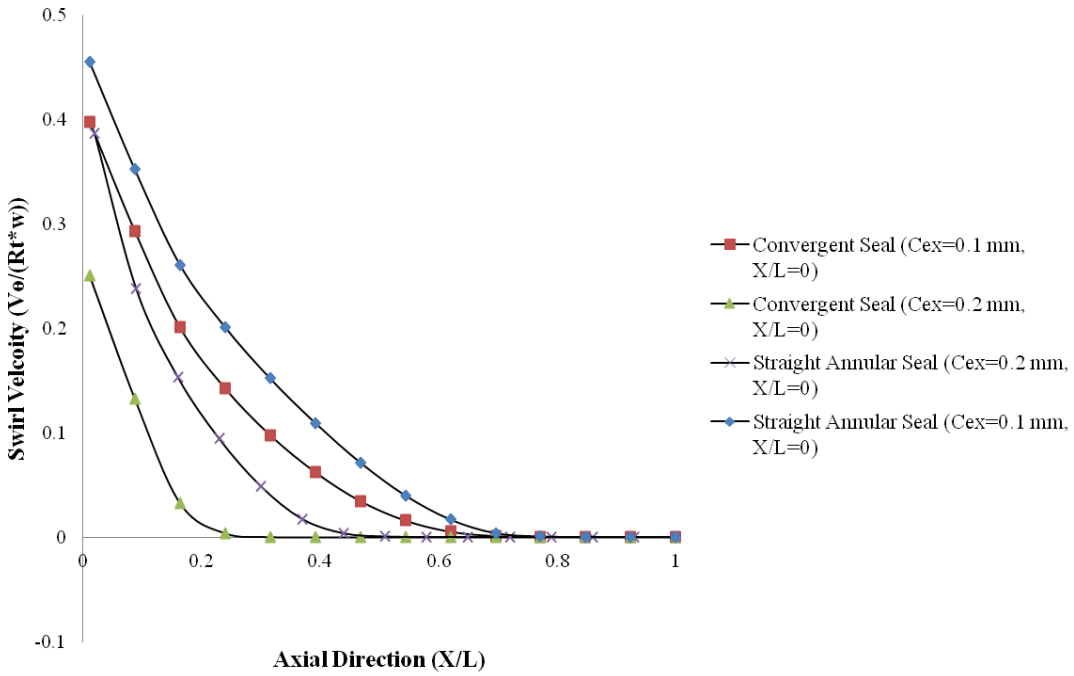

Fig. 27 Swirl velocity distributions for the convergent, and straight annular seal (water flow, X/L=0, 20,200 rpm)

As specified in the previous section, low seal clearance gives greater swirl velocity formation in the radial direction, and convergent seal configuration with 0.1 mm exit seal clearance provides the highest swirl velocity formation. Rhode [27] suggested considering the angular momentum conservation that annular seal configurations with low seal clearances provide very high swirl velocity accelerations, which causes low residence time.

In order to better understand the seal clearance effects on the swirl velocity distributions in the radial direction, bulk swirl velocities, which are taken from different points (X/L=0-0.02-0.04-0.06-1) through the seal length, will be analyzed. Bulk swirl velocities at these points are calculated taking the average of swirl velocity profiles.

In figure 28, average swirl velocity distributions, which are taken from different points through the seal length (X/L=0-0.02-0.04-0.06-1), for the convergent, and straight annular seal configurations are presented. Results show that the straight annular seal configuration with 0.1 mm exit seal clearance gives greater average swirl velocity distribution at the exit, and there is no significant difference in the average swirl velocities at the exit clearance for the convergent and straight annular seal configurations with 0.2 mm seal clearance. All cases have an average value near 0.5.

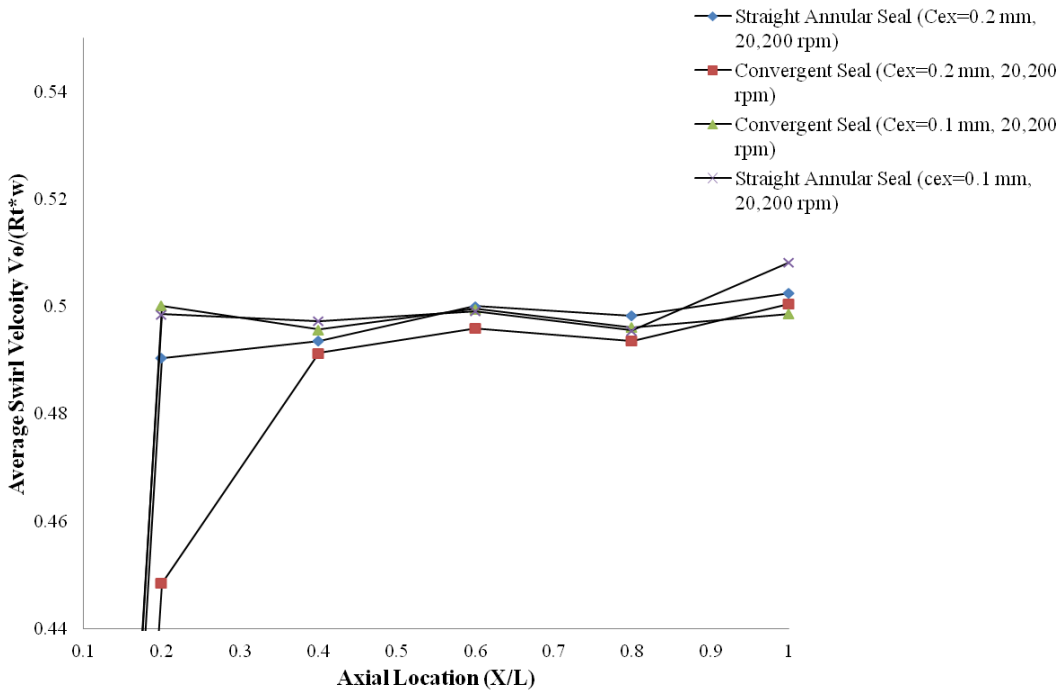

Fig. 28 Average swirl velocity distributions for the convergent, and straight annular seals (water flow, X/L=0, 20,200 rpm, X/L=0-0.02-0.04-0.06-1)

Swirl velocity is introduced to the system by the effects of rotational speed. As specified in the previous section, higher swirl formation is resulted from the high circumferential stress effects along the free shear layers. It can be deduced from the figure 28. that the decrease of the seal clearance causes the increase of the axial shear stress effects, which increase the turbulence effects in the boundary layer. Due to these turbulence effects, shear losses in the boundary layer increase, that is to say, dissipation rate of the kinetic energy, which is obtained from the flow pressure, increases based upon the linear inertia of the flow.

As in previous section, turbulent intensity variation in flow domains of both seal configurations will be analyzed as well. Rhode [27] proved by his study that seal configurations, which have larger seal clearance, have lower swirl velocity formation because residence time is shorter when fluid particles are close to the rotor wall. Residence time is knows as an average time, which is spent by fluid particles in flow domain. Residence time starts with entrance of a particular fluid particle to the system, and comes to an end by leaving of same particle to the system.

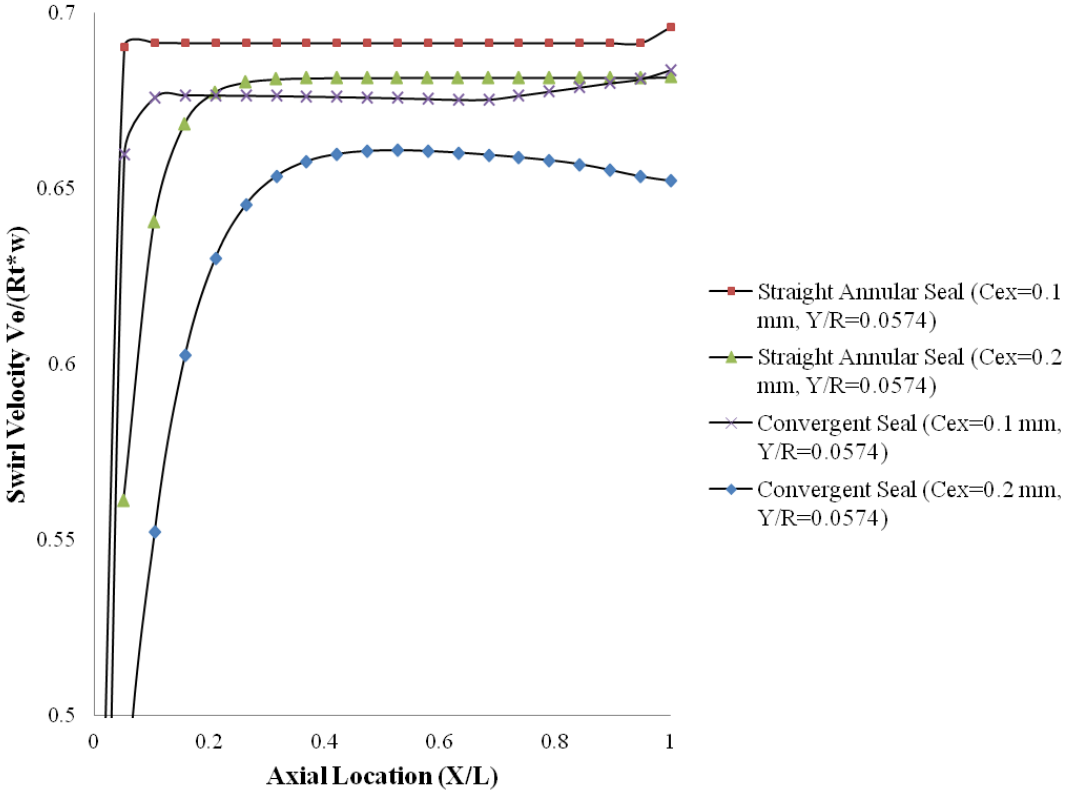

Fig. 29 Swirl velocity distributions for the convergent, and straight annular seal configurations (water flow, 20,200 rpm, Y/R=0.0574)

In figure 29, swirl velocity distributions in the axial direction for the convergent, and straight annular seal configurations are presented. These data are taken from a specified point in the radial direction (Y/R=0.0574). According to the figure 29, high seal clearance produces greater swirl velocity formation in the axial direction. At the inlet, significant variation in the swirl velocity is observed, and then swirl velocity is stable. The entrance length decreases with decreasing clearance, and the presence of the straight seal.

As specified in the previous section, Rhode [27] also performed same analyses to compare the leakage characteristics of the labyrinth, and annular seal configurations, and his results show that seal configurations with smaller exit clearances give greater swirl velocity formation, and swirl velocity increases in the axial direction, which is resulted from higher shear stress effects. His results are supported by this study. In the following section, average swirl velocity distributions, which are made non-dimensional by using the equations taken from the previous studies, will be presented.

In figure 30, turbulent intensity distributions on the rotor wall for the convergent, and straight annular seal configurations are presented. Rhode [27] also performed this analysis for the labytinth, and annualr seal configurations in order to see which seal configurations have more intense turbulent effects. His results showed that labyrinth seal configurations have more intense turbulent effects, which increase shear effects on the flow.

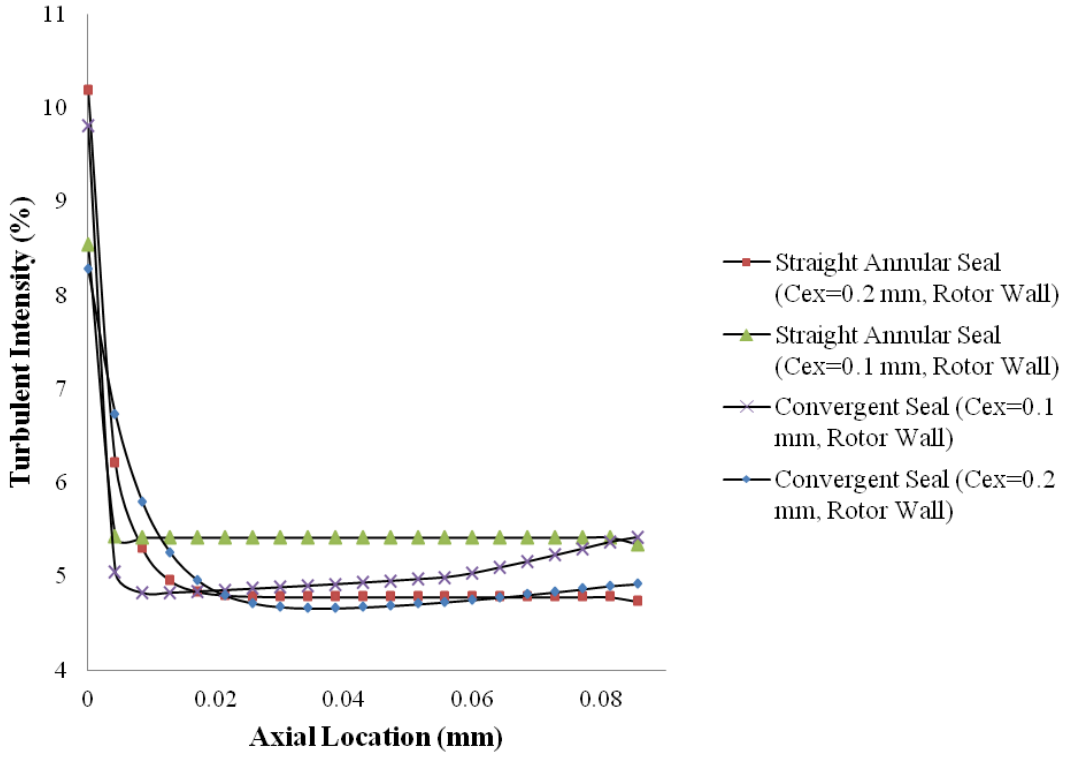

Fig. 30 Turbulent intensity for the convergent and straight annular seal (rotor wall, 20,200 rpm)

Results presented in figure 30 show that straight annular seal configuration with 0.1 mm exit seal clearance gives the gretaest turbulence intensity formation on the rotor wall, which is resulted from the high shear stress effects in the boundary layer. Straight, and convergent seal configurations with 0.2 mm exit seal clearance have about same turbulence intensity along the seal length. The convergent seal with 0.1 mm exit seal clearance has the turbulence intensity near the value of the straight annular seal with 0.2 mm exit seal clearance at the entrance, where the clearance is 0.2 mm then increases as clearance decreases.

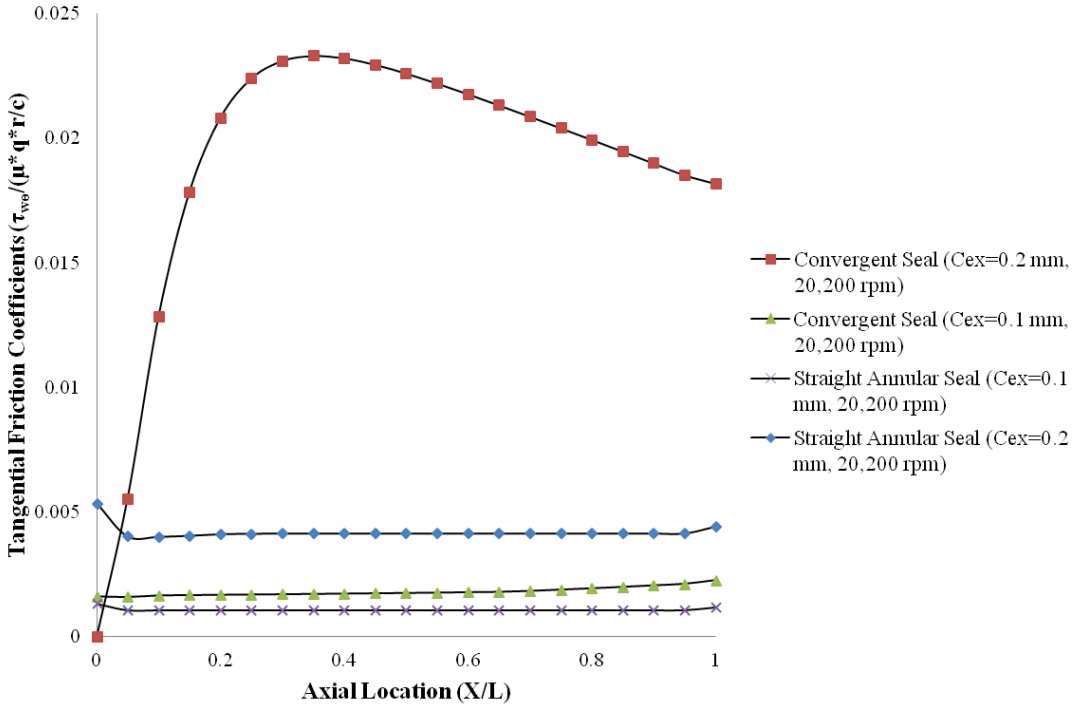

Fig. 31 Tangential friction coefficients for the convergent and straight annular seals (stator wall, 20,200 rpm)

In figure 31, friciton coefficients at 20,200 rpm shaft speed on the stator wall for the convergent, and straight annular seal configurations are presented. Results show that the highest friction coefficients are given by the convergent seal configuration with 0.2 mm exit seal clearance. In the entrance region, great increase is observed for this seal configuration, and then the tangential stress effects continuously decreases. In terms of other cases, uniform friction coefficient profiles are obtained. This is due to the larger seal clearance having higher axial flow rates, reducing the residence time of the fluid and the ability of the tangential shear stresses to accelerate the tangential velocity resulting a steeper velocity gradient near the wall further downstream in the seal.

Static pressure also has an effects on the increment of circumferential stresses on the wall. Circumferential forces,which are introduced to the flow domain by the effects of shaft speed, push the flow to the wall, and this causes the increment of static pressure. High static pressure formation in the radial direction provides high shear stress formation along the shear layers. In the following section, axial wall shear stress distributions along the stator wall will be analyzed.

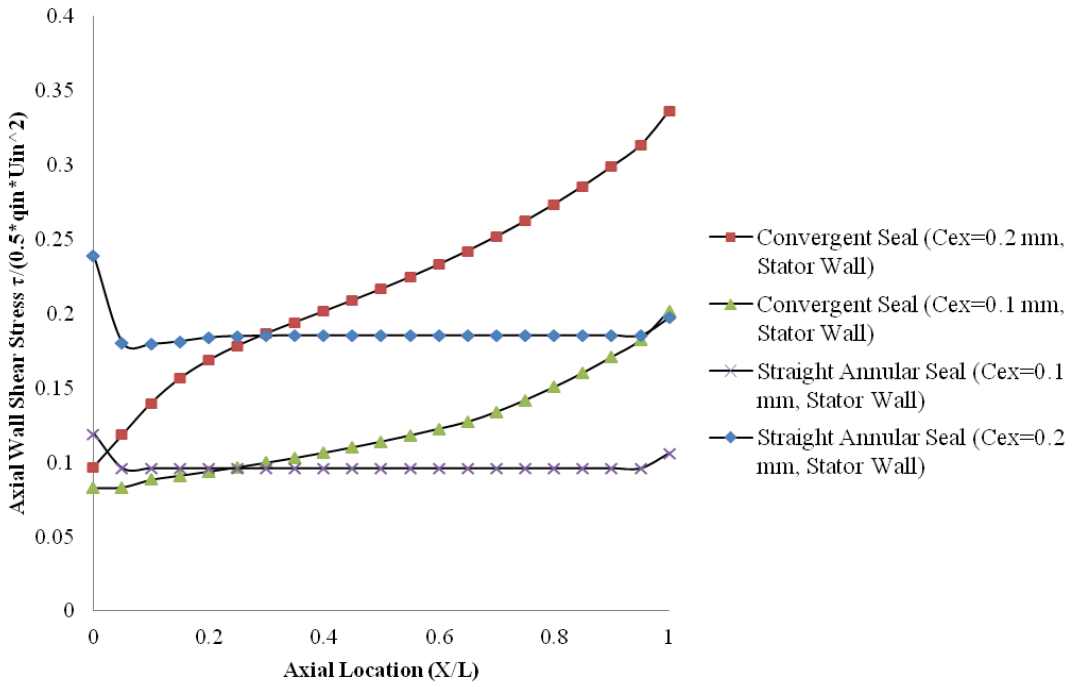

Fig. 32 Axial wall shear stress distributions for the convergent and straight annular seals (stator wall, 20,200 rpm)

In figure 32, axial wall shear stress distributions along the stator wall for the convergent, and straight annular seal configurations are presented. Results show that

axial wall shear stresses for the convergent seal configurations continuously increases along the seal length, and convergent seal configuration with smaller seal clearance gives greater axial wall shear stress formation. Uniform axial shear stress profiles are obtained for straight annular seal configurations, and annular seal with 0.1 mm seal clearance exhibits greater wall shear stress formation.

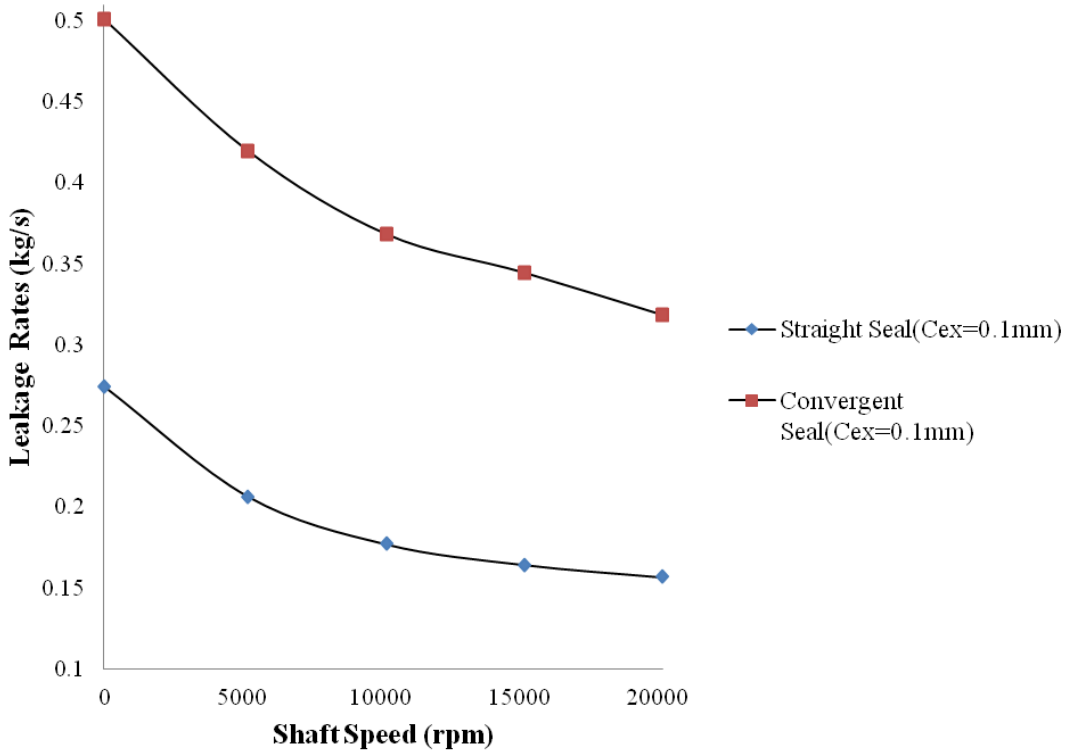

Fig. 33 Lekage rates for the convergent, and straight annular seal configurations (C_{ex}=0.1 mm, 20,200 rpm)

In figure 33, leakage rates for the convergent, and straight annular seal configurations with 0.1 mm exit seal clearances are presented. Results show that leakage

rate increases with the increase of the seal clearance. In general, larger seal clearance, and lower axial wall shear stress produce more leakage.

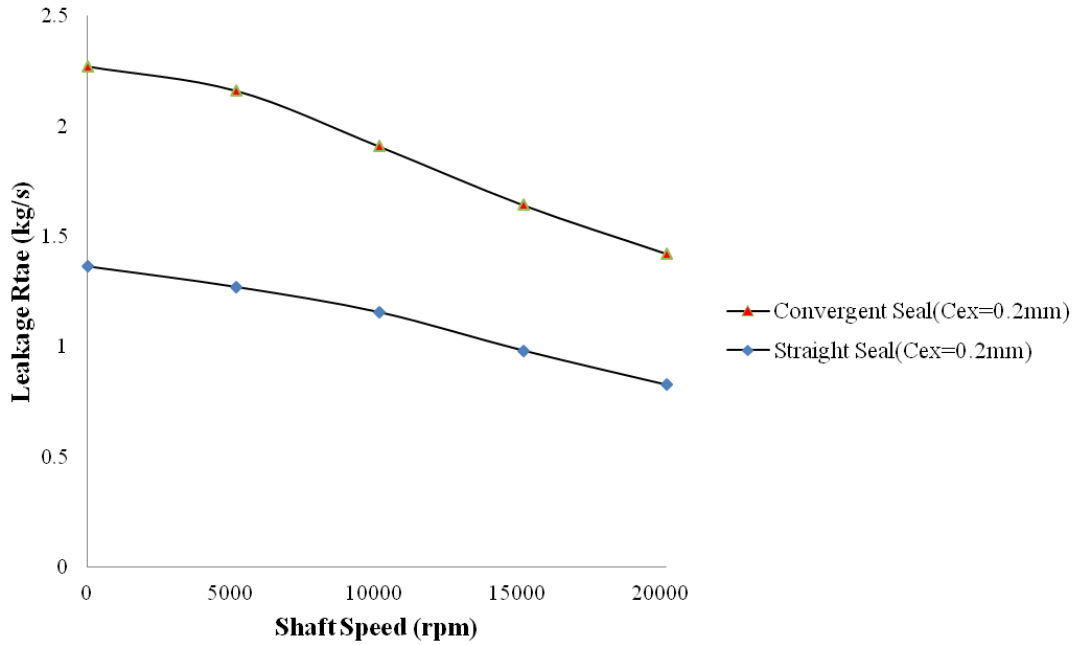

Fig. 34 Lekage rates for the convergent and straight annular seal (C_{ex}=0.2 mm, 20,200 rpm)

Figure 34 shows that leakage rate increases with the increase of the seal clearance, and decreases with the increase of the shaft speed. As specified in previous section, Rhode [27] performed a study to compare the leakage characteristics of the labyrinth, and annular seal configurations. Rhode [27] analyzed swirl velocity variations in axial and radial directions for the labyrinth and annular seal configurations, and he also applied different pressure ratios to see how the leakage rates change. In this study same analyses are performed with different seal configurations. Rhode [27] obtained a

result that secondary flow rate increases with increment of sealing clearance.

Greater swirl velocity formation is observed when smaller seal clearance is applied to both convergent and straight annular seal configurations. Rhode [27] explained this result by residence time, which is determined in previous section. In addition, analyses show that turbulent intensity increases by decreasing sealing clearance. Higher turbulence intensity means that turbulence shear layer effect will increase, which is also proved by Rhode [27].

Consequently, larger seal clearance results in increase of the leakage rate. With the increase of the clearance, axial momentum of the flow increases, which dominates the effects of circumferential stresses. Due to the decrement of turbulence effects, dissipation rate of the flow kinetic energy decreases, which results in higher leakage rate.

6.1.2. Effect of Surface Roughness on the Water Leakage

In this section, effects of the surface roughness on the leakage through the convergent, and straight annular seal configurations will be discussed. As specified in the previous section, three different roughness parameters (0.0004 mm, 0.0008 mm, 0.0016 mm) will be applied. Matsuzaki, and Kazamaki [29] performed a study to investigate effects of the surface roughness on the compressive stresses, and his results showed that compressive stresses increase with the increment of the surface roughness. He suggested that leakage decreases with the increment of the compressive stresses, which means higher surface roughness height on the wall. His results showed that higher surface roughness causes the increment of the plastic deformation at the outside of the

contacting surfaces. His results show that leakage suddenly stops because of the plastic deformation.

Childs, and Chang-Ho [7] performed a study to investigate effects of the surface roughness on the rotordynamic characteristics of seals. His results showed that damper seals decrease the cross-couples stiffness coefficients, which increases the stability of the system, and he also suggested that damper seal configurations provide better leakage characteristics than smooth seal configurations. Lucas, Danaila, Bonneau, and Frene [9] also performed a study to understand the effects of wall roughness on the pressure distribution, and his results showed that increment of surface roughness causes higher pressure loss, and lower pressure drop in the axial direction. In addition, he observed significant decrement in the leakage with the increment of the surface roughness.

In the following section, effects of the surface roughness heights on both the stator, and rotor walls will be discussed. Additionally, axial pressure gradients-to-axial wall shear stress ratio with respect to the different roughness heights will also be analyzed to investigate the effects of the surface roughness on the pressure distributions.

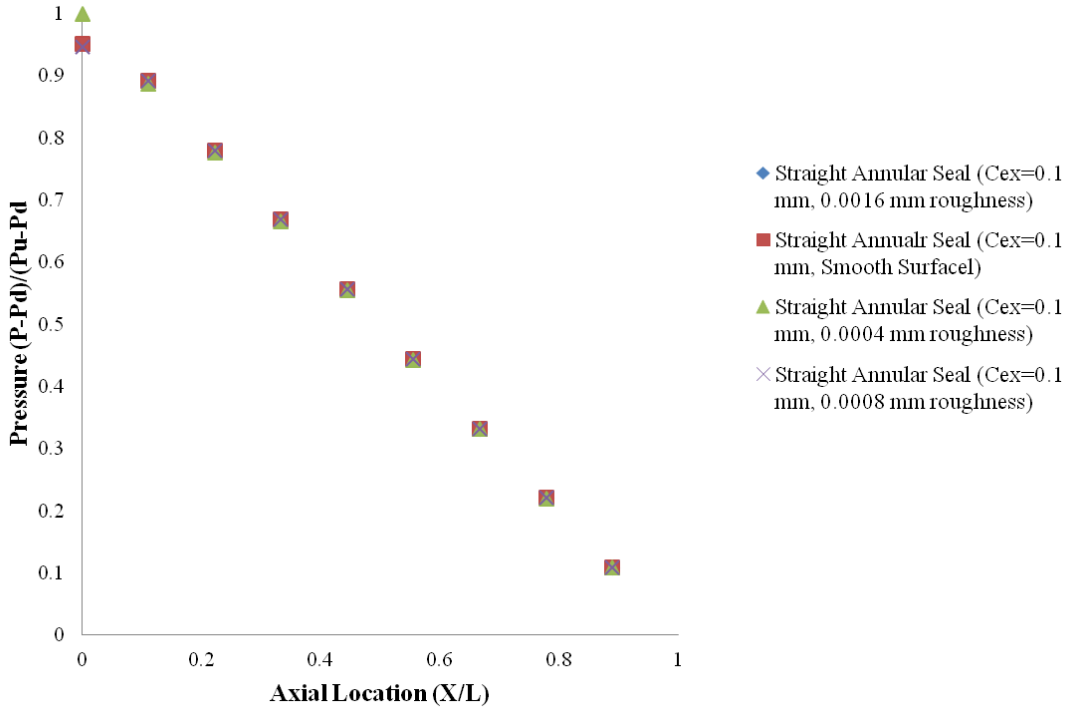

Fig. 35 Pressure distributions for the straight annular seals (C_{ex}=0.1 mm, rotor wall, water flow, roughness= 0-0.0004-0.0008-0.0016 mm)

In figure 35, pressure distributions on the rotor wall with respect to the different surface roughness parameters for the straight annular seal configuration with 0.1 mm, exit seal clearance are shown. Results show that pressure distributions for all cases are almost the same, and linear. In the following section, the pressure gradient variations based upon the different surface roughness parameters will be analyzed to investigate if the pressure gradient is dependent on surface roughness or not.

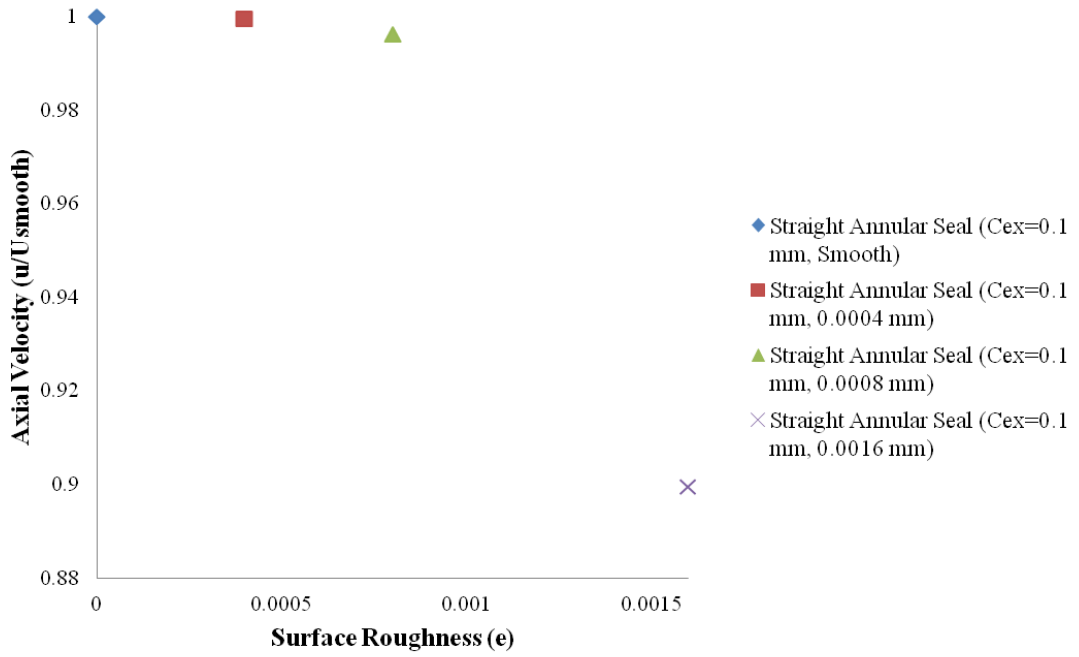

Fig. 36 Average axial velocity for the straight annular seal (C_{ex}=0.1 mm, water flow, surface roughness= 0-0.0004-0.0008-0.0016 mm)

In figure 36, the average axial velocity at the exit plane with respect to the different surface roughness parameters for the straight annular seal configurations with 0.1 mm exit seal clearances are presented. Results show that the increase of the surface roughness on both the rotor, and stator surfaces causes a decrease of axial velocity, which is resulted from the increase of the wall friction effects, especially for 0.0016 mm surface roughness height. Results show that the increase of the surface roughness causes 10 % decrease in the axial velocity at the exit plane. There is not a considerable variation in the axial velocity until the roughness increases from 0.0008 mm to 0.0016 mm.

Table 9 Non-dimensional boundary layer thickness (e+) for the straight annular seal (C_{ex}=0.1 mm, 20,200 rpm, rotor wall)

Roughness	e+
0	0
0.0004	0.218
0.0008	0.437
0.0016	0.855

In table 9, non-dimensional boundary layer thicknesses (e+) with respect to the different surface roughness heights for the straight annular seal configurations with 0.1 mm exit seal clearances are presented. Results show that e+ increases with the increase of the surface roughness height. Same analysis is also performed for the convergent seal configurations.

In figure 37, the average axial velocity distributions based upon different surface roughness parameters for the convergent seal configurations with 0.1 mm exit seal clearances are shown. Results show that average axial velocity decreases by the increase of surface roughness, which increases the shear stresses affecting the shear layers.In the following section, average axial velocity distributions with respect to the different surface roughness heights for the convergent seal configurations will be analyzed.

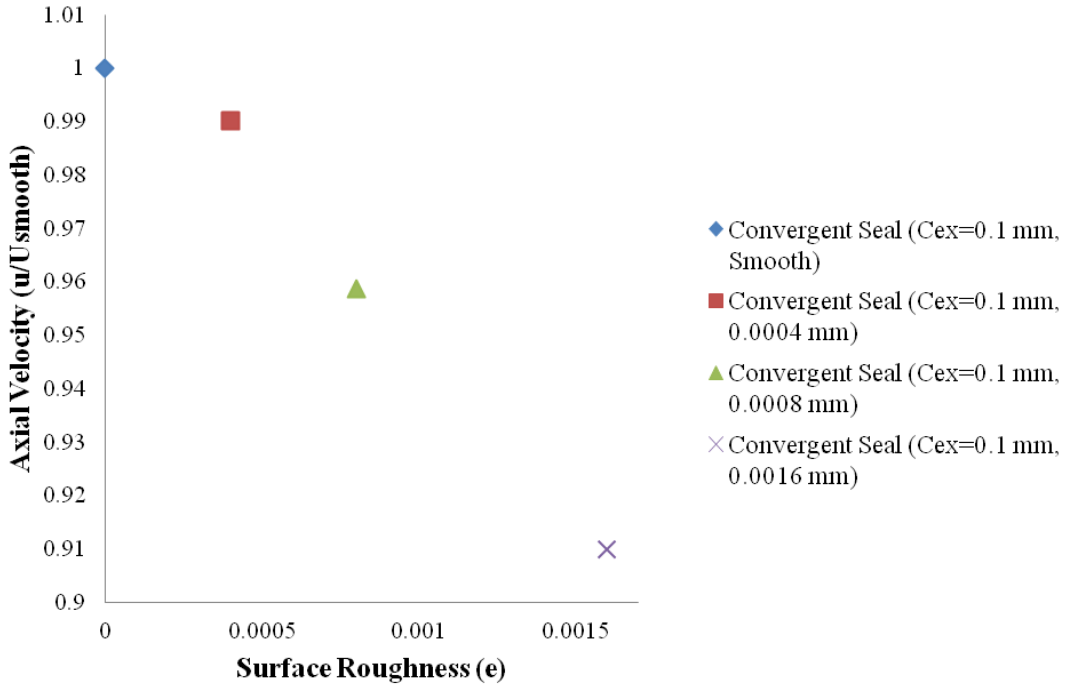

Fig. 37 Average axial velocity at the exit plane for the convergent seals (C_{ex}=0.1 mm, water flow, surface roughness= 0-0.0004-0.0008-0.0016 mm)

Unlike the straight annular seal configurations, the axial velocity increases through the seal length for the convergent seal configurations due to the decrease of the flow area for the incompressible flow. Results show that the increase of the roughness height causes 9 % decrease in the axial velocity at the exit.

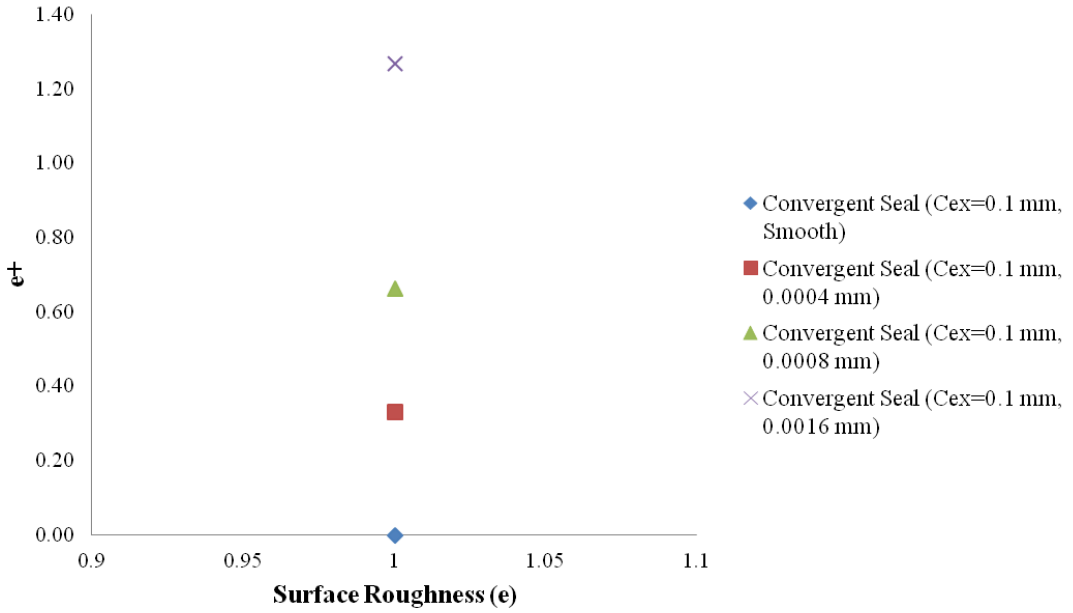

Fig. 38 e+ at the exit plane for the convergent seals (C_{ex}=0.1 mm, water flow, surface roughness= 0-0.0004-0.0008-0.0016 mm)

In figure 38, e+ at the exit plane for the convergent seal configurations with 0.1 mm exit seal clearances are presented. Results show that e+ increases with the increase of the surface roughness height.

In table 10, e+ at the exit plane for the straight annular, and convergent seal configurations with 0.1 mm exit seal clearances are presented. Results show that convergent seal configurations give higher e+ formation at the exit plane. This is due to the convergent channel causing the fluid to accelerate resulting in a thinner boundary layer, hence larger value for e+.

Table 10 Non-dimensional boundary layer thickness (e+) for the straight annular, and convergent seal (C_{ex}=0.1 mm, 20,200 rpm, rotor wall)

Roughness	Straight Annular	Convergent
0	0	0
0.0004	0.219	0.331
0.0008	0.437	0.662
0.0016	0.855	1.268

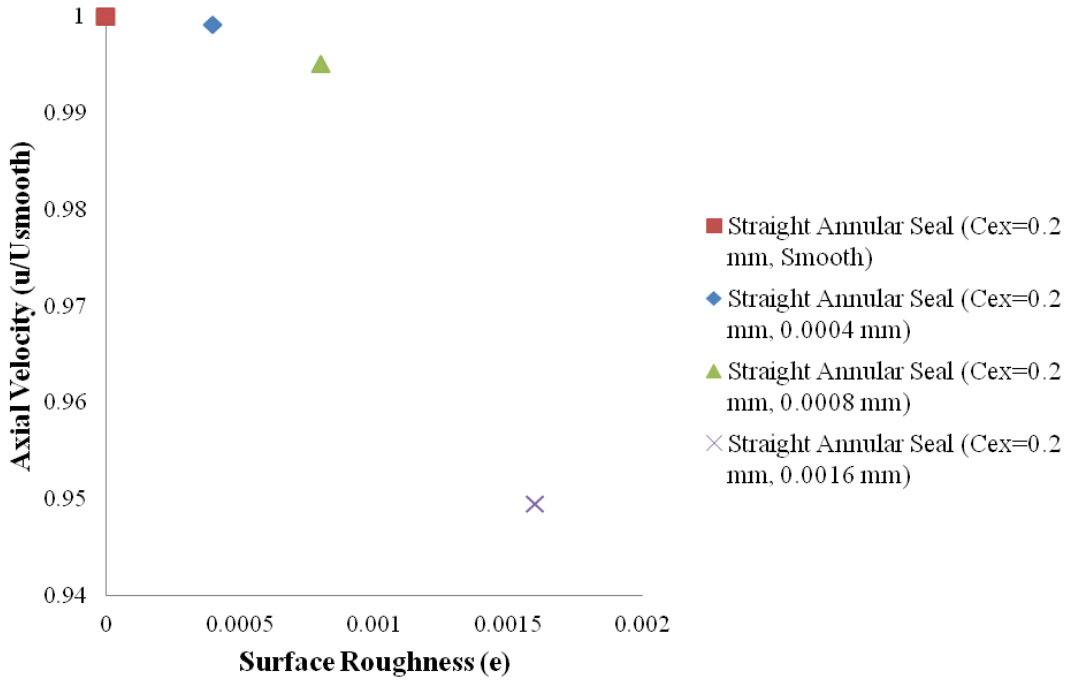

Fig. 39 Average axial velocity for the straight annular seals (C_{ex}=0.2 mm, water flow, surface roughness= 0-0.0004-0.0008-0.0016 mm)

Figure 39 shows that the axial velocity decreases the by the increase of the surface roughness, especially for 0.0016 mm surface roughness. Results show that the

increase of the surface roughness height causes 5 % decrease in the axial velocity at the exit plane. This is half the value for the 0.1 mm clearance straight seal.

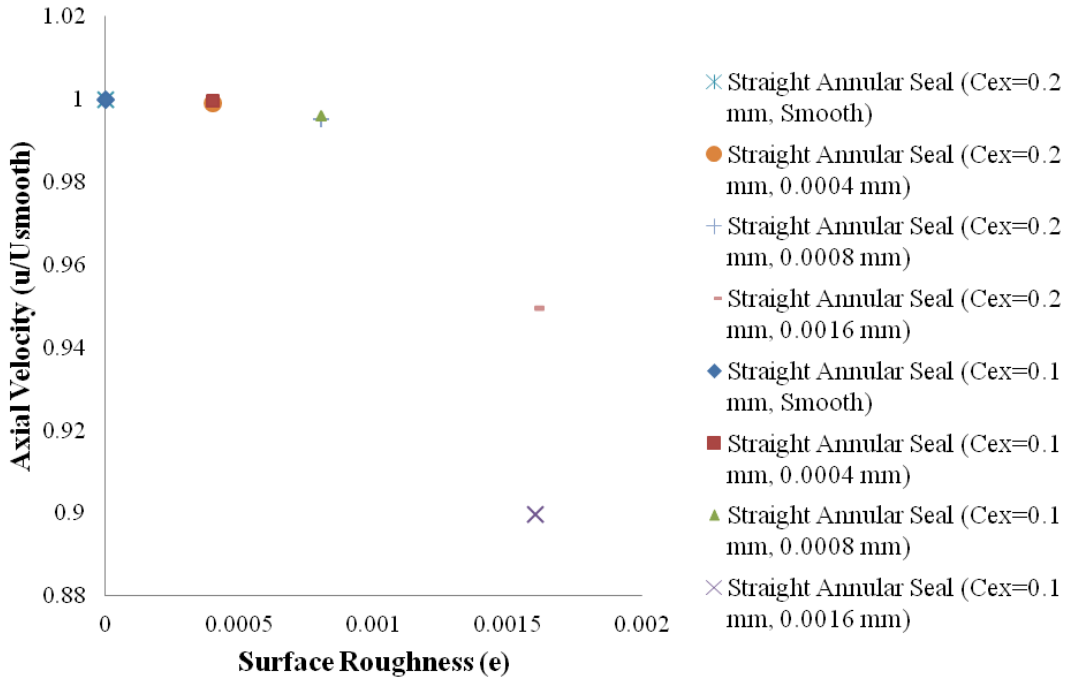

Fig. 40 Average axial velocity for the straight annular seals (C_{ex}=0.1-0.2 mm, water flow, surface roughness= 0-0.0004-0.0008-0.0016 mm)

In figure 40, the average axial velocity at the exit plane with respect to the different surface roughness parameters for both straight annular seal configurations with 0.1, and 0.2 mm exit seal clearances are presented. Results show that there is not significant difference between axial velocities until the increase from 0.0008 mm to 0.0016mm. Additionally, higher seal clearance causes 5 % increase in the axial velocity when surface roughness is set at 0.0016 mm.

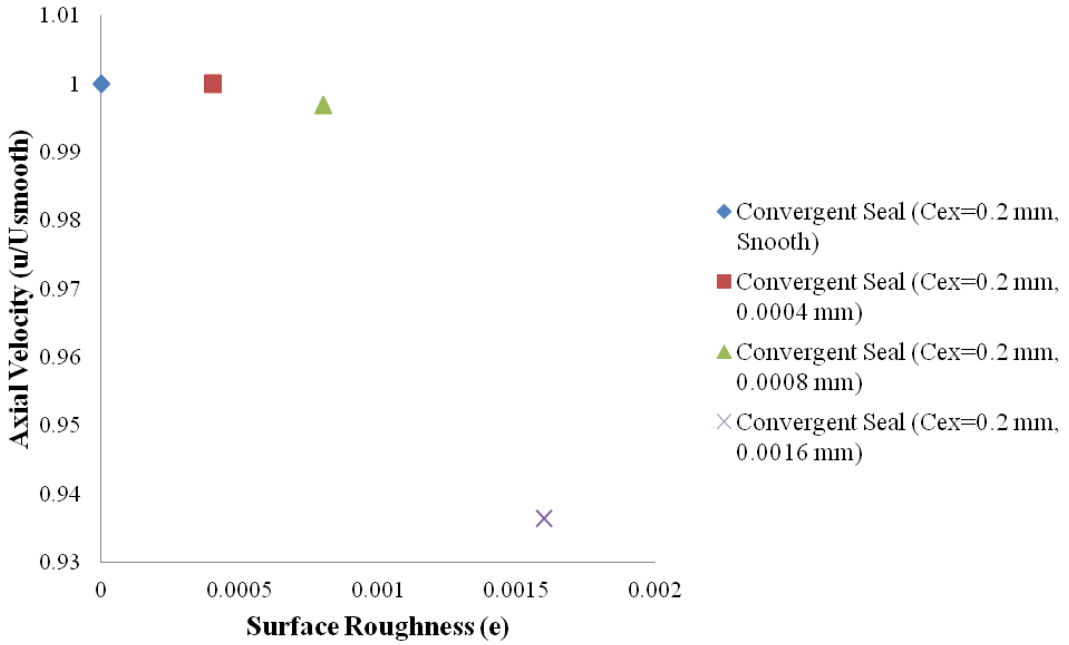

Fig. 41 Average axial velocity at the exit plane for the convergent seals (C_{ex}=0.2 mm, water flow, surface roughness= 0-0.0004-0.0008-0.0016 mm)

In figure 41, the average axial velocity at the exit plane with respect to the different surface roughness parameters for the convergent seal configurations with 0.2 mm exit seal clearances are presented. Results show that there is no significant decrease in axial velocity profiles until the increase from 0.0008 mm to 0.0016 mm surface roughness heights. In addition, increase of the roughness heights causes 6 % decrease in the axial velocity.

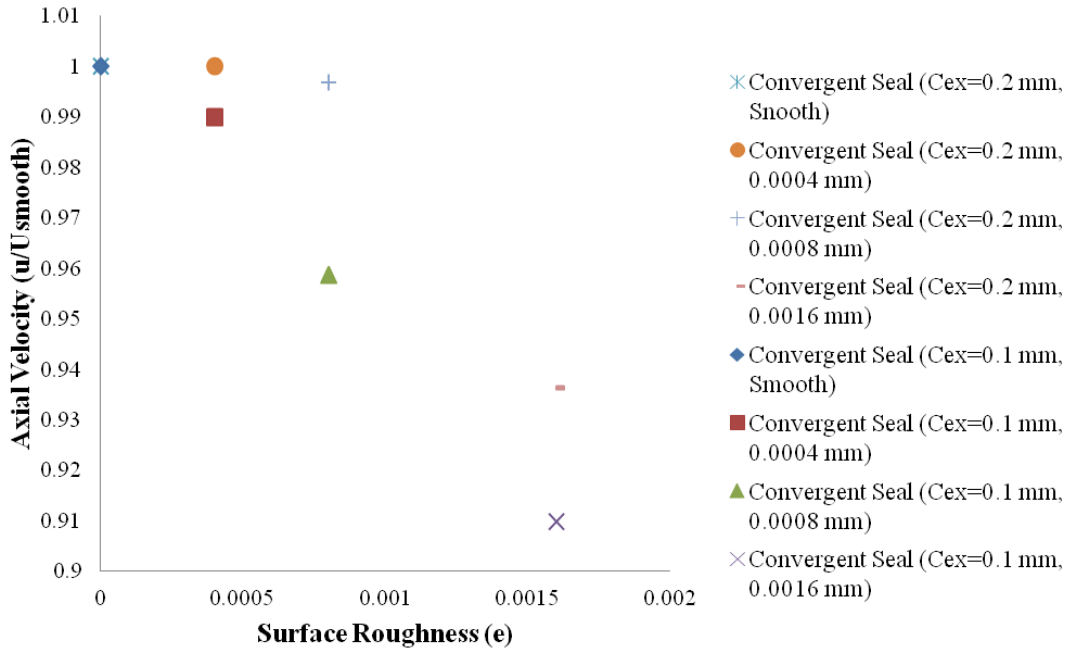

Fig. 42 Average axial velocity for the convergent seals (C_{ex}=0.1-0.2 mm, water flow, surface roughness= 0-0.0004-0.0008-0.0016 mm)

In figure 42, the average axial velocity at the exit plane with respect to the different surface roughness parameters for the convergent seal configurations with 0.1, and 0.2 mm exit seal clearances are presented. Results show that higher seal clearance causes the increase in the axial velocity at the exit plane. Additionally, the increase of the surface roughness height gives lower average axial velocity.

Table 11 Non-dimensional boundary layer thickness (e+) for the straight annular, and convergent seal (C_{ex}=0.1-0.2 mm, 20,200 rpm, rotor wall, X/L=1)

Straight Annular		Convergent	
0.1 mm	0.2 mm	0.1 mm	0.2 mm
0	0	0	0
0.219	0.319	0.331	0.438
0.437	0.639	0.662	0.876
0.855	1.267	1.2681	1.764

In table 11, non-dimensional boundary layer thicknesses (e+) with respect to different seal clearances are presented. Results show that increase of the seal clearance causes higher e+, and convergent seal configurations exhibit greater e+ formation with respect to the straight annular seal configurations. Convergent seals give higher flow acceleration, which suppress boundary layer. Because of that reason, non-dimensional boundary layer thickness increases. In the following section the axial pressure gradient-to-axial wall shear stress ratios for different surface roughness heights will be analyzed to better see the effects of the roughness height on the axial pressure gradient. In the following section, pressure gradient-to-axial wall shear stress ratios with respect to the different surface roughness heights will be anayzed.

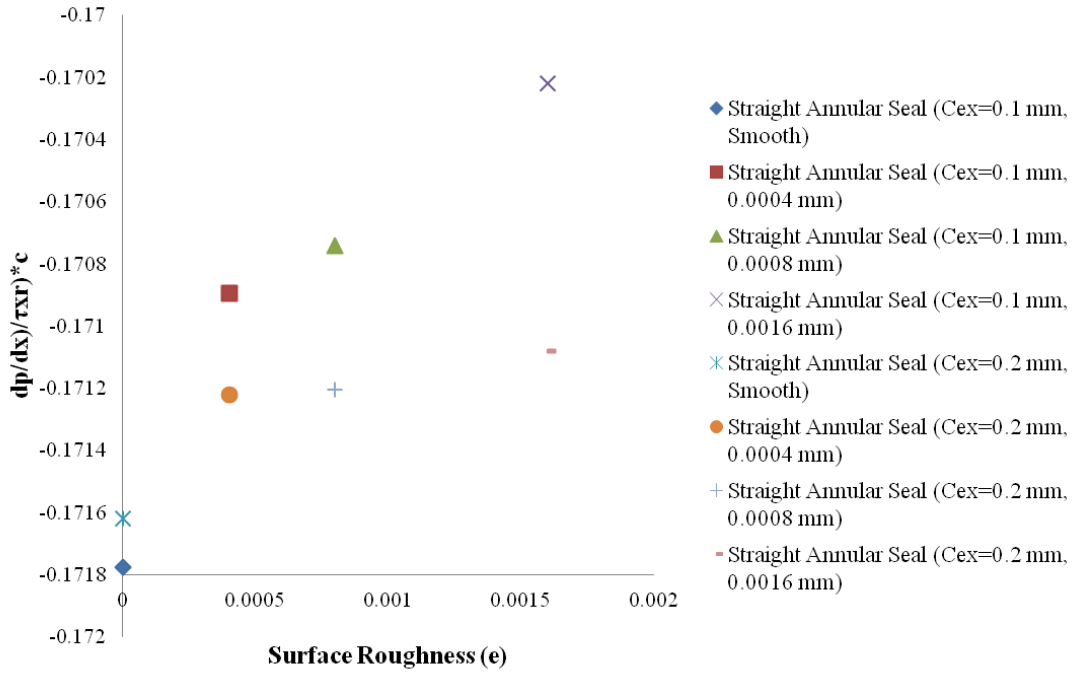

Fig. 43 $(dp/dx)/\tau_{xy}*c$ versus x for the straight annular seals (C_{ex}=0.1-0.2 mm, water flow, surface roughness= 0-0.0004-0.0008-0.0016 mm)

In figure 43, axial pressure gradient-to-axial wall shear stress ratios with respect to the different surface roughness for the straight annular seal configurations with 0.1 mm, and 0.2 mm exit seal clearances are presented. These parameters are taken from the mid section of the rotor wall for all cases. Results show that this ratio increases with the increase of the surface roughness, which causes the increase of the wall shear stress while pressure gradient variations is almost negligible. Additionally, figure 43 shows that axial pressure gradient is the same when the surface roughness height increases, which causes the decrease of the average axial velocity. Since axial pressure gradient is hold constant across the seal, higher surface roughness height causes higher axial wall shear stress, which causes lower axial velocity.

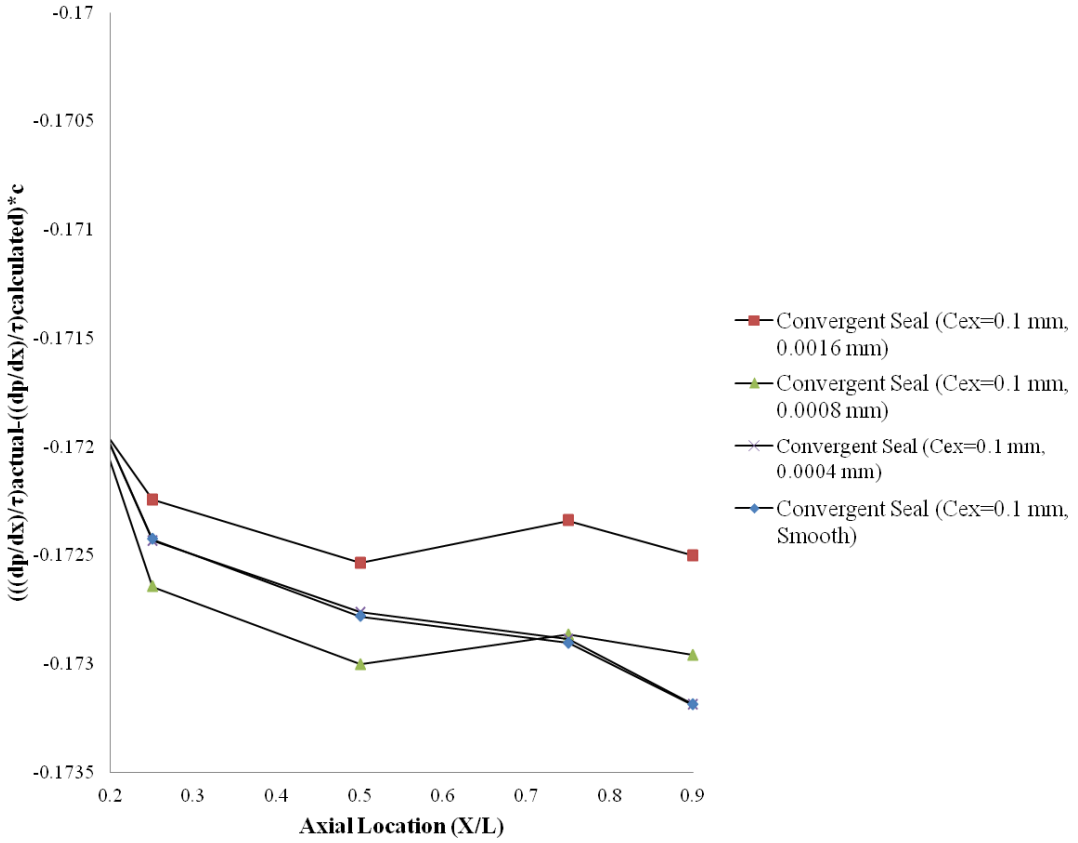

Fig. 44 $((dp/dx)/\tau_{xr}-(dp/dx)/\tau_{xr})*c$ versus x for the convergent seals (C_{ex}=0.1 mm, water flow, surface roughness= 0-0.0004-0.0008-0.0016 mm)

In figure 44, axial pressure gradient-to-axial wall shear stress ratios for the convergent seal configurations with 0.1 mm exit seal clearances are presented. When the exit plane is considered, it can be deduced that the increase of surface roughness cause the slight variation of these ratios. When these ratios are made non-dimensional by multiplying with clearance, these ratios are between 0.172-0.173 ranges, which are slightly different from the straight annular seal configurations. In addition, pressure gradients for the convergent seals are slightly larger than the ones for the straight annular seal configurations but flow is accelerating making boundary layer thinner. Table 12

shows that convergent seal configurations give greater e+ than straight annular seal configurations, which causes surface roughness to stick further out of boundary layer causing more drag.

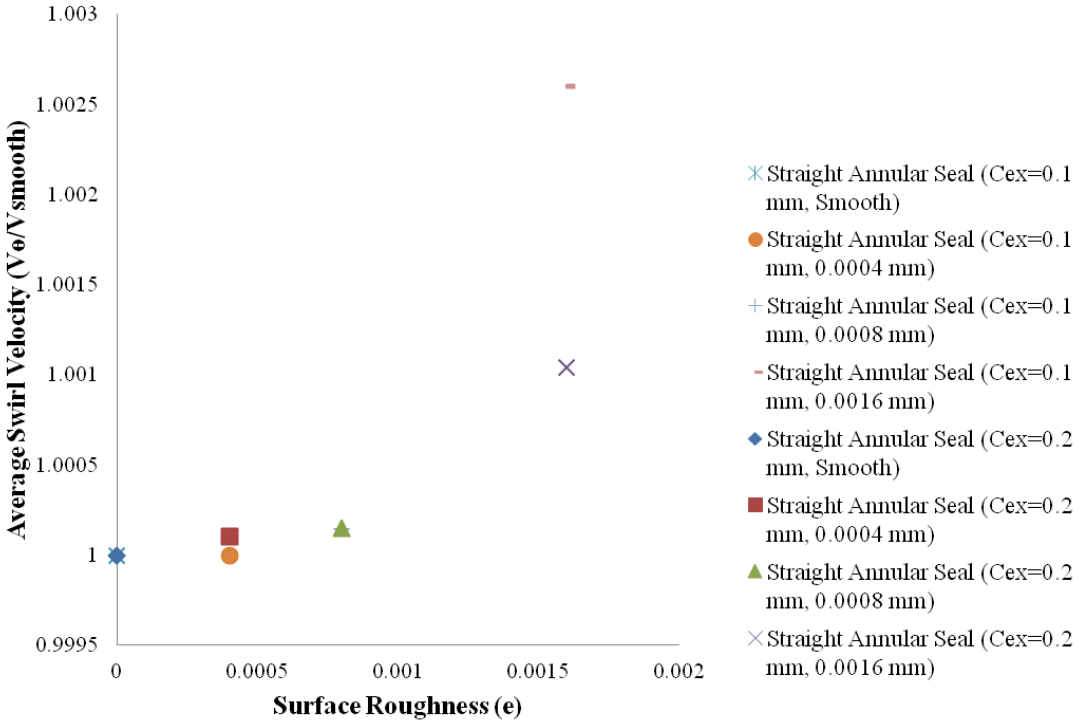

Fig. 45 Average swirl velocity distributions at the exit plane for the straight annular seals (C_{ex}=0.1-0.2 mm, 20,200 rpm, X/L=1, water flow)

Figure 45 shows that average swirl velocity does not change considerably by the variation of the surface roughness height. Results show that there is 0.3 % variation in the swirl velocity for the straight annular seal configurations with 0.1 mm exit seal clearances. 0.3 % change is not a significant increased in rotor drag, which is offset by the similar increase in stator drag resulting a net change in average swirl velocity of

about 0 %. In terms of straight seal configurations with 0.2 mm exit seal clearances, there is 0.0012 % about 0.33 value for the 0.1 mm exit seal clearances. This shows that larger seal clearance decreases the effects of the surface roughness upon swirl velocity. Additionally, larger seal clearance causes higher axial velocity. 0.02 % increase is observed in the average axial velocity for the straight annular seal configuration when the seal clearance is increased from 0.1 mm to 0.2 mm.

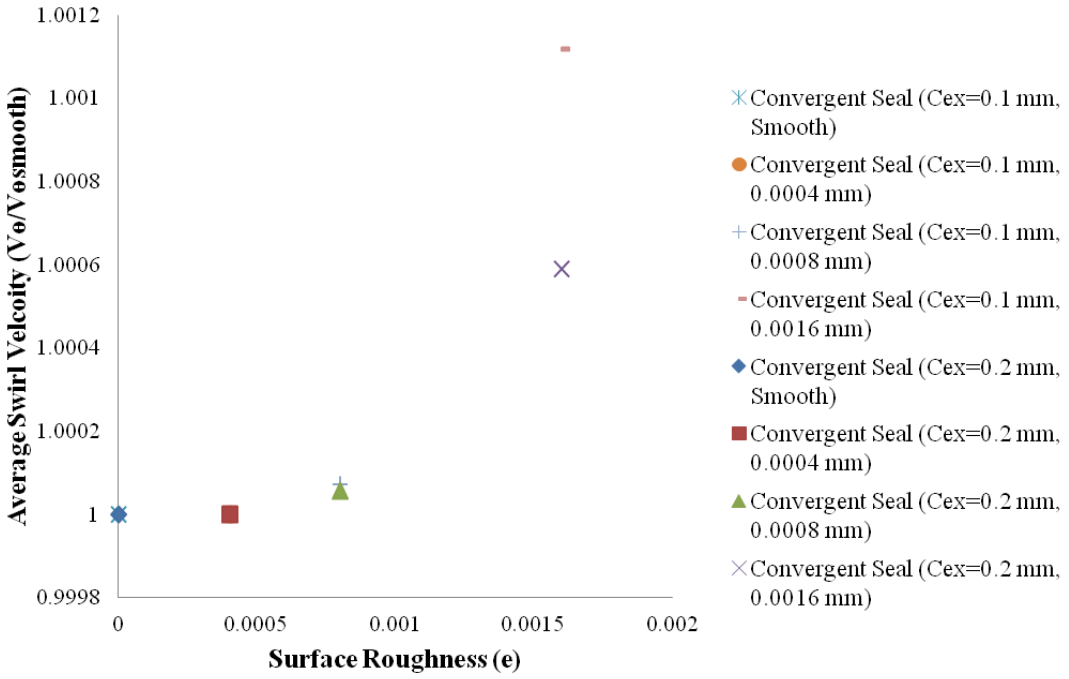

Fig. 46 Average swirl velocity distributions at the exit plane for the convergent seals (C_{ex}=0.1-0.2 mm, 20,200 rpm, X/L=1, water flow)

In figure 46, average swirl velocities at the exit plane with respect to the different surface roughness heights for the convergent seal configurations with 0.1 mm, and 0.2

mm exit seal clearances are presented. Results show that there is even less change predicted than for the straight seal.In addition, the effect of the uniform surface roughness on the average swirl velocity is not significant. As a consequence of that, surface roughness will not help to reduce swirl and increase the stability.

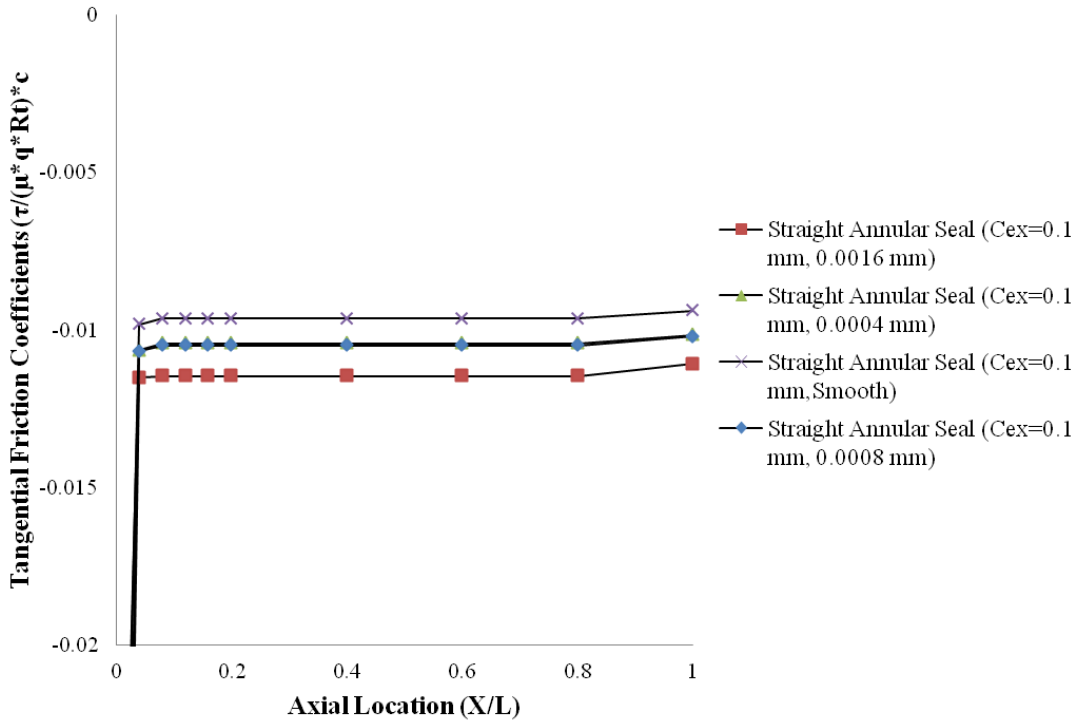

Fig. 47 Tangential friction coefficients for the straight annular seals (C_{ex}=0.1 mm, 20,200 rpm, rotor wall, water flow)

In figure 47, tangential friction coefficients on the rotor wall with respect to the different surface roughness heights for the straight annular seal configurations with 0.1 mm exit seal clearances are presented. Results show that friction coefficients increase

with the increase of the surface roughness heights. Friction coefficients for the 0.0004 mm, and 0.0008 mm surface roughness heights are almost same, but there is a considerable increase for 0.0016 mm roughness height.

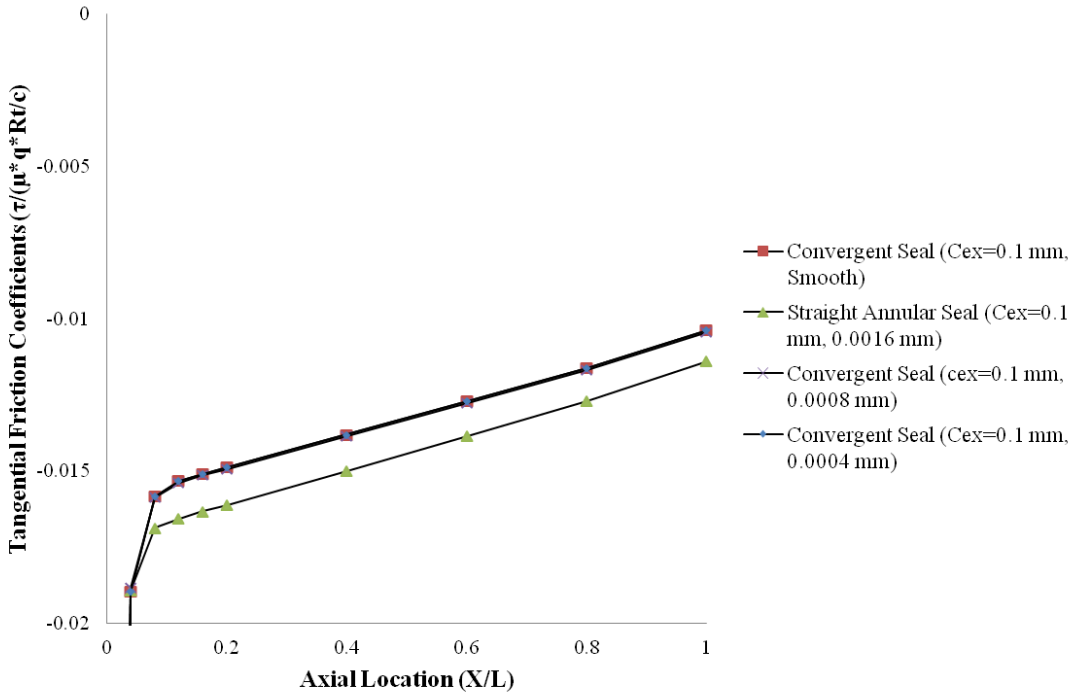

Fig. 48 Tangential friction coefficients for the convergent seals (C_{ex}=0.1 mm, 20,200 rpm, rotor wall, water flow)

In figure 48, the tangential friction coefficients on the rotor wall with respect to the different surface roughness heights for the convergent seal configurations with 0.1 mm exit seal clearances are presented. Results show that there is not a considerable variation in the circumferential stress profiles on the rotor wall for the 0, 0.0004 mm, and 0.0008 mm surface roughness heights. On the other hand, 0.0016 mm roughness

height causes an increase of the friction coefficients. There is about a 50 % increase in the tangential friction coefficients for the 0.0016 roughness at the end. Unlike the straight annular seal configurations, tangential friction coefficients for the convergent seal configurations continuously increase up to the seal exit. At the end, friction coefficients for the straight annular, and convergent seal configurations are almost same.

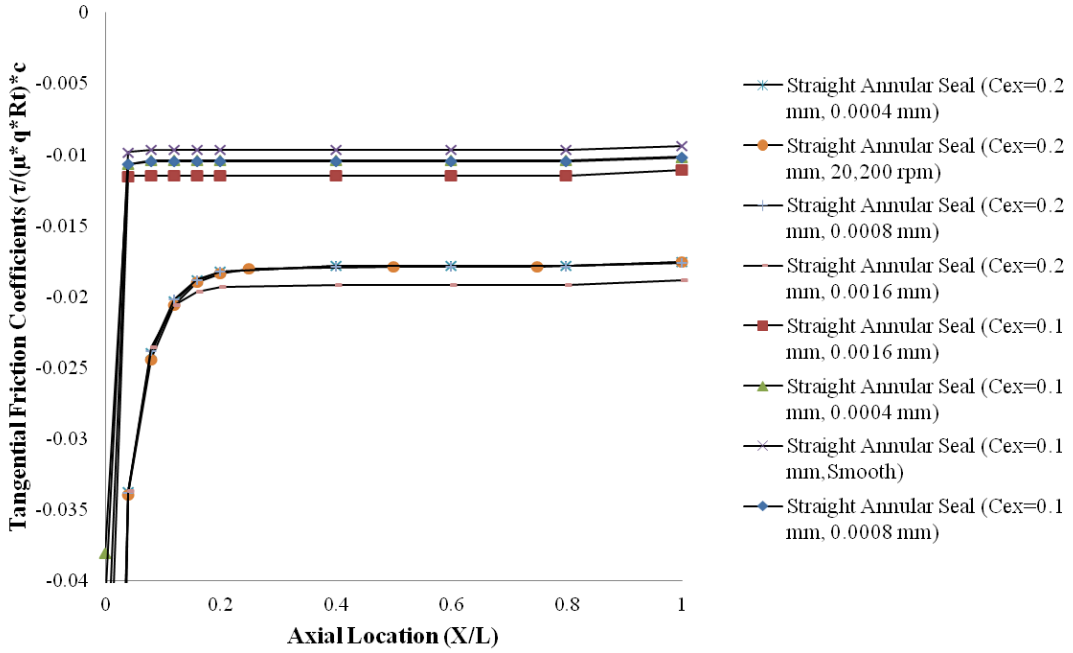

Fig. 49 Tangential friction coefficients for the straight annular seals (C_{ex}=0.1-0.2 mm, 20,200 rpm, rotor wall, water flow)

In figure 49, tangential friction coefficients on the rotor wall with respect to the different surface roughness heights for the straight annular seals with 0.1, and 0.2 mm exit seal clearances are presented. Straight annular seal configurations with 0.2 mm exit

seal clearances exhibit about 80 % larger tangential friction coefficient formations, which can be resulted from having higher tangential stresses. Additionally, results show that the larger seal clearance exhibits a longer entrance region.

Table 12 Entrance region length for the straight annular seals (C_{ex}=0.1-0.2 mm, surface roughness height=0-0.0004-0.0008-0.0016 mm)

Roughness (mm)	Cex=0.1 (mm)	Cex=0.2 (mm)
0	0.039	0.19
0.0004	0.039	0.19
0.0008	0.039	0.19
0.0016	0.039	0.19

Table 12 includes the entrance region length with respect to the different roughness heights for the straight annular seal configurations with 0.1, and 0.2 mm exit seal clearances. Results show that the roughness height has not a significant impact on the entrance region length but the increase of the seal clearances causes an increase of the entrance region length. In the following section, comparison of the tangential friction coefficients on the rotor wall for the convergent seal configurations with 0.1 and 0.2 mm exit seal clearances will be performed.

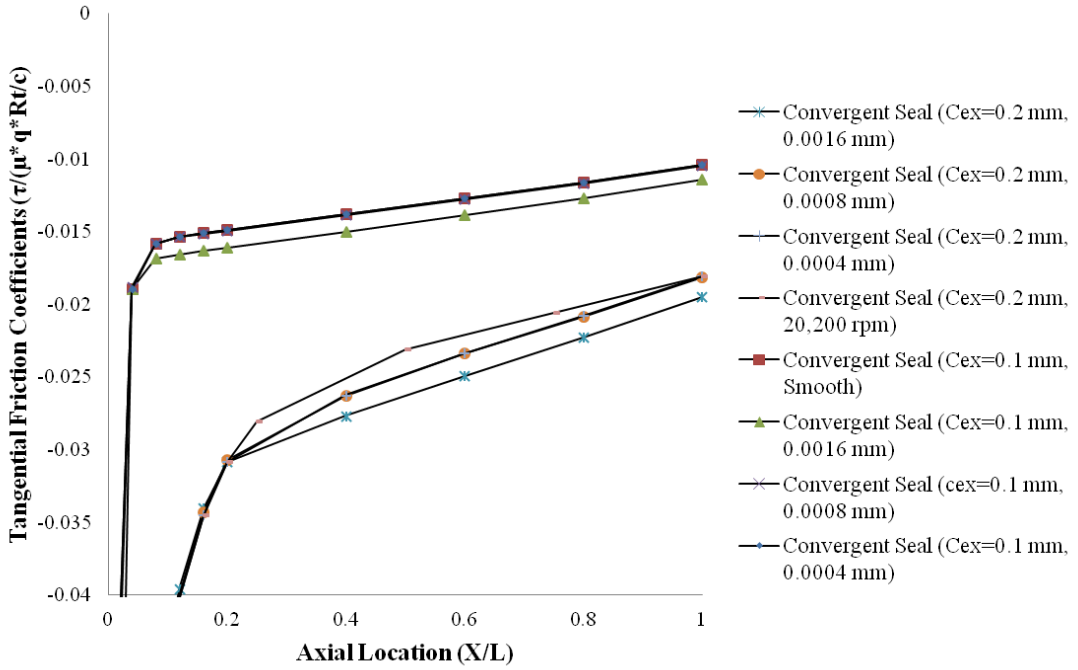

Fig. 50 Tangential friction coefficients for the convergent seals (C_{ex}=0.2 mm, 20,200 rpm, rotor wall, water flow)

Figure 50 shows that tangential friction coefficients increase with the increase of the surface roughness heights for the convergent seal configurations. Tangential friction coefficients for the 0.0004 mm, and 0.0008 mm roughness heights are almost same. In addition, tangential friction coefficients increase for the all cases along the rotor wall, and larger clearance causes higher friction coefficients as well. There is about 70 % increase in the friction coefficients for the seal configurations with 0.2 mm exit seal clearances. Additionally, the increase of the seal clearance causes an increase of the entrance region length.

Table 13 Entrance region length for the convergent seals (C_{ex}=0.1-0.2 mm, surface roughness height=0-0.0004-0.0008-0.0016 mm)

Roughness (mm)	Cex=0.1 (mm)	Cex=0.2 (mm)
0	0.079	0.249
0.0004	0.079	0.249
0.0008	0.079	0.249
0.0016	0.079	0.249

Table 13 includes the entrance region length with respect to the different roughness heights for the convergent seal configurations with 0.1, and 0.2 mm exit seal clearances. Results show that the roughness height has not a significant impact on the entrance region length but the increase of the seal clearances causes an increase of the entrance region length.

In the following section, tangential friction coefficient distributions on the stator walls with respect to the different surface roughness heights for the convergent, and straight annular seal configurations will be analyzed. As discussed in the previous section, straight annular seals give a constant tangential friction coefficients after the entrance region but tangential frication coefficients for the convergent seals continuously decreases due to the axial flow acceleration after the entrance region.

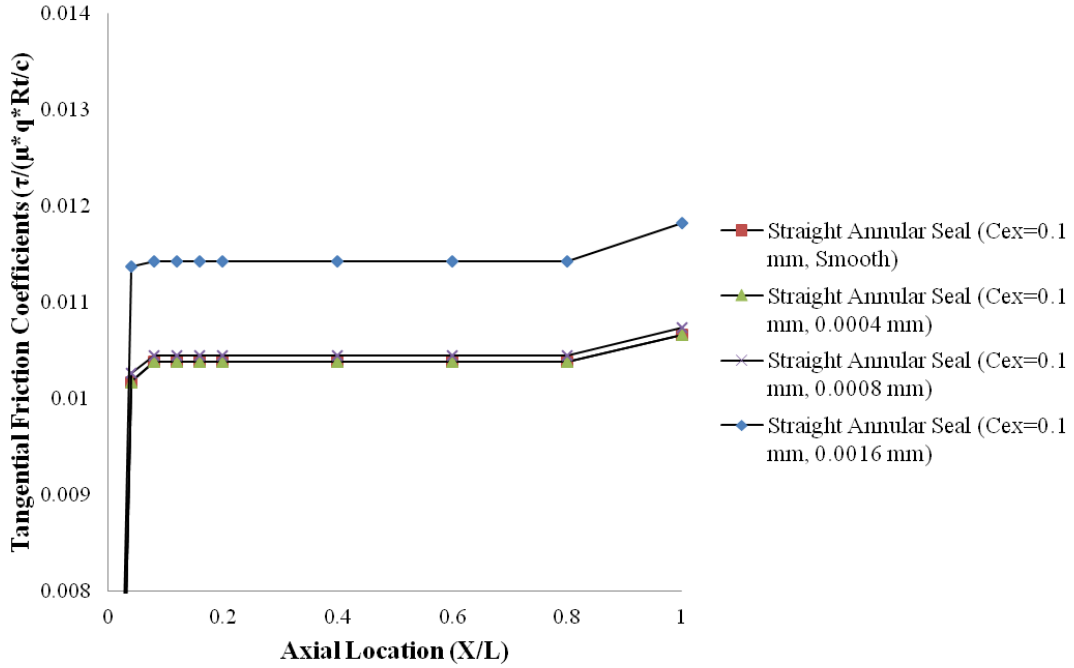

Fig. 51 Tangential friction coefficients for the straight annular seals (C_{ex}=0.1 mm, 20,200 rpm, stator wall, water flow)

In figure 51, tangential friction coefficients on the stator wall with respect to the different surface roughness heights for the straight annular seal configurations with 0.1 mm exit seal clearances are presented. Results show that friction coefficients increase with the increase of the surface roughness height. In addition, significant increase is given by 0.0016 mm roughness. According to figures 48 and 51, it can be said that tangential friction coefficients on both the rotor, and stator walls for the straight annular seal configurations with 0.1 mm exit seal clearances are almost same. There is about 0.87 % increase observed in tangential friction coefficients on the rotor wall compared to the those on the stator wall.

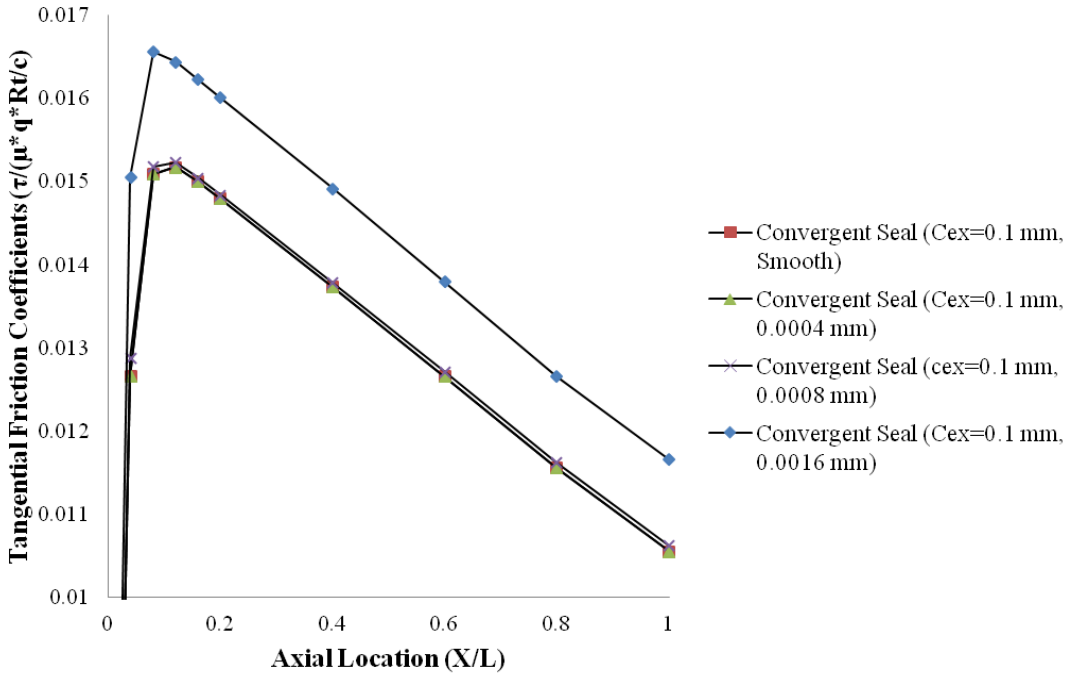

Fig. 52 Tangential friction coefficients for the convergent seal configurations (C_{ex}=0.1 mm, 20,200 rpm, stator wall, water flow)

In figure 52, tangential friction coefficients on the stator wall with respect to the different surface roughness heights for the convergent seal configurations with 0.1 mm exit seal clearances are presented. Results show that there is not a significant variation in the tangential friction coefficients until the increase from 0.0008 mm to 0.0016 mm surface roughness. Additionally, friction coefficients for the all cases decreases along the stator wall after the entrance region. After the entrance region, about 29 % decrease is observed in the tangential friction coefficients. In addition, about 2 % increase is observed for the tangential friction coefficients on the stator wall compared to the those on the rotor wall.

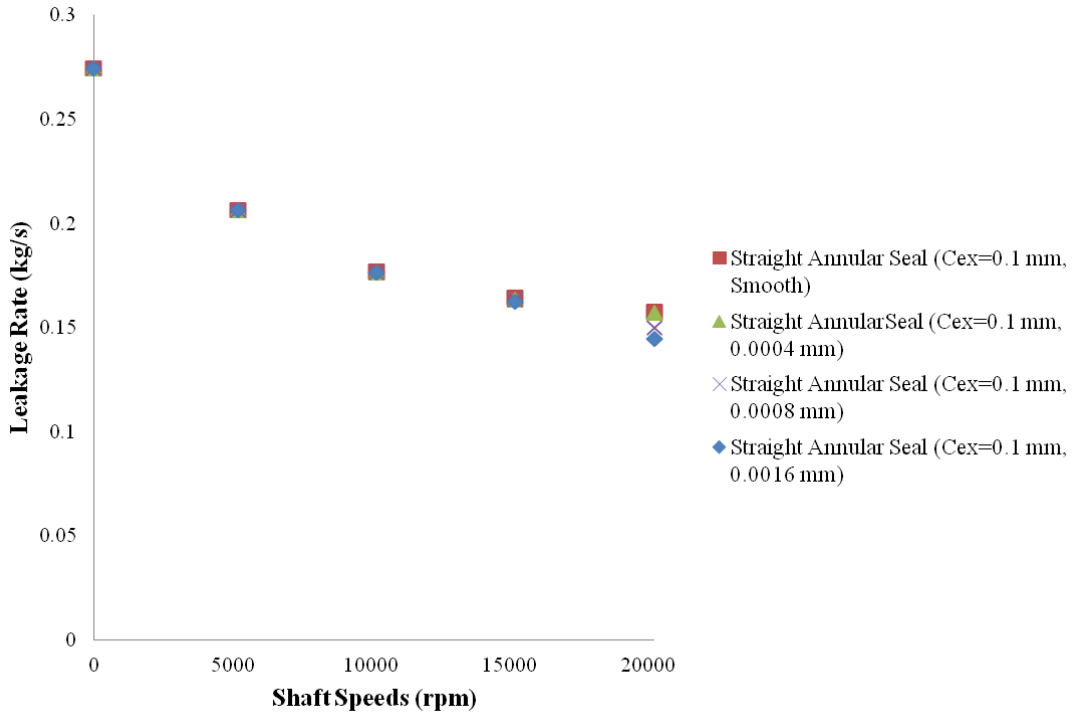

Fig. 53 Leakage rates for the straight annular seal configurations (C_{ex}=0.1 mm, 0-20,200 rpm, water flow)

In figure 53, leakage rates with respect to the different surface roughness heights for the straight annular seal configurations with 0.1 mm exit seal clearances are shown. Results show that leakage rate slightly decreases with the increase of the surface roughness, and effects of the surface roughness are more apparent at higher shaft speeds. There is 25 % reduction in the leakage rate when roughness is set at 0.0016 mm. Affect is not linear with occurring at low shaft speed. Same analysis is also performed for the convergent seal configurations, and results are presented in following section.

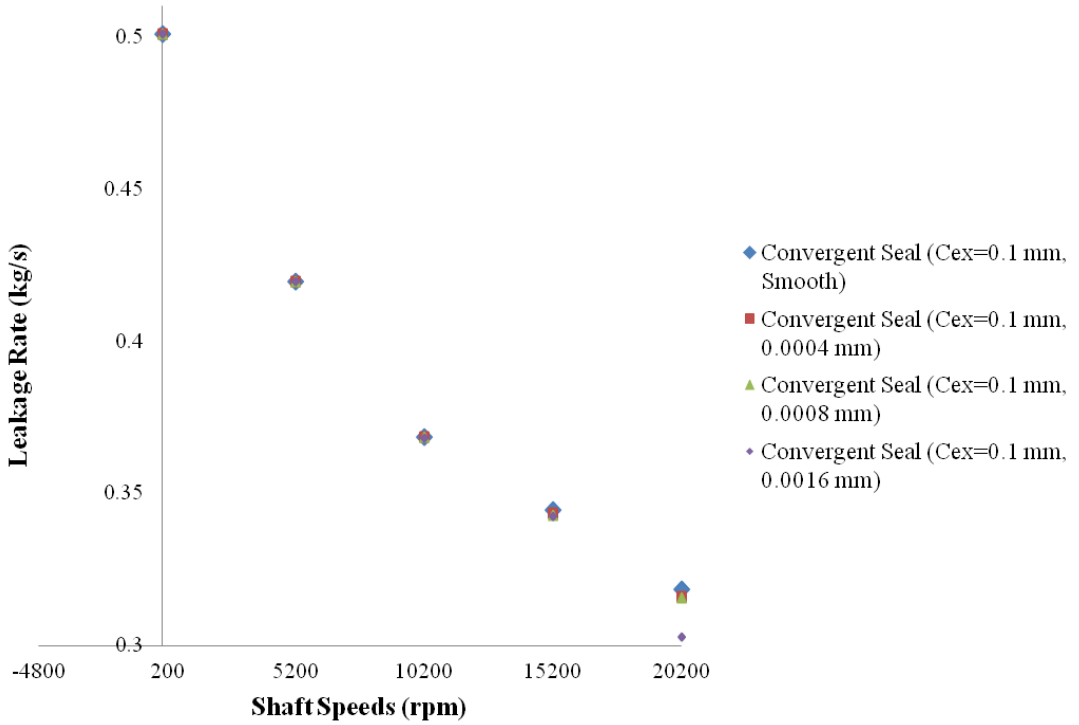

Fig. 54 Leakage rates for the convergent seal configurations (C_{ex}=0.1 mm, 0-20,200 rpm, water Flow)

Figure 54 shows that leakage rate for the convergent seal configurations with 0.1 mm exit seal clearances slightly decreases with the increase of the surface roughness, especially at 0.0016 mm surface roughness height. As is in the straight annular seal configurations, effects of the surface roughness heights on the leakage rate are more apparent at higher shaft speeds. Results are more linear than the those of the straight annular seals. There is almost 25% decrease in the mass flow rate with the increased shaft speed. Figure 32 shows that axial wall shear stress distribution is more linear for the convergent seal configurations. Pressure energy accelerates the fluid, which

overcomes friction. When the seal clearance is constant, there is no flow acceleration so all goes into the friction.

6.2. Effect of Seal Clearance, Shaft speed, Pressure Ratio, and Surface Roughness on the Leakage for the Air Flow

In this section, results obtained from the analyses, which are performed by using air as a working fluid, will be presented in order to understand the effects of the seal clearance, shaft speed, pressure ratio, and surface roughness on the leakage. The same seal configurations are tested, but different boundary conditions are applied. Inlet boundary conditions for all cases are the same but exit ones are different, because different pressure ratios are applied.

Two different boundary conditions are applied to the seal configurations with 0.1 mm exit seal clearance, and four different boundary conditions are used for seal configurations with 0.2 mm exit seal clearance. In the following section, average axial velocity, and swirl velocity distributions based upon different shaft speeds, and surface roughness heights will be presented.

Inlet gage pressure for each seal configurations is 70 bar. There are two pressure ratios (0.17, 0.53), which are applied to the seal configurations with 0.1 mm exit seal clearances, and four pressure ratios (0.28, 0.39. 0.48, 0,65) for the seal configurations with 0.2 mm exit seal clearances. Due to different boundary conditions, seal configurations with different exit seal clearances will not be compared to each other in terms of leakage characteristics. The same analyses performed in the previous section

will be followed to investigate how the leakage rate changes with variation of the seal geometry.

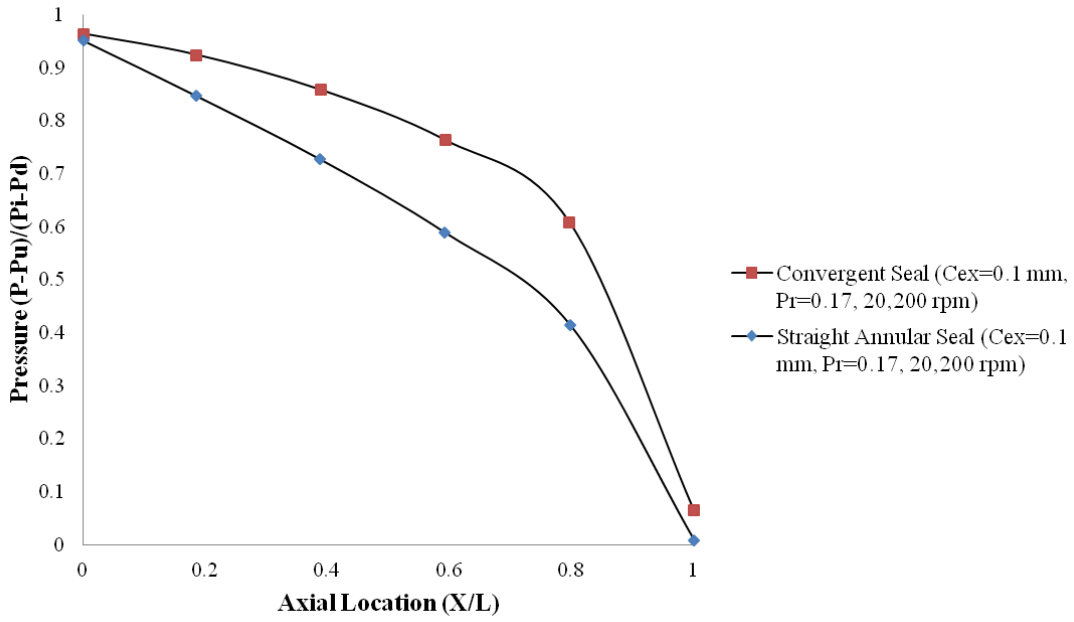

Fig. 55 Pressure distributions for the straight annular, and convergent seal configurations (C_{ex}=0.1 mm, 0-20,200 rpm, air flow, Pr=0.17)

In figure 55, static pressure distributions along the rotor wall for the convergent and straight annular seal configurations with 0.1 mm exit seal clearances, and 0.17 pressure ratios are presented. Results show that pressure distributions are not linear for both seal configurations, and there is a sharp decrease in the pressure after X/L=0.8 because of the high Mach number. These analyses are performed when the shaft speed is set at 20,200 rpm.

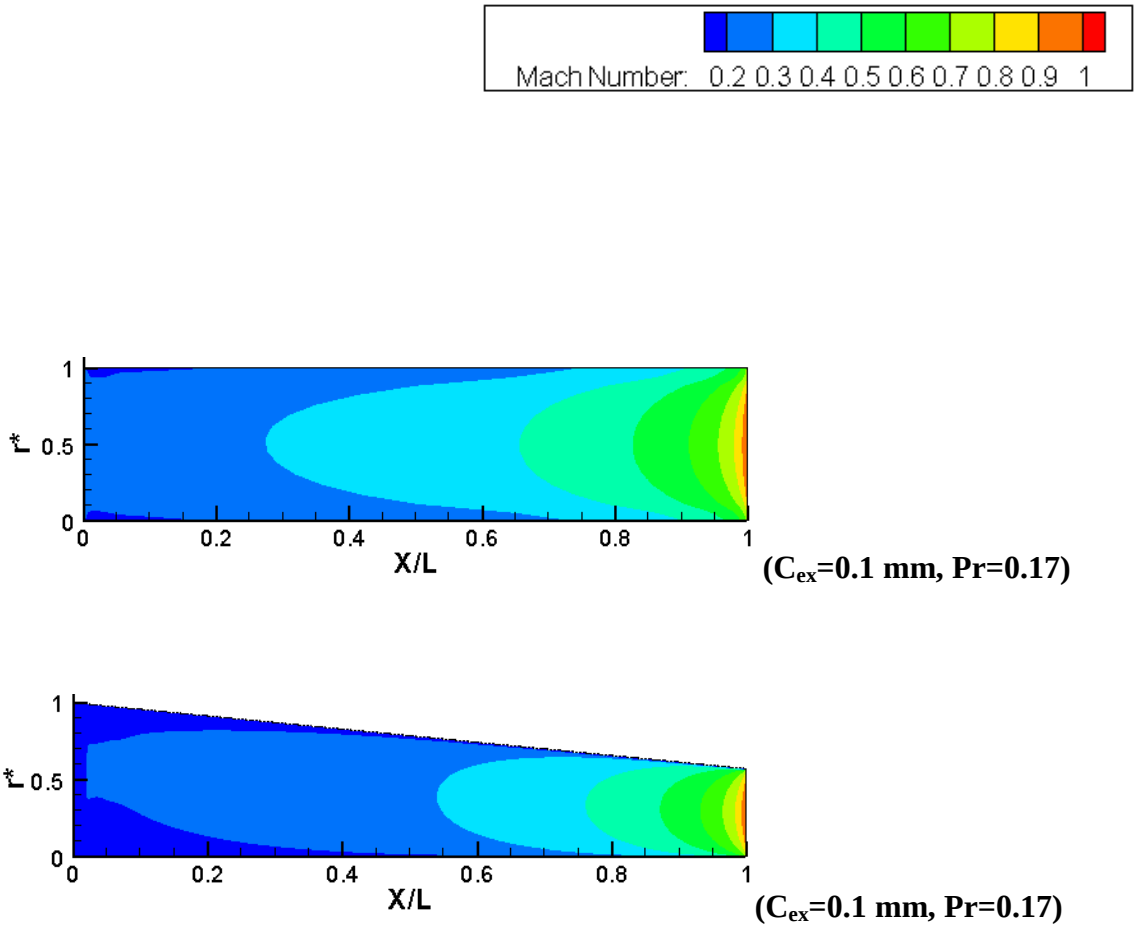

Fig. 56 Mach number distributions for the straight annular and convergent seal configurations (C_{ex}=0.1 mm, 20,200 rpm, air flow, Pr=0.17)

In figure 56, Mach number distributions along the axial direction for the convergent, and straight annular seal configurations with 0.1 mm exit seal clearances, and 0.17 pressure ratios are presented. Results show that Mach number increases along the axial direction for both seal configurations. For this pressure ratio, flow is choked so the Mach number at the exit has a value of one.

Table 14 Static pressures at the seal inlet, and exit for the convergent, and straight annular seals (C_{ex}=0.1mm, 0-20,200 rpm, rotor wall, X/L=1)

Seal Type	Cex (mm)	Pr	Rpm	Pi (bar)	Pe (bar)
Straight Annular	0.1	0.17	0	70	12.49
Straight Annular	0.1	0.17	5200	70	12.47
Straight Annular	0.1	0.17	10200	70	12.43
Straight Annular	0.1	0.17	15200	70	12.42
Straight Annular	0.1	0.17	20200	70	12.41
Straight Annular	0.1	0.53	0	70	37.11
Straight Annular	0.1	0.53	5200	70	37.11
Straight Annular	0.1	0.53	10200	70	37.10
Straight Annular	0.1	0.53	15200	70	37.10
Straight Annular	0.1	0.53	20200	70	37.10
Convergent	0.1	0.17	0	70	16.11
Convergent	0.1	0.17	5200	70	15.90
Convergent	0.1	0.17	10200	70	14.75
Convergent	0.1	0.17	15200	70	14.50
Convergent	0.1	0.17	20200	70	13.13
Convergent	0.1	0.53	0	70	37.17
Convergent	0.1	0.53	5200	70	37.16
Convergent	0.1	0.53	10200	70	37.10
Convergent	0.1	0.53	15200	70	37.10
Convergent	0.1	0.53	20200	70	37.01

Table 14 includes the pressure distributions at the inlet, and exit planes for the convergent, and straight annular seal configurations with 0.1 mm exit seal clearances. In addition, effects of the pressure ratio, and shaft speed on the exit pressure are also presented in this table. Results show that exit pressure is higher than expected for these seal configurations due to the choked flow. Straight annular seals with 0.17 pressure ratio shows about 4 % increase in the static pressure at the exit plane, and this ratio decreases to about 0.278 % for the same seal configurations with 0.53 pressure ratio.

Additionally, there is about 10 % increase in the pressure at the exit plane for the convergent seal configurations, and variation in the exit pressures for the same seal configurations with 0.53 pressure ratios is almost same with straight annular seal configurations with 0.53 pressure ratios.

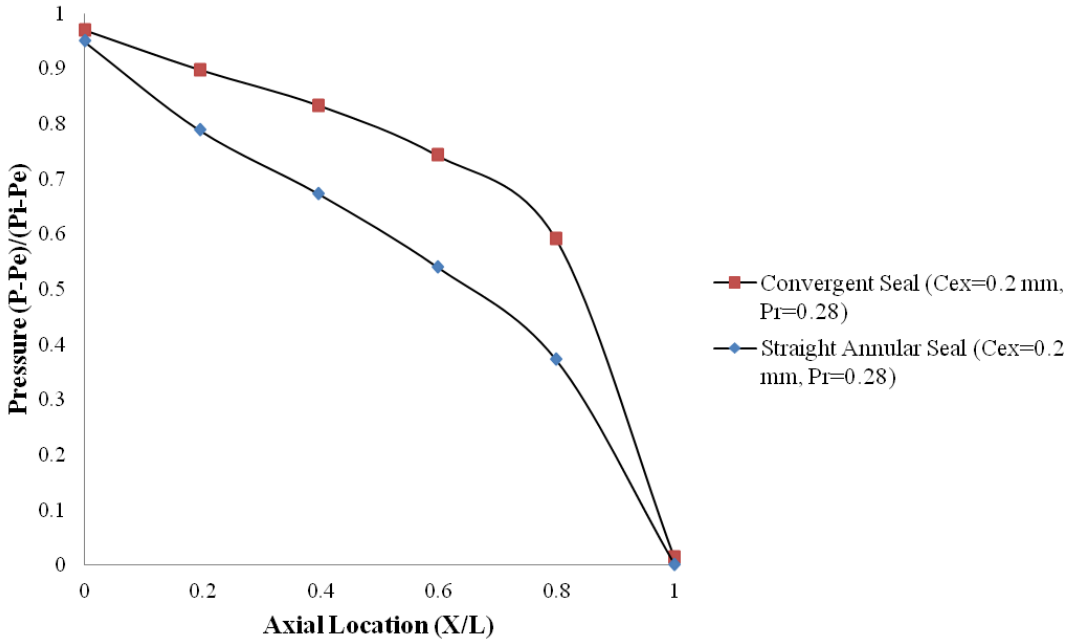

Fig. 57 Pressure distributions for the straight annular and convergent seal configurations (C_{ex}=0.2 mm, 0-20,200 rpm, air flow, Pr=0.28)

In figure 57, the static pressure distributions along the rotor wall for the convergent, and straight annular seal configurations with 0.2 mm exit seal clearances, and 0.28 pressure ratios are presented. Results show that there is a sharper decrease in the pressure after X/L= 0.8, which is caused by the increase in the Mach number.

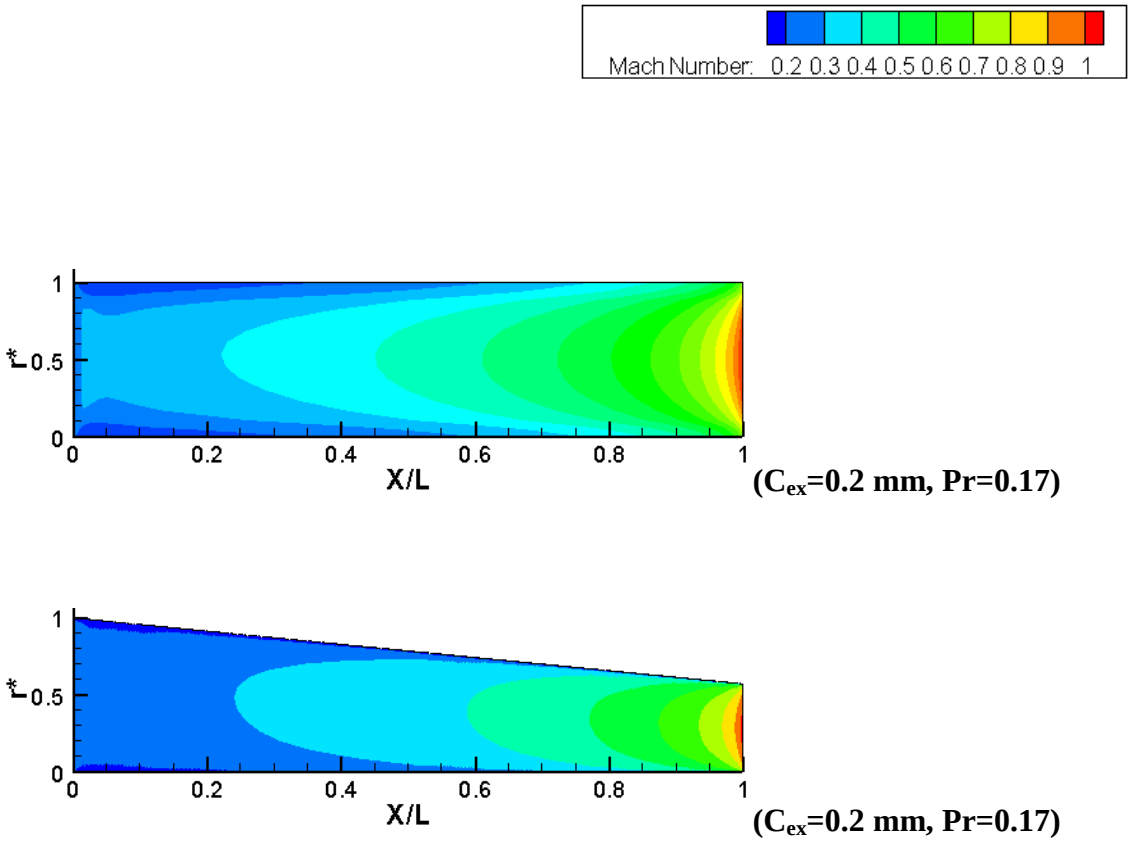

Fig. 58 Mach number distributions for the straight annular and convergent seal configurations (C_{ex}=0.2 mm, 20,200 rpm, air flow, Pr=0.28)

In figure 58, Mach number distributions along the axial direction for the convergent, and straight annular seal configurations with 0.2 mm exit seal clearances, and 0.28 pressure ratios are presented. Results show that Mach number increases along the axial direction for both seal configurations, which causes shaper pressure decrease after X/L= 0.8 where the Mach number exceeds 0.6 in value.

Table 15 Static pressures at the seal inlet, and exit for the convergent and straight annular seals (C_{ex}=0.2 mm, 0-20,200 rpm, rotor wall, X/L=1)

Seal Type	Cex (mm)	Pr	Rpm	Pi (bar)	Pe (bar)
Straight Annular	0.2	0.28	0	70	19.6
Straight Annular	0.2	0.28	5200	70	19.6
Straight Annular	0.2	0.28	10200	70	19.6
Straight Annular	0.2	0.28	15200	70	19.6
Straight Annular	0.2	0.28	20200	70	19.6
Convergent	0.2	0.28	0	70	20
Convergent	0.2	0.28	5200	70	20
Convergent	0.2	0.28	10200	70	19.7
Convergent	0.2	0.28	15200	70	19.7
Convergent	0.2	0.28	20200	70	19.7

Table 15 includes the inlet, and exit pressures for the straight, and convergent seal configurations with respect to the different shaft speeds are presented. Results show that there is a slight increase in the exit pressures due to the increase of the Mach number. According to the pressure ratio, which is presented in table 15, expected exit pressure is 19 bar. Table 15 shows that there is a slight increase in the exit pressure due to the increase of the mach number at the exit plane. In the following section, the axial pressure gradient-to-axial wall shear stress ratios for the straight annular seal configurations will be analyzed.

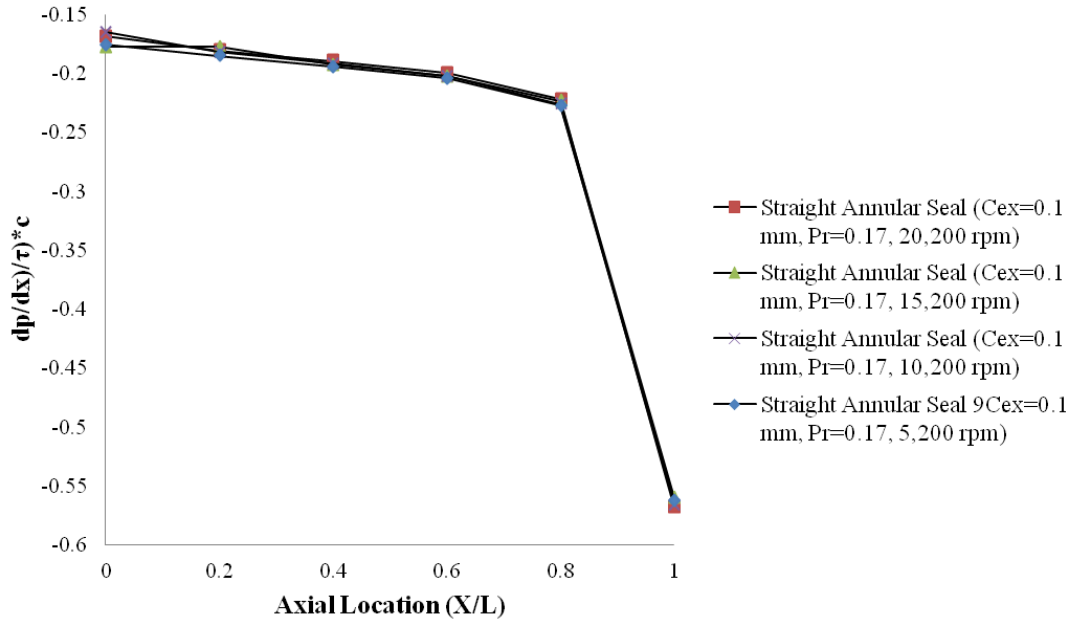

Fig. 59 ($(dp/dx)/\tau_{xy}$)*c for the straight annular seal configurations (C_{ex}=0.1 mm, 0-20,200 rpm, air flow, Pr=0.17)

In figure 59, the pressure gradient-to-axial wall shear stress ratios for the straight annular seal configurations with 0.1 exit seal clearances for different shaft speeds are presented. These ratios are made non-dimensional by multiplying the seal clearances. Results show that shaft speeds does not have a significant effect on this ratio. Because this flow is compressible, constant pressure gradient distributions are not obtained. In addition, the axial pressure gradients for all cases decrease very rapidly after X/L=0.8 where the Mach number exceeds 0.6. Magnitude of the axial pressure gradients increases along the axial direction making the axial velocity radial gradient at wall larger, which causes higher axial wall shear stress.

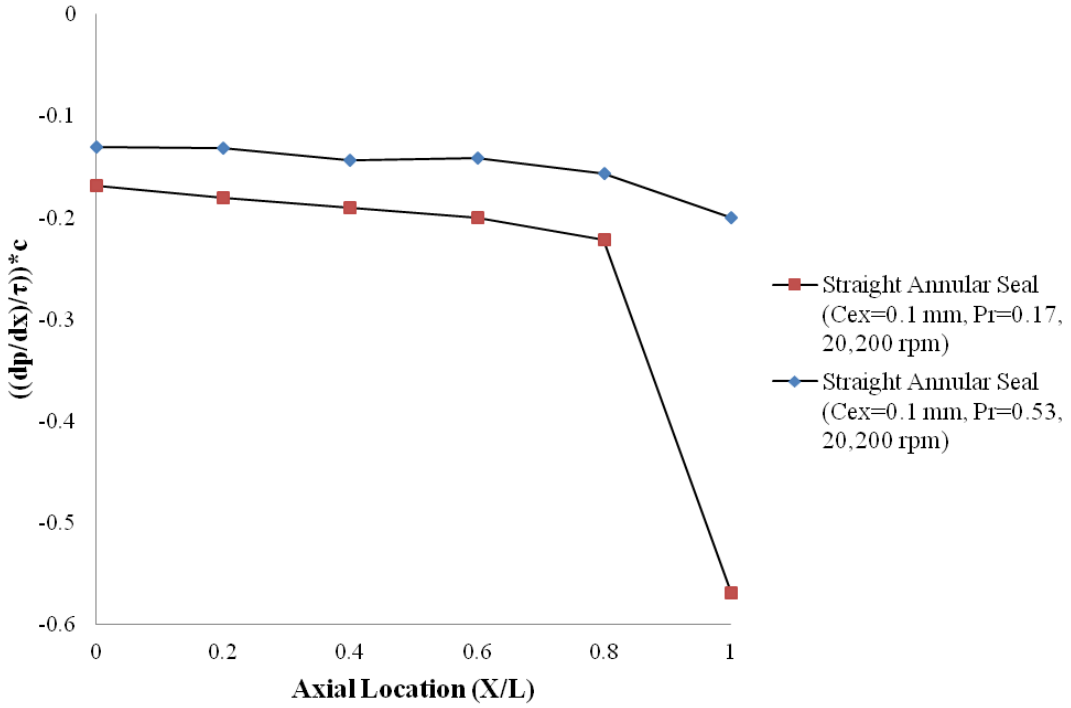

Fig. 60 $((dp/dx)/\tau_{xy})*c$ for the straight annular seal configurations (C_{ex}=0.1 mm, 0-20,200 rpm, air flow, Pr=0.17-0.53)

In figure 60, the pressure gradient-to-axial wall shear stress ratios for the straight annular seal configurations with 0.1 exit seal clearances for different pressure ratios are presented. These ratios are made non-dimensional by multiplying the seal clearances. For the higher pressure ratio, the flow is not choked so the mass flow rate is lower. Also the ratio is smaller and does not suddenly increase in magnitude near the exit as does the smaller pressure ratio. Additionally, these analyses are also performed based upon the different surface roughness heights, and presented in the following section. Rate of this pressure gradient-to-axial wall shear stress ratio is related to the Mach number variation in the axial direction.

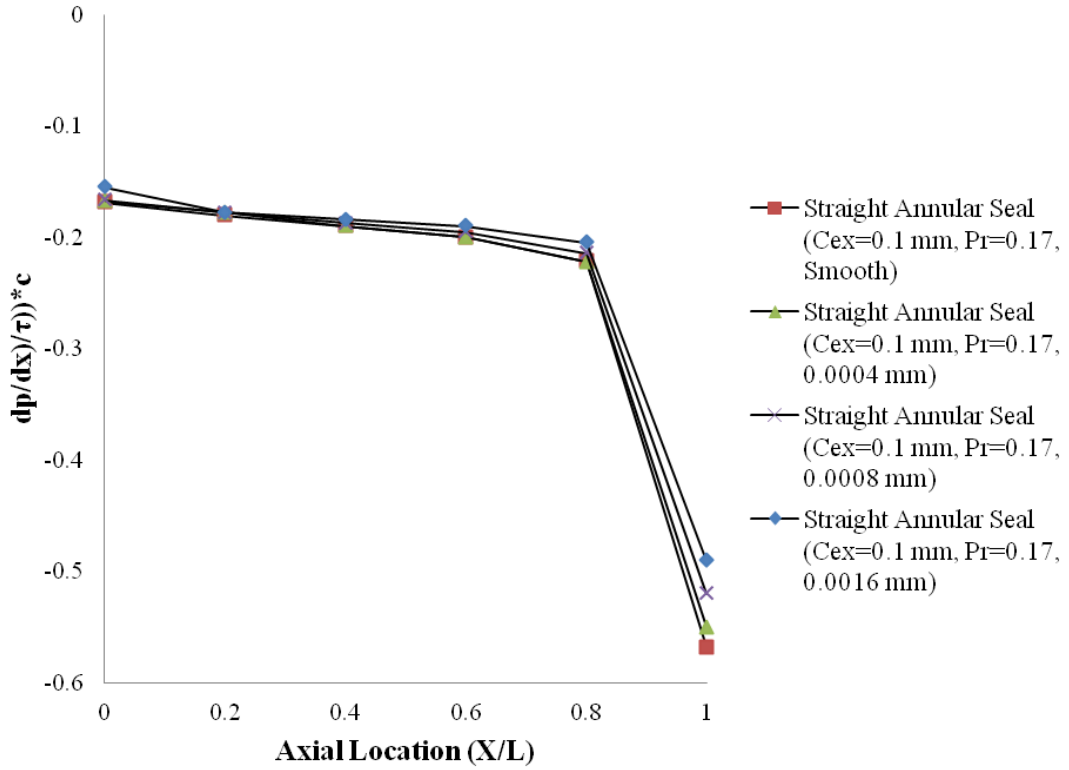

Fig. 61 ($(dp/dx)/\tau_{xy}$)*c for the straight annular seals (C_{ex}=0.1 mm, 0-20,200 rpm, air flow, surface roughness = 0-0.0004 mm-0.0008 mm-0.0016 mm)

In figure 61, the pressure gradient-to-axial wall shear stress ratios with respect to the different surface roughness heights for the straight annular seal configurations with 0.1 mm exit seal clearances are presented. Results show that there is not significant variation in this ratio for different surface roughness heights excepts near the exit where the Mach number approaches one. Additionally, these ratios decrease for all cases up to the seal exit. As Mach number, and axial velocity increase along the axial direction, magnitude of the axial wall shear stress increases as well. Additionally, difference between the axial pressure gradient-to-axial wall shear stress ratios at the exit plane is

due to the surface roughness. As for incompressible flow, larger axial velocity makes boundary layer thinner, and roughness height protrudes further into higher speed flow.

Rhode [27] also observed pressure distribution in the axial direction versus different seal clearances for labyrinth and annular seal conifurations. His results suggested that pressure drop increases with the increment of seal clearance. In addition, he observed that pressure drop in annular seal configurations is higher compared to the labyrinth seals.

As specified in the introduction section, the decrement of leakage rate is a cost-effective way to increase the aerodynamic performance of a turbo-Machinery system. The rotating seal configurations are used for enhancing aerodynamic efficiency. Estimating the leakage rate through these rotating seal configurations under different working conditions has a particular importance. In order to actualize this purpose, there are many research performed.

In this section, effects of rotor speed, pressure ratio, and surface roughness on the leakage rate for both convergent and straight annular seal configurations will be discussed. Five rotor speeds will be applied to all flow simulations. In following section, pressure distributions, swirl velocity variation, swirl shear, and axial wall shear stress distributions under the effects of rotor speed will be analyzed.

It is also deduced from the previous studies that shaft rotation has an impact on the pressure distribution. Rotational speed introduces circumferential forces to the system, which push the flow towards to the stator wall, and causes the increment of

static pressure. Greater swirl velocity formation in the system also has important effects on circumferential stresses on the rotor and stator walls.

In the following section, average axial, and swirl velocity distributions with respect to the different shaft speeds, pressure ratios, and surface roughness heights for all seal configurations will be presented to better understand the lekaage characteristics of these seal configurations. In the following section, average axial velocity distributions with respect to the different shaft speeds, pressure ratios, seal clearances, and roughness heights will be analyzed.

Figure 62 shows the average axial velocity distributions along the axial direction for the straight annular seal configurations with 0.1 mm exit seal clearances, and 0.17 pressure ratios. Axial velocities are made non-dimensional divided by the mass average inlet velocities of each case. Results show that shaft speeds have no significant effects on the axial velocity formation, and axial velocities increase along the axial direction. As specified in the previous section, this flow is compressible, and density of the flow along the axial direction decreases, which causes the increase of the axial velocity. Fanno flow case is shown in figure 62.

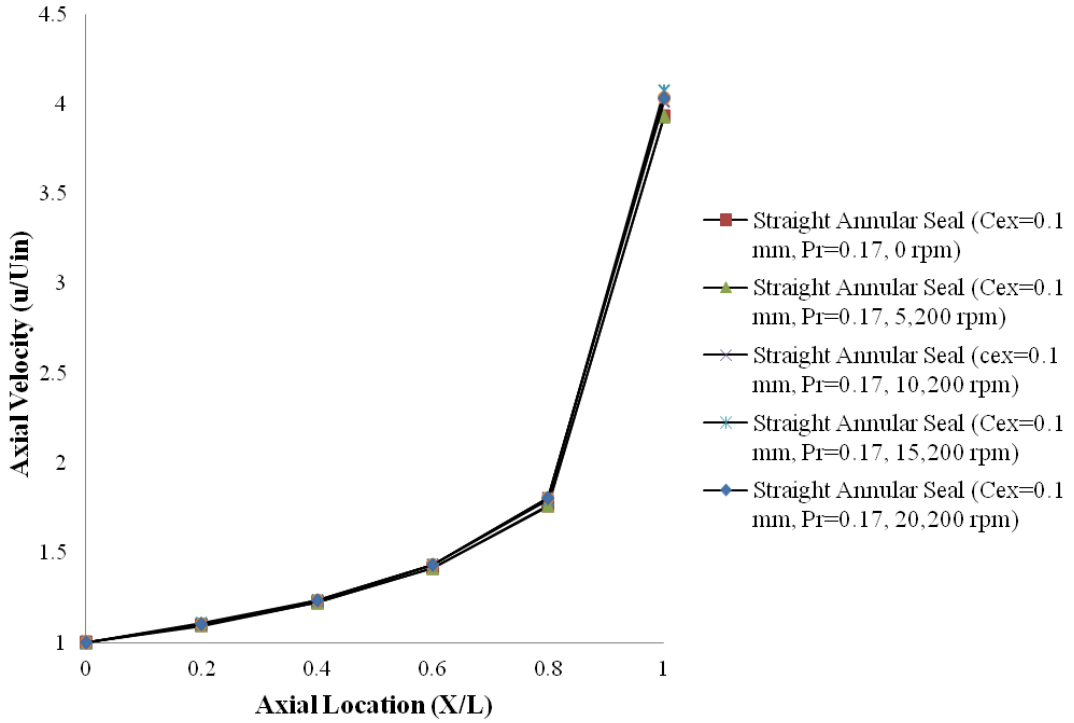

Fig. 62 Average axial velocity distributions for the straight annular seals (C_{ex}=0.1 mm, Pr=0.17, 0-20,200 rpm, X/L=0-0.2-0.4-0.6-0.8-1)

This result also shows that flow inertia increases continuously up to the seal exit. For the pressure ratio presented, the flow is choked at the exit. The axial velocity increases rapidly over the last 20 % of the seal length in the same manner as presented in Fanno flow. In addition, it can be deduce from the figure 62 that the increase of the shaft speed has not a significant impact on the average axial velocity formation along the axial direction.

Table 16 Bulk axial velocity at the inlet (straight annular seals, C_{ex}=0.1 mm, Pr=0.17, 0-20,200 rpm)

rpm	Uin (m/s)
0	83.9
5200	83.9
10200	81.4
15200	80.8
20200	80.2

In table 16, bulk axial velocities with respect to the different shaft speeds for straight annular seal configurations with 0.1 mm exit seal clearances are presented in order to better understand the effects of shaft speeds on the axial velocity. Results show that there is 4 % decrease in the bulk axial velocity with the increase of the shaft speed, which can be resulted from the increase of the circumferential stress effects on the flow. It can be deduced from table 16 that increase of the shaft speed causes the decrease of the axial wall shear stress, which gives longer residence time. As a consequence of this, effects of the tangential shear increase.

Same analyses are also performed for the convergent seal configurations, and results will be presented in the following section. Additionally, effects of the seal clearance on the average axial velocity formation will be discussed as well.

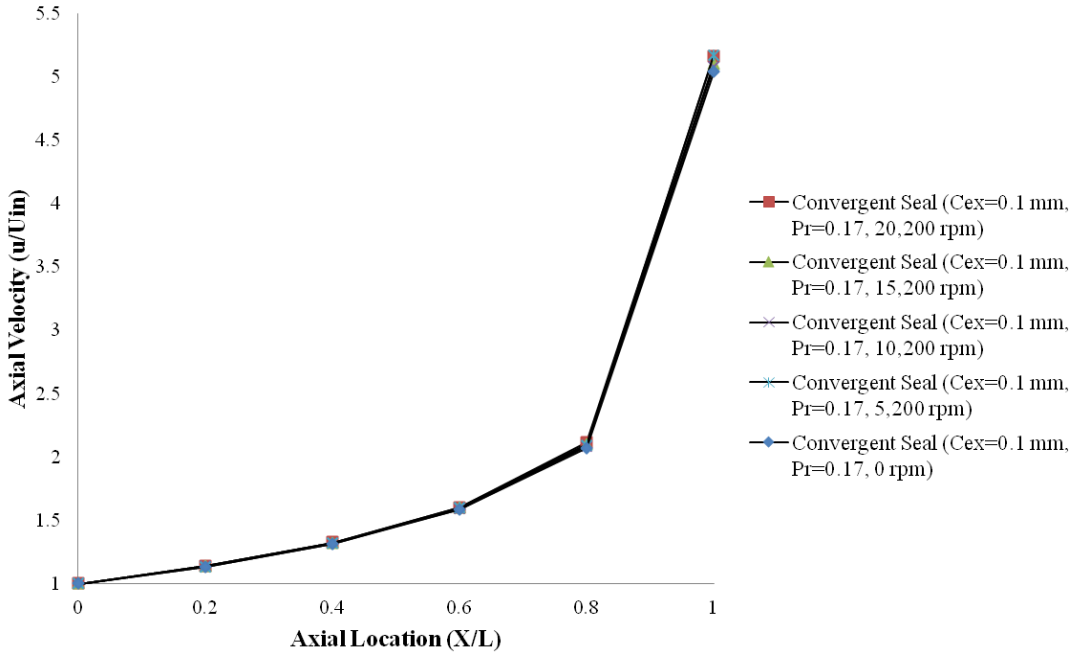

Fig. 63 Average axial velocity distributions for the convergent seals (C_{ex}=0.1 mm, Pr=0.17, air flow, 0-20,200 rpm, X/L=0-0.2-0.4-0.6-0.8-1)

Figure 63 shows the average axial velocity distributions along the axial direction for the convergent seal configurations with 0.1 mm exit seal clearances, and 0.17 pressure ratios. Axial velocities are made non-dimensional divided by the mass average inlet velocities of each case. Results show that shaft speeds do not have significant effects on the axial velocity formation for the convergent seal configuration as well, and axial velocities increase along the axial direction, which is caused by the decrement of the surface area, and flow density. Figure 63 shows that there is about 100 % increase in the axial velocity-to-bulk inlet velocity ratios from the seal inlet to X/L=0.8 for the convergent seal configurations. In terms of the straight annular seal configurations, 80 % increase is observed. Due to the convergence geometry, convergent seals produce larger

variation in axial velocity ratio. In addition, axial velocity increases rapidly after X/L= 0.8 due to the Fanno acceleration.

Table 17 Bulk axial velocity at the inlet (convergent seals, C_{ex}=0.1 mm, Pr=0.17, 0-20,200 rpm)

rpm	Uin (m/s)
0	67.5
5200	67.0
10200	66.7
15200	65.9
20200	65.0

In Table 17, bulk axial velocities with respect to the different shaft speeds for the convergent seal configurations with 0.1 mm exit seal clearances are presented in order to better understand the effects of shaft speeds on the axial velocity. Results show a 3 % decrease in the bulk axial velocity with the increase of the shaft speed, which can be resulted from the increase of the circumferential stress effects on the flow. Straight annular seal configurations shows 4 % decrease in the bulk inlet axial velocity as presented in previous section. Additionally, results show that straight annular seal configurations exhibits higher bulk axial velocity formations at the inlet compared to the convergent seal configurations, which can be due to the flow area at the inlet. The same analyses are also performed for the same seal configurations with 0.2 mm exit seal clearances, and results will be presented in the following section.

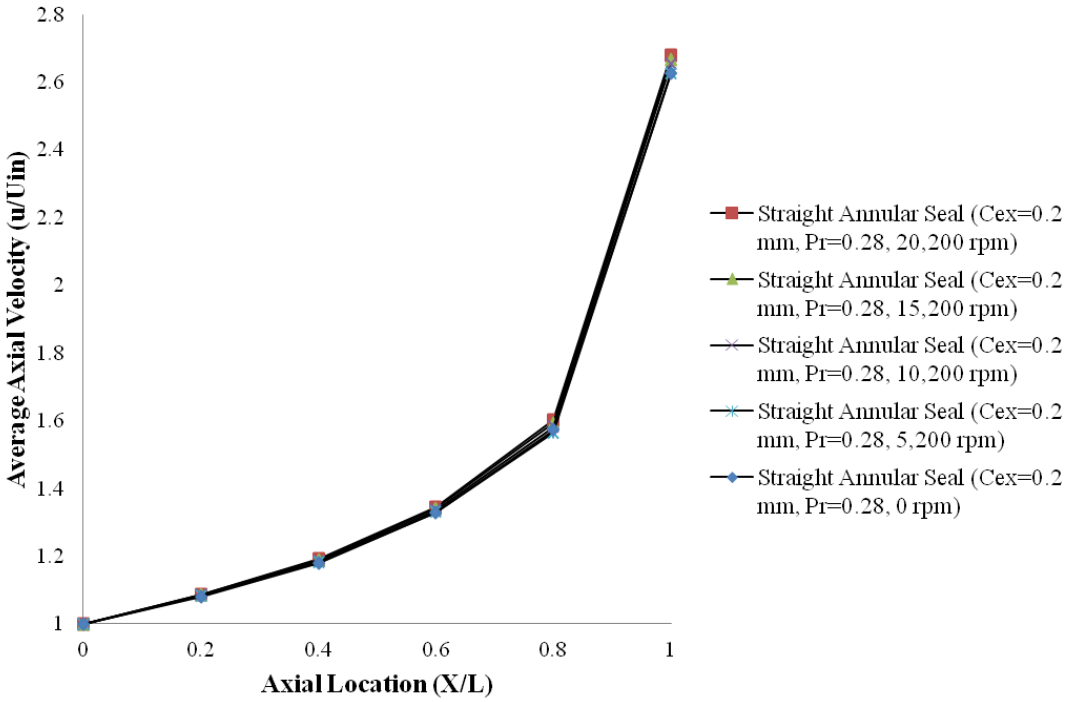

Fig. 64 Average axial velocity distributions for the straight annular seals (C_{ex}=0.2 mm, Pr=0.28, 0-20,200 rpm, X/L=0-0.2-0.4-0.6-0.8-1)

Figure 64 shows the average axial velocity distributions along the axial direction for the straight annular seal configurations with 0.2 mm exit seal clearances, and 0.28 pressure ratios. Results show that shaft speeds does not have significant effects on the axial velocity formation as specified in the previous section. Additionally, axial velocity-to-bulk inlet velocity ratio at the exit plane for straight annular seals with 0.2 mm exit seal clearances is about 2.8 while this ratio for the same seal configurations with 0.1 mm exit seal clearances is 4, which is resulted from the lower flow area. Flow is choked for these cases as well. Hence as shown in table 16, bulk inlet velocities are larger for the straight annular seal configurations with 0.2 mm exit seal clearances. Additionally, exit velocities for straight annular seals with 0.1, and 0.2 mm exit seal clearances are almost

same but smaller axial velocity-to-bulk inlet velocity ratio is obtained for the seal configurations with 0.2 mm seal clearances.

Table 18 Bulk axial velocity at the inlet (straight annular seals, C_{ex}=0.2 mm, Pr=0.28, 0-20,200 rpm)

rpm	Uin (m/s)
0	120.5
5200	120.1
10200	117.4
15200	116.6
20200	115.4

Table 18 shows that the increase of the shaft speed causes 4 % decrease in the bulk inlet axial velocity about the same as the 0.1 mm seal clearance case. Increase of the seal clearance does not alter variation in the bulk inlet velocity while shaft speed changes. Additionally, results show that average axial inlet velocity decreases with the increase of the seal clearance. Convergent seal configurations give lower average inlet velocities at the exit plane due to the higher surface area at the inlet. At the exit plane, greater axial velocity formations are observed in the convergent seal configurations due to the axial flow acceleration along the axial direction.

In the following section, average axial velocity distributions for the convergent seal configurations with 0.2 mm exit seal clearances will be analyzed.

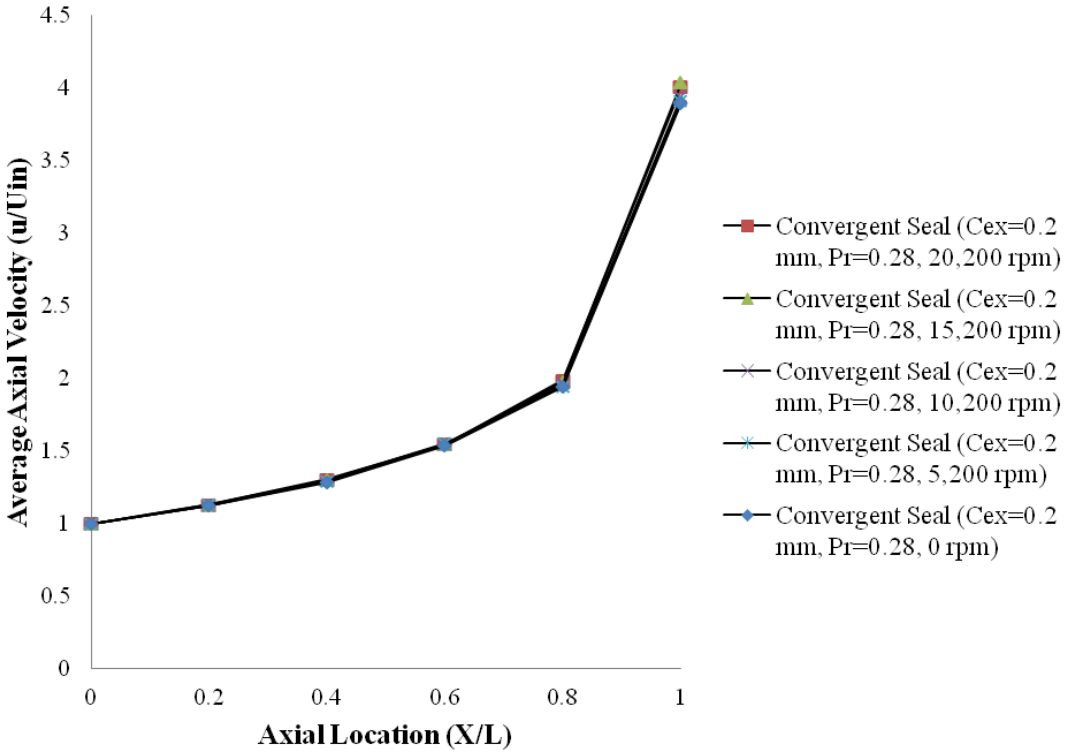

Fig. 65 Average axial velocity distributions for the convergent seals (C_{ex}=0.2 mm, Pr=0.28, air flow, 0-20,200 rpm, X/L=0-0.2-0.4-0.6-0.8-1)

Figure 65 shows the average axial velocity distributions along the axial direction for the convergent seal configurations with 0.2 mm exit seal clearances, and 0.28 pressure ratios. Results show that flow is choked (Mach number=1) at the exit so inlet bulk axial velocity is lower due to larger inlet seal clearance than bulk inlet axial velocity for the straight annular seal configurations with 0.2 mm exit seal clearances. Therefore, exit axial velocity-to-inlet axial velocity ratios for the convergent seal configurations with 0.2 mm exit seal clearances are larger than those for the straight annular seal configurations with same exit seal clearances.

Table 19 Bulk axial velocity at the inlet (convergent seals, C_{ex}=0.2 mm, Pr=0.28, 0-20,200 rpm)

rpm	Uin (m/s)
0	84.8
5200	84.5
10200	83.8
15200	83.4
20200	82.2

In table 19, bulk axial velocities with respect to the different shaft speeds for the straight annular seal configurations with 0.2 mm exit seal clearances are presented in order to better understand the effects of shaft speeds on the axial velocity. Results show that increase of the shaft speed causes 3 % decrease in the bulk inlet velocity for the convergent seal configurations with 0.2 mm exit seal configurations, which is slightly less than 0.1 mm exit seal clearance case. In addition to that, the straight annular seal configurations give greater axial velocity formations compared to the convergent seal configurations, which can be resulted from the flow area at the inlet. Additionally, larger seal clearance reduces effects of the swirl velocity gradient on the flow.

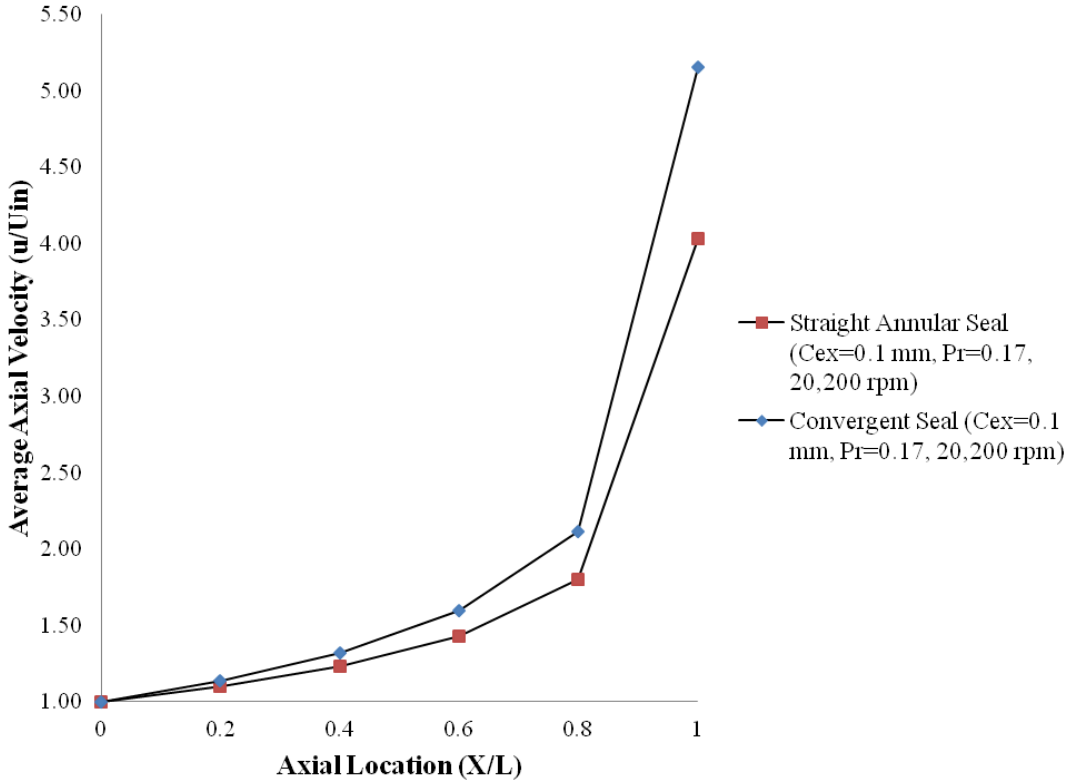

Fig. 66 Average axial velocity for the convergent and straight annular seals (C_{ex}=0.1 mm, Pr=0.17, 0-20,200 rpm, X/L=0-0.2-0.4-0.6-0.8-1)

Figure 66 shows the average axial velocity distributions along the axial direction for the convergent, and straight annular seal configurations with 0.1 mm exit seal clearances, and 0.17 pressure ratios. Results show that convergent seal configurations give greater axial velocity formations, which are due to the increase of the seal clearances. Rhode [27] also performed the same analysis to understand the effects of seal clearance on the axial velocity formation for the annular, and labyrinth seal configurations. He applied two different seal clearances (0.051 cm, 0.013 cm), and axial velocity distributions were analyzed when shaft speed was set at 20,200 cpm. His results show that annular seal configurations give greater axial velocity formations. Same

analysis is also performed same type of seal configurations with 0.2 mm exit seal clearances.

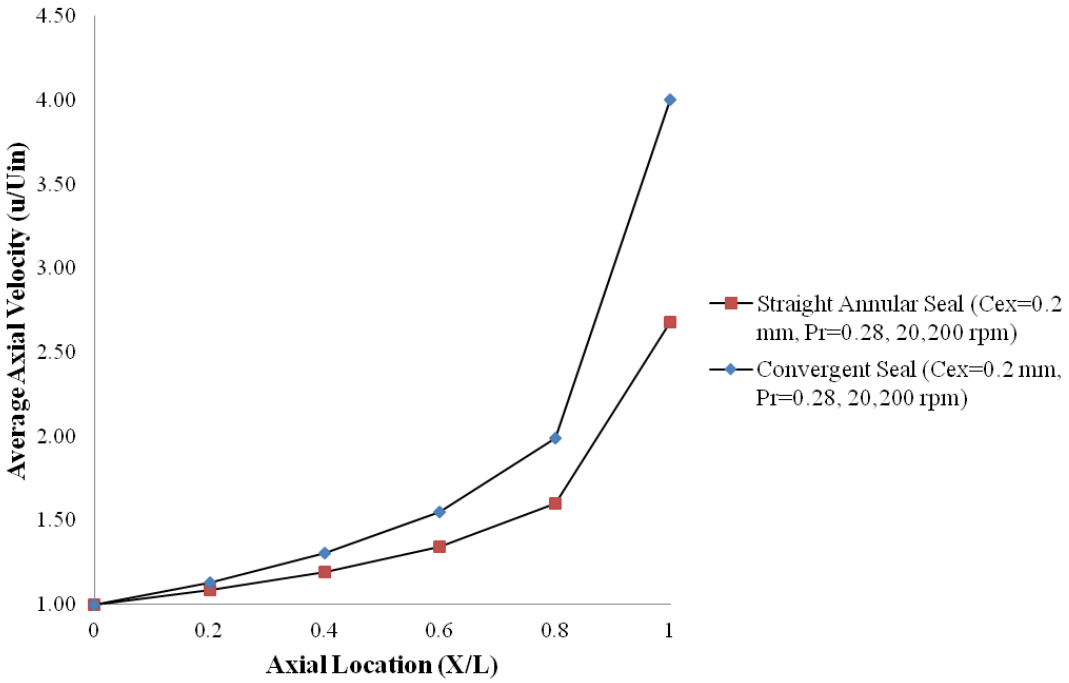

Fig. 67 Average axial velocity for the convergent and straight annular seals (C_{ex}=0.2 mm, Pr=0.28, air flow, 0-20,200 rpm, X/L=0-0.2-0.4-0.6-0.8-1)

Figure 67 shows the average axial velocity distributions along the axial direction for the convergent, and straight annular seal configurations with 0.2 mm exit seal clearances, and 0.28 pressure ratios. Shaft speed for both case is set at 20,200 rpm. Results show that convergent seal configurations give greater axial velocity formations, which can be caused by the increase of the seal clearances. This will cause the decrease

of the circumferential stresses on the flow, and effects of the tangential forces will be dominated by the flow inertia.

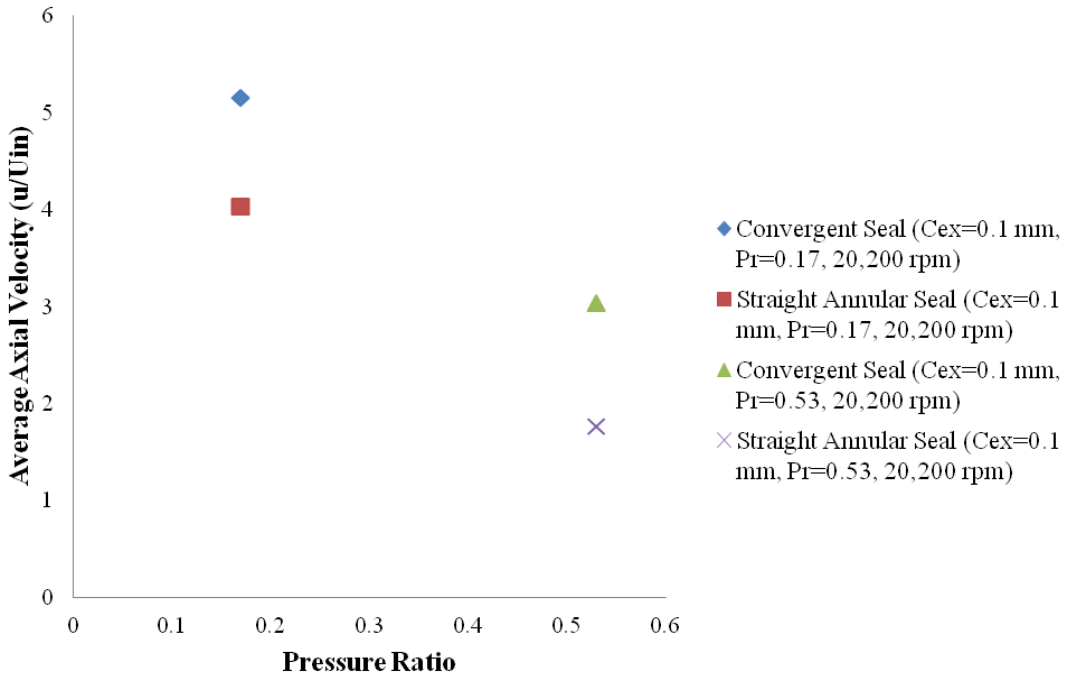

Fig. 68 Average axial velocity for the convergent and straight annular seals (C_{ex}=0.1 mm, Pr=0.17-0.53, air flow, 20,200 rpm, X/L=1)

Figure 68 shows the average axial velocity distributions along the axial direction for the convergent, and straight annular seal configurations with 0.1 mm exit seal clearances, and 0.17-0.53 pressure ratios. Shaft speeds for both cases are set at 20,200 rpm. Axial velocity distributions at the exit plane for these seal configurations are analyzed. Results show that the decrease of the pressure ratio causes the decrease of the

axial velocities. Higher pressure ratio shows that pressure drop along the axial direction is lower, which means low linear inertia.

Figure 69 shows the average axial velocity distributions along the axial direction for the convergent, and straight annular seal configurations with 0.2 mm exit seal clearances, and 0.28-0.39-0.48-0.65 pressure ratios. Results show that the increase of the pressure ratios cause the decrease of the axial velocities, and convergent seal configurations exhibit greater axial velocity formation compared to the straight annular seal configurations.

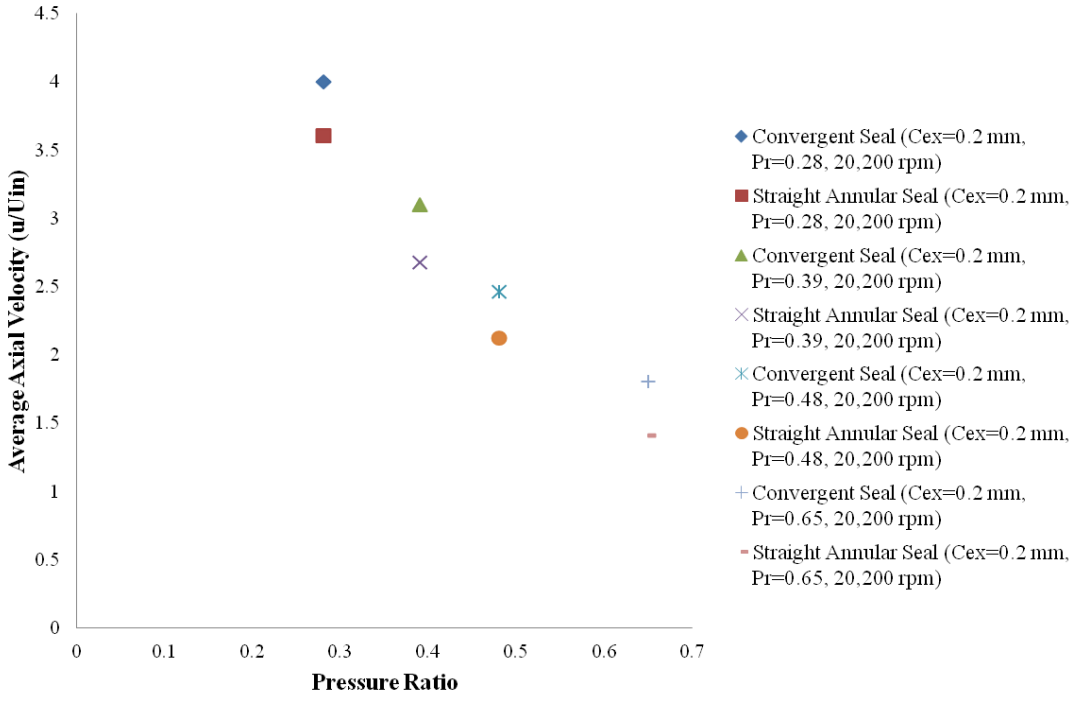

Fig. 69 Average axial velocity for the convergent and straight annular seals (C_{ex}=0.1 mm, Pr=0.28-0.39-0.48-0.65, air flow, 20,200 rpm, X/L=1)

In the following section, average axial velocity distributions with respect to the different surface roughness heights will be analyzed. As specified in the previous section, three different surface roughness heights (0.0004 mm, 0.0008 mm, 0.0016 mm) are applied to the both rotor, and stator walls.

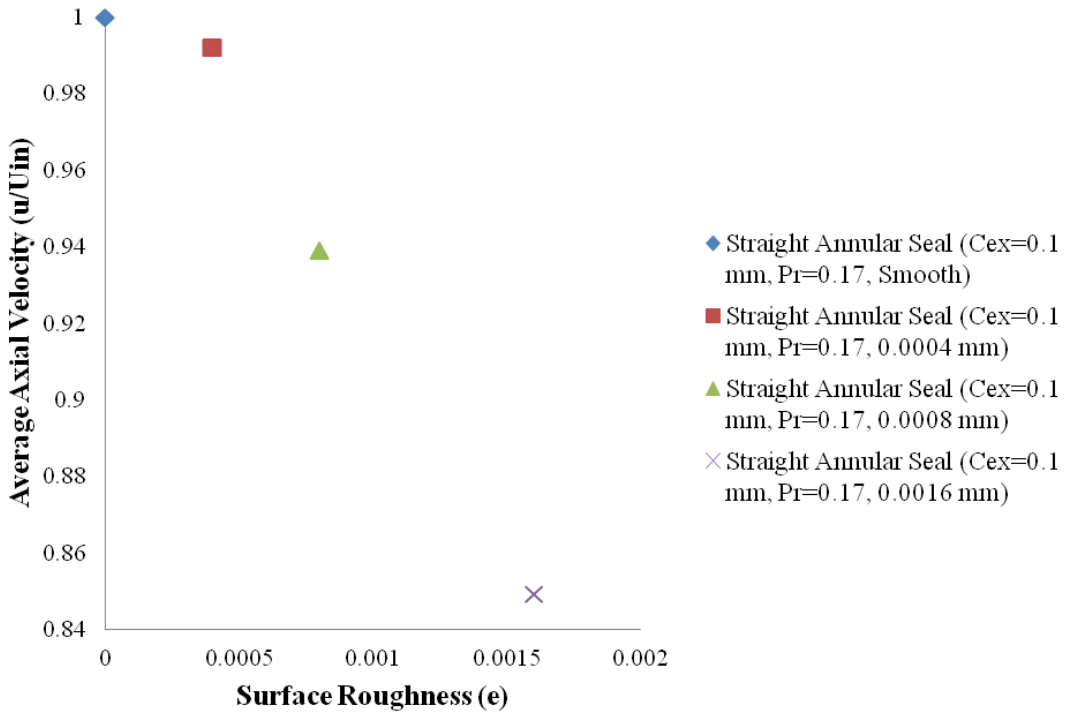

Fig. 70 Average exit axial velocities for the straight annular seals (C_{ex}=0.1 mm, roughness=0-0.0004-0.0008-0.0016 mm, 20,200 rpm, X/L=1, Pr=0.17)

]

In figure 70, the average exit axial velocity distributions with respect to the different surface roughness heights for the straight annular seals with 0.1 mm exit seal clearances, and 0.17 pressure ratios are presented. These analyses are performed when shaft speed is set at 20,200 rpm. As specified in the previous section, surface roughness

are applied to both rotor, and stator walls. Average axial velocities are collected from the exit planes of these seal configurations. Additionally, the increase of the surface roughness height at the exit causes about 11 % decrease in the Mach number at the exit. In this figure, non-dimensional axial velocity distributions are presented, and axial velocities are made non-dimensional with average axial velocity for the smooth surfaces. It can be deduced from this figure that the increase of the surface roughness causes the decrease of the axial velocity, which can be resulted from the effects of friction forces on the wall. There is about 15 % decrease in the axial velocity with the increase of the roughness height. The same analyses are also performed for the water flow as presented in previous section, and the increase of the roughness height causes about 10 % decrease in the axial velocity for the water flow.

Table 20 Non-dimensional boundary layer thickness (e+) for the straight annular seal (C_{ex}=0.1 mm, 20,200 rpm, rotor wall, X/L=1, Pr=0.17)

Roughness	e+
0	0
0.0004	0.771
0.0008	1.516
0.0016	2.876

Table 20 includes non-dimensional boundary layer thicknesses with respect to the different roughness heights for the straight annular seal configurations with 0.1 mm exit seal clearances. Results show that non-dimensional boundary layer thickness

increases with the increase of the roughness. There is about 73 % increase in the non-dimensional boundary layer thickness with the increase of the roughness height.

Lucas, Danaila, Bonneau, and Frene [9] also performed a study to investigate the effects of the roughness on the turbulence flow through annular seals. He suggested with his study that increase of surface roughness causes higher pressure loss, and lower pressure drop in annular seals, which is caused by the duct loss coefficient at the inlet.

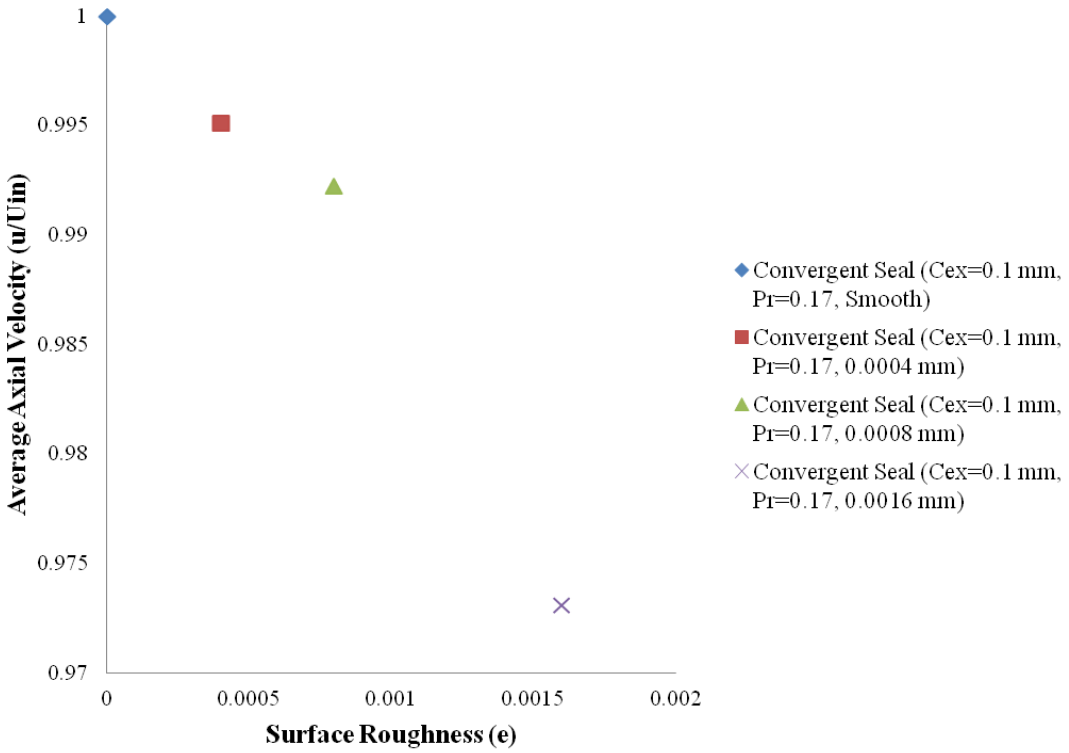

Fig. 71 Average exit axial velocities for the convergent seals (C_{ex}=0.1 mm, roughness=0-0.0004-0.0008-0.0016 mm, 20,200 rpm, X/L=1, Pr=0.17)

In figure 71, average exit axial velocity distributions with respect to the different surface roughness heights for the convergent seals with 0.1 mm exit seal clearances, and

0.17 pressure ratios are presented. Results show that convergent seal configurations with smooth surfaces give the highest axial velocity, and the increase of the surface roughness height causes the decrease of the axial velocity. The same analyses are also performed for the same seal configurations with higher seal clearances. There is about 3 % decrease in the axial velocity with the increase of the roughness height.

Table 21 Non-dimensional boundary layer thickness (e+) for the convergent seal (C_{ex}=0.1 mm, 20,200 rpm, rotor wall, X/L=1, Pr=0.17)

Roughness	e+
0	0
0.0004	0.926
0.0008	2.138
0.0016	4.776

Table 21 includes non-dimensional boundary layer thicknesses with respect to the different roughness heights for the convergent seal configurations with 0.1 mm exit seal clearances. Results show that there is about 79 % increase in the non-dimensional boundary layer thickness with the increase of the roughness height. Effects of the surface roughness height on the non-dimensional boundary layer thickness is almost the same for both seal configurations. Additionally, convergent seal geometry causes the increase of the non-dimensional boundary layer, which is caused by the higher axial velocity, which makes boundary layer thinner. There is about 39 % increase in the e+ for the convergent seal configurations compared to the straight annular ones. In addition,

convergent seal configurations exhibit larger non-dimensional boundary layer thickness than straight annular seal configurations.

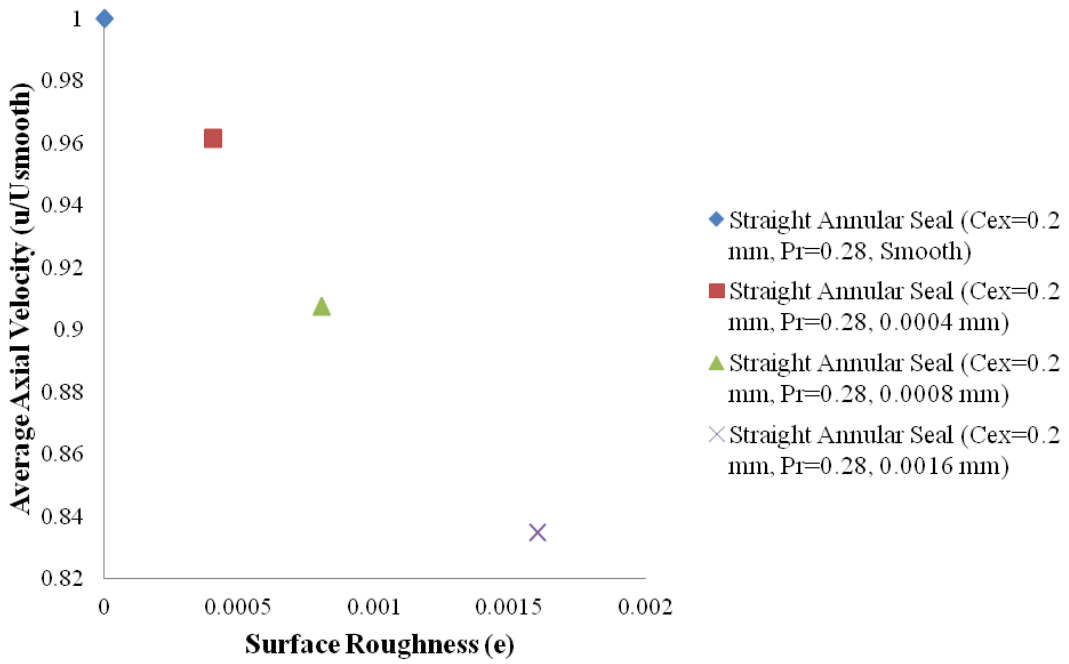

Fig. 72 Average exit axial velocity for the straight annular seals (C_{ex}=0.2 mm, roughness=0-0.0004-0.0008-0.0016 mm, air flow, 20,200 rpm, X/L=1, Pr=0.28)

In figure 72, the average exit axial velocity distributions with respect to the different surface roughness heights for the straight annular seals with 0.2 mm exit seal clearances, and 0.28 pressure ratios are presented. These analyses are performed when the shaft speed is set at 20,200 rpm. Results show an increase of the surface roughness height causes the decrease of the axial velocity, which decreases the linear inertia of the flow. Due to the decrease of the linear inertia, effects of the circumferential stresses,

which are introduced to the system by the swirl velocity, on the flow increase. There is about 16 % decrease in the axial velocity with the increase of the roughness height.

Table 22 Non-dimensional boundary layer thickness (e+) for the straight annular seal (C_{ex}=0.2 mm, 20,200 rpm, rotor wall, X/L=1, Pr=0.28)

Roughness	e+
0	0
0.0004	0.592
0.0008	1.177
0.0016	2.342

Table 22 includes non-dimensional boundary layer thicknesses with respect to the different roughness heights for the straight annular seal configurations with 0.2 mm exit seal clearances. Results show that there is about 75 % increase in the non-dimensional boundary layer thickness with the increase of the roughness height.

In figure 73 average exit axial velocities at the exit plane with respect to the different surface roughness heights for the convergent seal configurations with 0.2 mm exit seal clearances are presented. Results show that there is about 5 % decrease in the axial velocity with the increase of the roughness height.

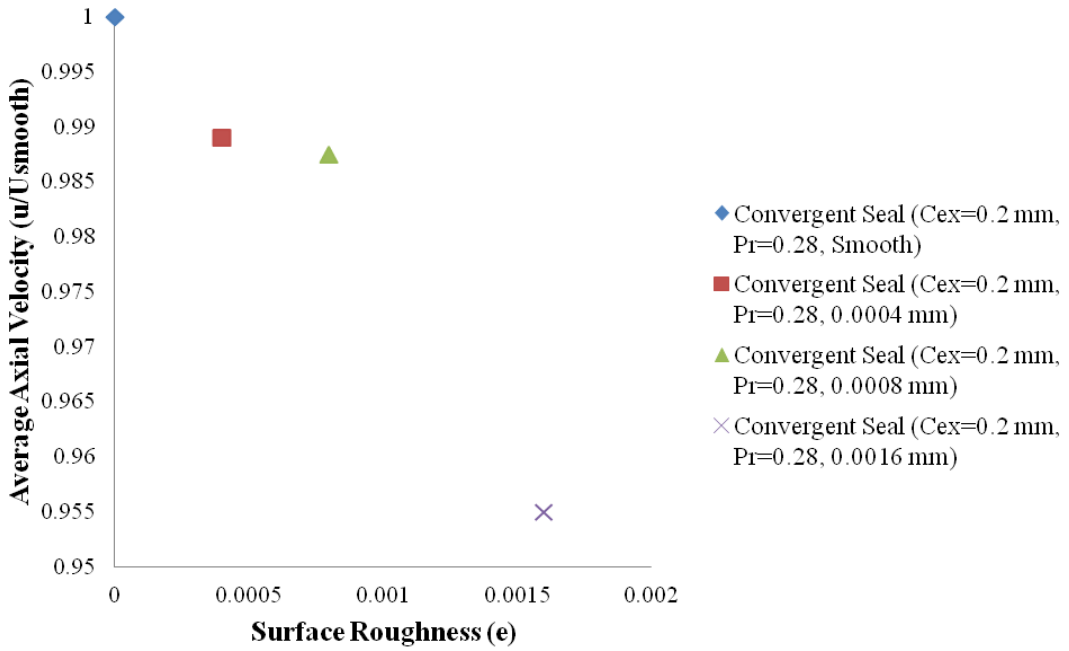

Fig. 73 Average exit axial velocity for the convergent seals (C_{ex}=0.2 mm, roughness=0-0.0004-0.0008-0.0016 mm, 20,200 rpm, X/L=1, Pr=0.28)

Table 23 includes non-dimensional boundary layer thicknesses with respect to the different roughness heights for the convergent seal configurations with 0.2 mm exit seal clearances. Results show that there is about 79 % increase in the non-dimensional boundary layer thickness with the increase of the roughness height. The convergent seal configurations gives about 37 % higher the non-dimensional boundary layer thickness than straight annular seal configurations, which is resulted from the higher axial velocity formation in the convergent seal configurations, which makes boundary layer thinner.

Table 23 Non-dimensional boundary layer thickness (e+) for the convergent seal (C_{ex}=0.2 mm, 20,200 rpm, rotor wall, X/L=1, Pr=0.28)

Roughness	e+
0	0
0.0004	0.777
0.0008	1.734
0.0016	3.744

In the previous section, axial exit velocity distribution with respect to the different surface roughness height for both straight annular, and convergent seal configurations are presented. Results show that average axial velocity decreases with the increase of the roughness height. The non-dimensional boundary layer thicknesses are also analyzed, and results show that the increase of the roughness height makes non-dimensional boundary layer thickness higher, which causes the increase of the drag affecting the flow. When leakage rate is analyzed with respect to the different surface roughness heights for both convergent, and straight annular seal configurations, it can be seen that leakage rate decreases with the increase of the roughness height. The increase of the drag on the flow makes linear inertia of the flow lower, which increases the dissipation rate of the flow kinetic energy. There is about 24-20 % decrease in the leakage rate with the increase of the roughness height.

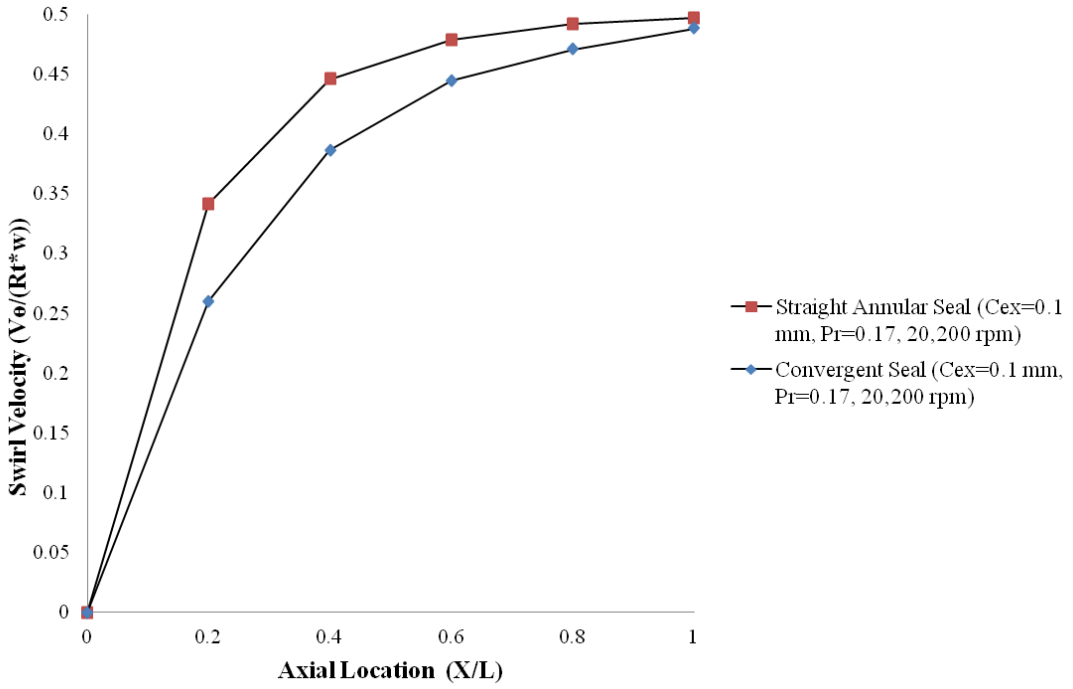

Fig. 74 Average swirl velocity distributions for the straight annular and convergent seals (C_{ex}=0.1 mm, air flow, 20,200 rpm, Pr=0.17)

In figure 74, average swirl velocity distributions along the axial direction for the convergent, and straight annular seal configurations with 0.1 mm exit seal clearances, and 0.17 pressure ratios are shown. Additionally, shaft speed is set at 20,200 rpm for both cases. Results show that swirl velocity increases up to the exit plane, and the straight annular seal configuration produces greater swirl velocity distribution, which is caused by the lower seal clearance. The straight annular seal configuration develops about 2 % higher swirl velocity at the exit plane than the convergent seal configuration. Swirl velocities at the exit plane for both seal configurations are almost equal with a value of 0.5.

As specified previously, Rhode [27] performed a study to investigate the leakage characteristics of annular and staggered labyrinth seal configurations. He also analyzed the swirl velocity distributions in the axial and radial directions with respect to the different seal clearances for these seal configurations. His results show that staggered labyrinth seal configurations exhibits greater swirl formation, and swirl velocity decreases with the increase of the seal clearances. He suggested that higher seal clearances cause the decrease of the residence time, which results in the decrease of the swirl velocity, and the increase of the circumferential stress effects along the shear layer, which provides greater swirl velocity formations. Additionally, it can be deduced from these analyses that increase of the seal clearance provides better stability due to the decrease of the swirl velocity.

The same analyses are also performed same seal configurations with different seal clearances, and results will be presented in the following section. In the following section, average swirl velocity distributions for different seal configurations will be analyzed.

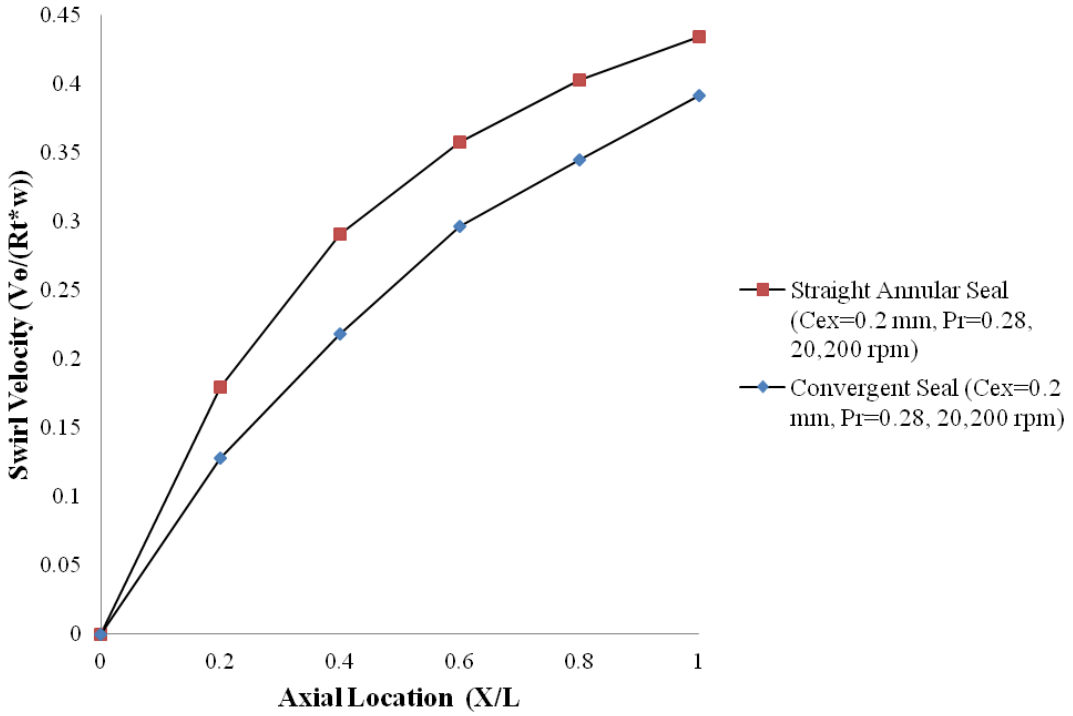

Fig. 75 Average swirl velocity distributions for the straight annular and convergent seals (C_{ex}=0.2 mm, 20,200 rpm, Pr=0.28)

In figure 75, the average swirl velocity distributions along the axial direction for the convergent, and straight annular seal configurations with 0.2 mm exit seal clearances, and 0.28 pressure ratios are shown. Additionally, shaft speed is set at 20,200 rpm for both case. Results show that swirl velocity increases up to the exit plane, with the straight annular seal configuration producing about 10 % higher swirl velocity at the exit plane than convergent seal, which is caused by the lower seal clearance. In addition, higher swirl velocity shows circumferential stress effects are higher, which causes the decrease of the linear inertia of the flow, and the increase of the dissipation rate of the flow kinetic energy. These data show that the smaller residence time caused by the larger

clearance and resulting higher leakage rate prohibit the average swirl velocity from reaching the 0.5 value seen for the smaller clearance. The seal would have to be longer to achieve the 0.5 value.

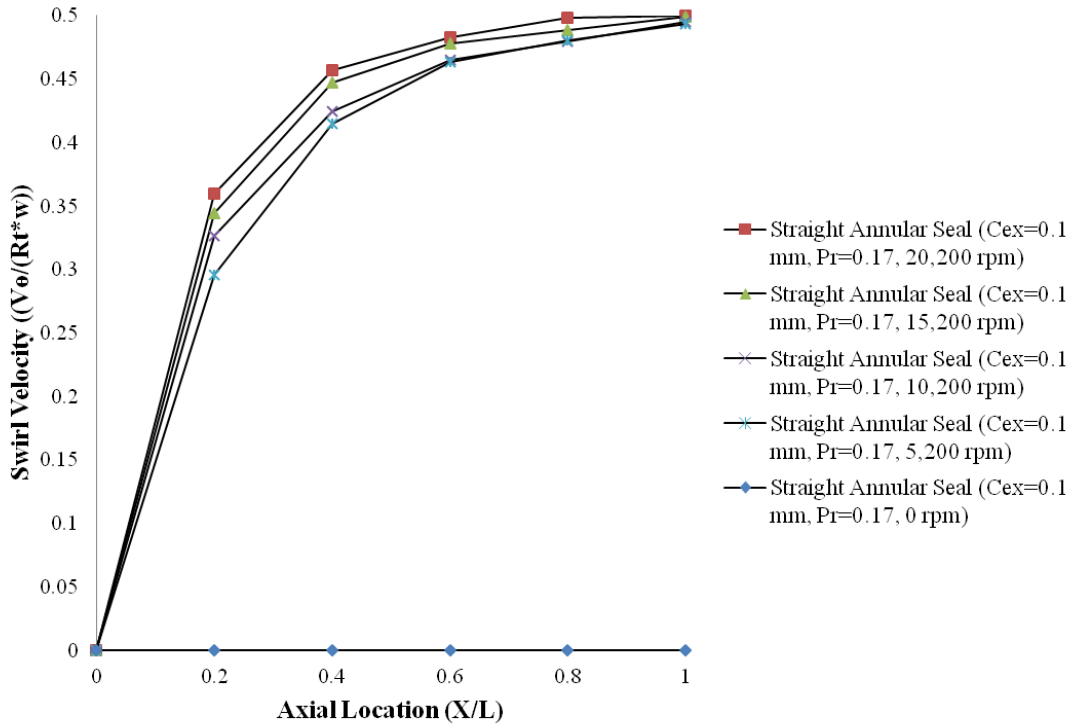

Fig. 76 Average swirl velocity distributions for the straight annular seals (C_{ex}=0.1 mm, 20,200 rpm, X/L=0-0.2-0.4-0.6-0.8-1, Pr=0.17)

In figure 76, the average swirl velocity distributions along the axial direction with respect to the different shaft speeds for the straight annular seal configurations with 0.1 mm exit seal clearances, and 0.17 pressure ratios are shown. Results show that swirl velocity increases with the increase of the shaft speed, and there is about 1 % increase in the swirl velocity with the increase of the shaft speed. The increase of the shaft speed

causes the increase of the centrifugal forces, which push the flow to the stationary stator wall. This causes the increase of the static pressure in the radial direction, and circumferential stresses on the wall.

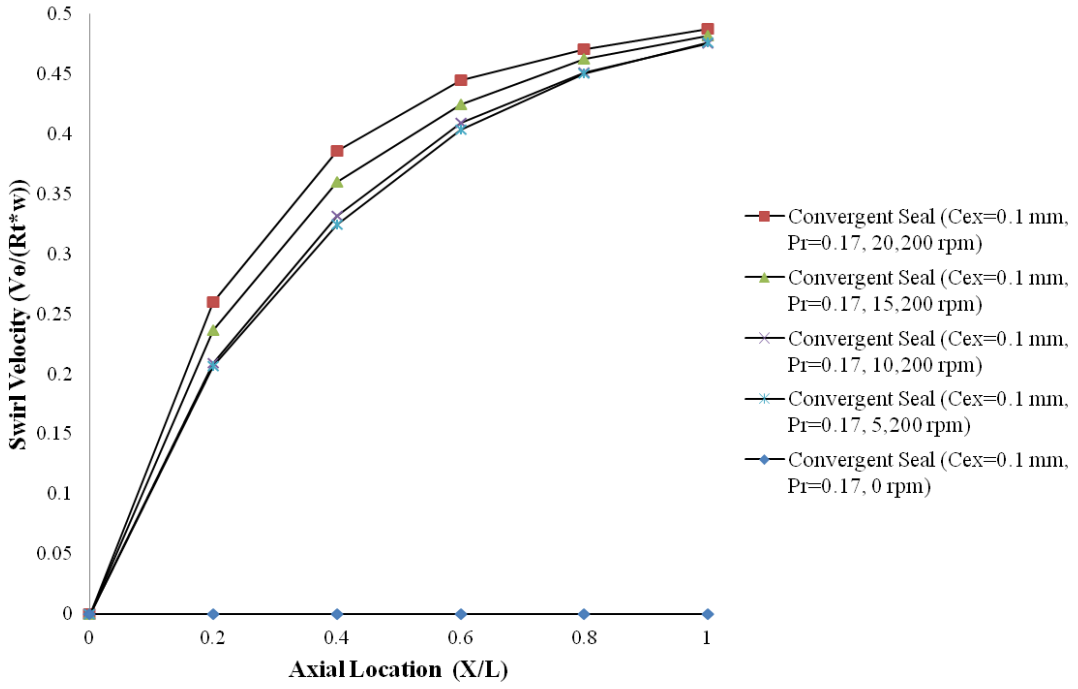

Fig. 77 Average swirl velocity distributions for the convergent seals (C_{ex}=0.1 mm, air flow, 20,200 rpm, X/L=0-0.2-0.4-0.6-0.8-1, Pr=0.17)

In figure 77, the average swirl velocity distributions along the axial direction with respect to the different shaft speeds for the convergent seal configurations with 0.1 mm exit seal clearances, and 0.17 pressure ratios are shown. Results show that swirl velocity increases with the increase of the shaft speed, and there is about 2 % increase in the swirl velocity with the increase of the shaft speed.. Additionally, increase in the swirl

velocity with the increase of the shaft speed for the convergent seal configurations is higher than straight annular ones.

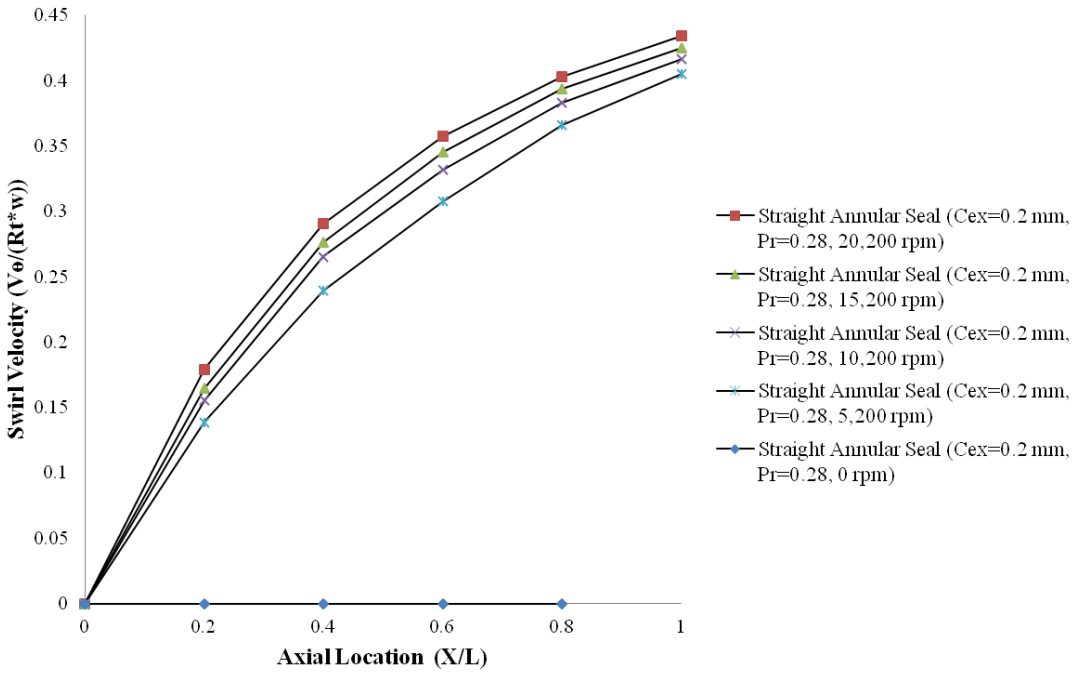

Fig. 78 Average swirl velocity distributions for the straight annular seals (C_{ex}=0.2 mm, 20,200 rpm, X/L=0-0.2-0.4-0.6-0.8-1, Pr=0.28)

In figure 78, the average swirl velocity distributions along the axial direction with respect to the different shaft speeds for the straight annular seal configurations with 0.2 mm exit seal clearances, and 0.28 pressure ratios are presented. Results show that swirl velocity increases with the increase of the shaft speed, which increases the effects of the tangential stresses on the flow. There is about 7 % increase in the swirl velocity with the increase of the shaft speed.

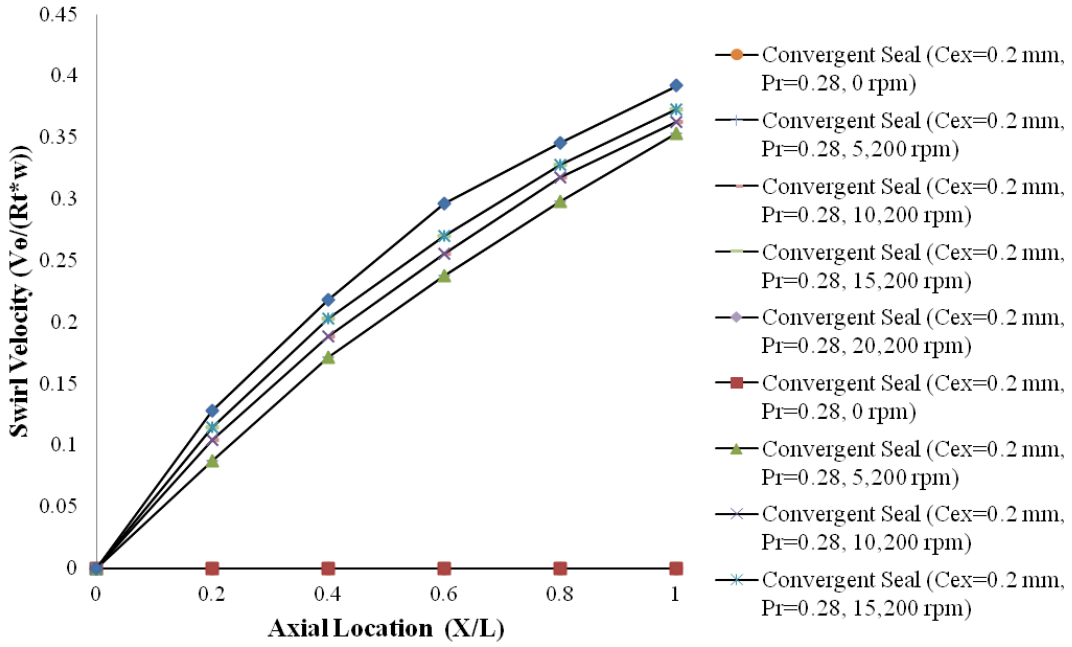

Fig. 79 Average swirl velocity distributions for the straight annular seals (C_{ex}=0.2 mm, 20,200 rpm, X/L=0-0.2-0.4-0.6-0.8-1, Pr=0.28)

In figure 79, the average swirl velocity distributions along the axial direction with respect to the different shaft speeds for the convergent seal configurations with 0.2 mm exit seal clearances, and 0.28 pressure ratios are presented. Results show that swirl there is about 10 % increase in the swirl velocity with the increase of the shaft sped while the straight annular seal configurations exhibit 7 % increase. Additionally, straight annular seal configurations produces higher swirl velocity than convergent seal configurations.

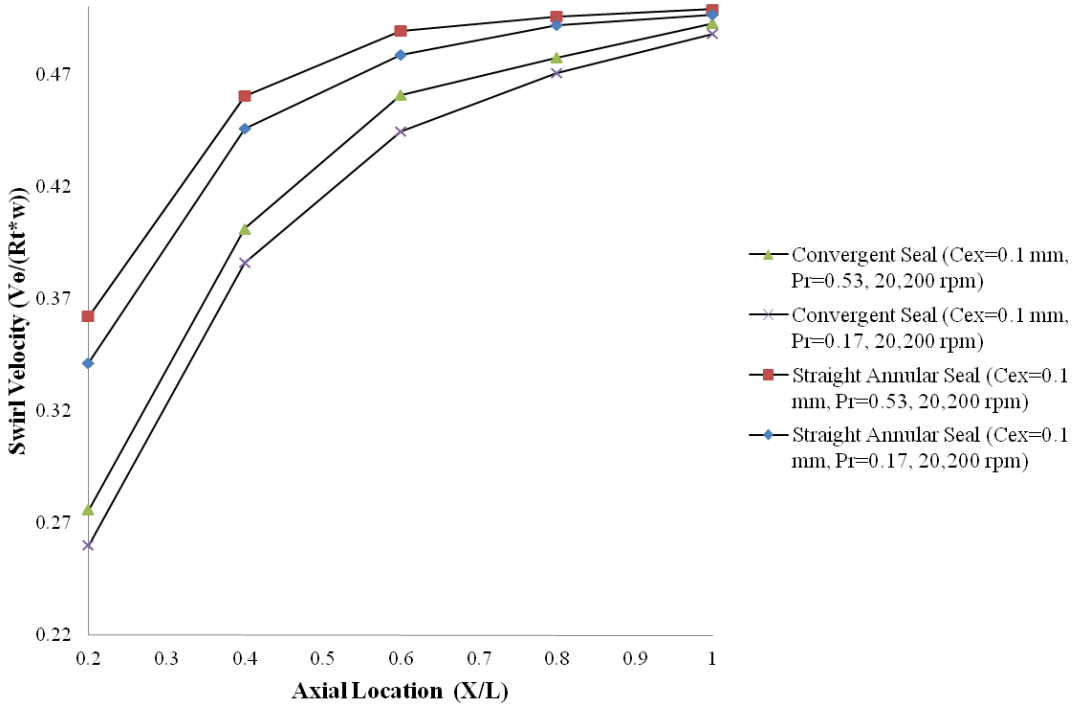

Fig. 80 Average swirl velocity for the straight annular and convergent seals (C_{ex}=0.1 mm, 20,200 rpm, X/L=0-0.2-0.4-0.6-0.8-1, Pr=0.17-0.53)

In figure 80, the average swirl velocity distributions along the axial direction with respect to the different pressure ratios for the straight annular and convergent seal configurations with 0.1 mm exit seal clearances are presented. Shaft speeds for both case are set at 20,200 rpm. Results show that swirl velocity increases with the decrease of the pressure ratio. This is due to the lower axial velocity, which increase the residence time of the fluid allowing the tangential shear to generate a larger tangential velocity. Additionally, straight seal configurations give higher swirl velocity formations compared to the convergent seal configurations.

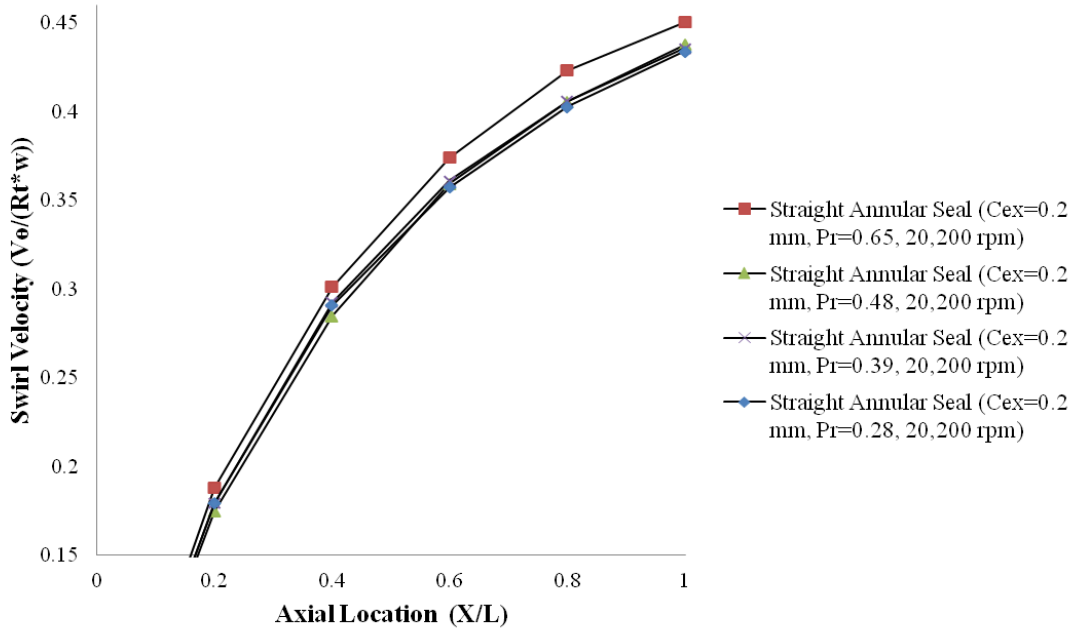

Fig. 81 Average swirl velocity for the straight annular seals (C_{ex}=0.2 mm, 20,200 rpm, X/L=0-0.2-0.4-0.6-0.8-1, Pr=0.0.28-0.39-0.48-0.65)

In figure 81, the average swirl velocity distributions along the axial direction with respect to the different pressure ratios for the straight annular seal configurations with 0.2 mm exit seal clearances are presented. Shaft speeds are set at 20,200 rpm. Results show that 0.65 pressure ratio gives the highest swirl velocities along the axial direction. Again lower average axial velocity produces higher residence time, which causes the increase of the tangential velocity. The same analyses are also performed for the convergent seal configurations with 0.2 mm exit seal clearances, and results are same.

Swirl velocity distributions with respect to the different surface roughness heights are also analyzed, and results will be presented in the following section. Additionally, there is about 16 % decrease in the leakage rate with the decrease of the

pressure ratio. The decrease of the pressure ratio cause the increase in the swirl velocity, which is caused by the lower residence time.

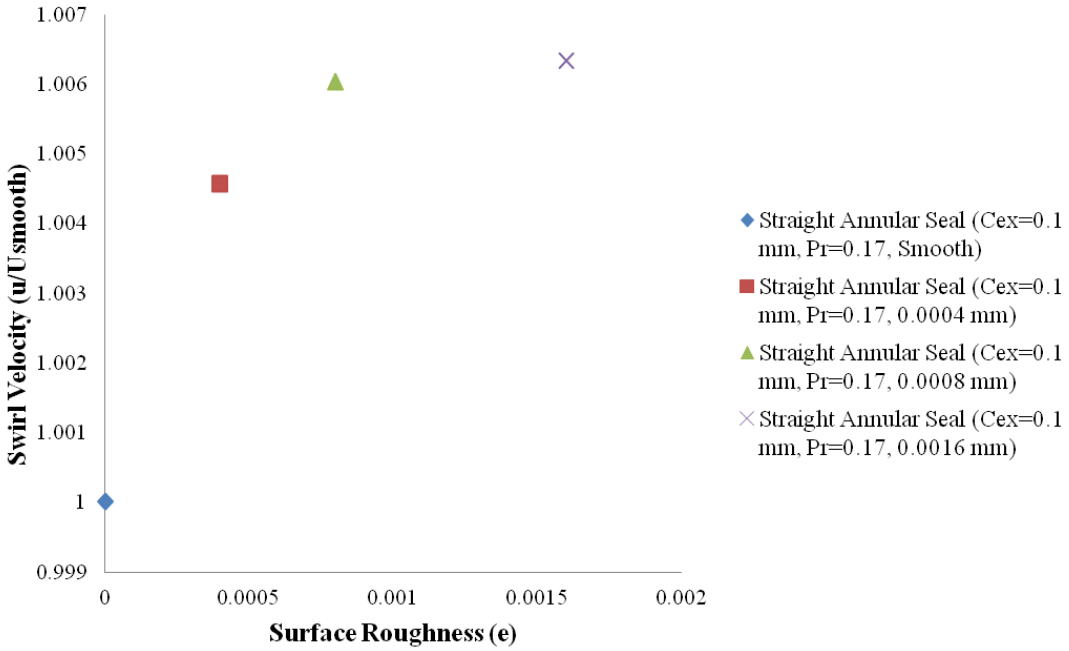

Fig. 82 Average swirl velocity for the straight annular seals (C_{ex}=0.1 mm, 20,200 rpm, X/L=1, Pr=0.17, roughness=0-0.0004-0.0008-0.0016 mm)

In figure 82, the average swirl velocity distributions along the axial direction with respect to the different surface roughness heights for the straight annular seal configurations with 0.1 mm exit seal clearances are presented. Shaft speeds are set at 20,200 rpm. Average swirl velocities at the exit planes of these seal configurations are presented. Results show that there is about 0.63 % increase in the swirl velocity with the increase of the surface roughness height. The increase of the roughness causes the increase of the circumferential stresses affecting along the free shear layers, which

provides greater swirl velocity formation. However, both the stator, and rotor surfaces were roughened resulting in a very small change in tangential velocity because shear stresses on both rotor, and stator surfaces balance each other. The same analyses are also performed for the water flow, and about 0.27 % increase in the average swirl velocity is observed.

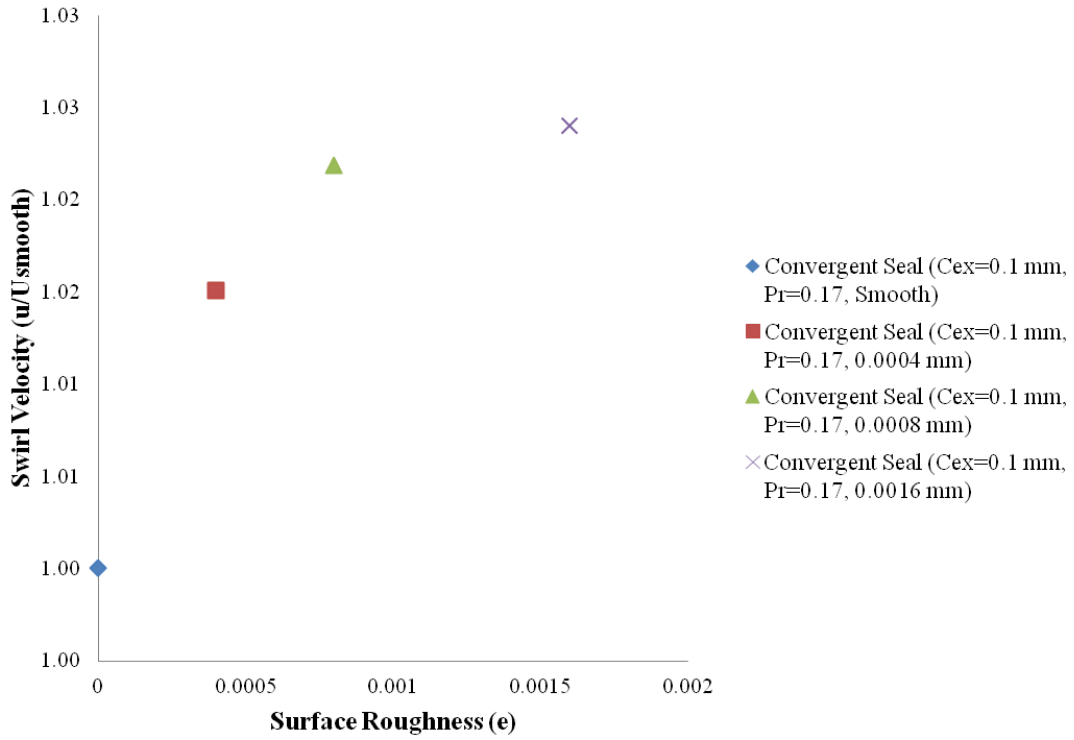

Fig. 83 Average swirl velocity for the straight annular seals (C_{ex}=0.1 mm, 20,200 rpm, X/L=1, Pr=0.17, roughness=0-0.0004-0.0008-0.0016 mm)

In figure 83, the average swirl velocity distributions along the axial direction with respect to the different surface roughness heights for the convergent seal configurations with 0.1 mm exit seal clearances are presented. Shaft speeds are set at

20,200 rpm. Results show that there is about 2 % increase in the swirl velocity with the increase of the surface roughness height. Same analyses are also performed convergent seal configurations. In the following section, average velocity distributions for the convergent seal configurations with 0.2 mm exit seal clearances, and 0.28 pressure ratios will be presented.

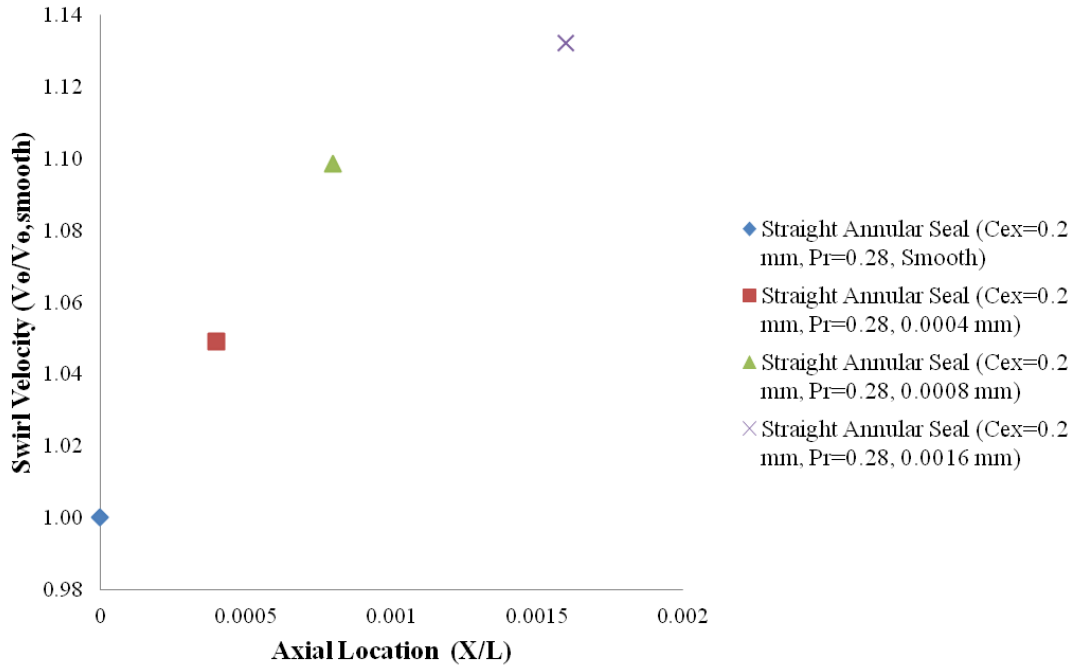

Fig. 84 Average swirl velocity for the straight annular seals (C_{ex}=0.1 mm, 20,200 rpm, X/L=1, Pr=0.17, roughness=0-0.0004-0.0008-0.0016 mm)

In figure 84, the average swirl velocity distributions along the axial direction with respect to the different surface roughness heights for the straight annular seal configurations with 0.2 mm exit seal clearances are presented. Shaft speeds are set at

20,200 rpm. Results show that there is about 13 % increase in the swirl velocity with the increase of the surface roughness height.

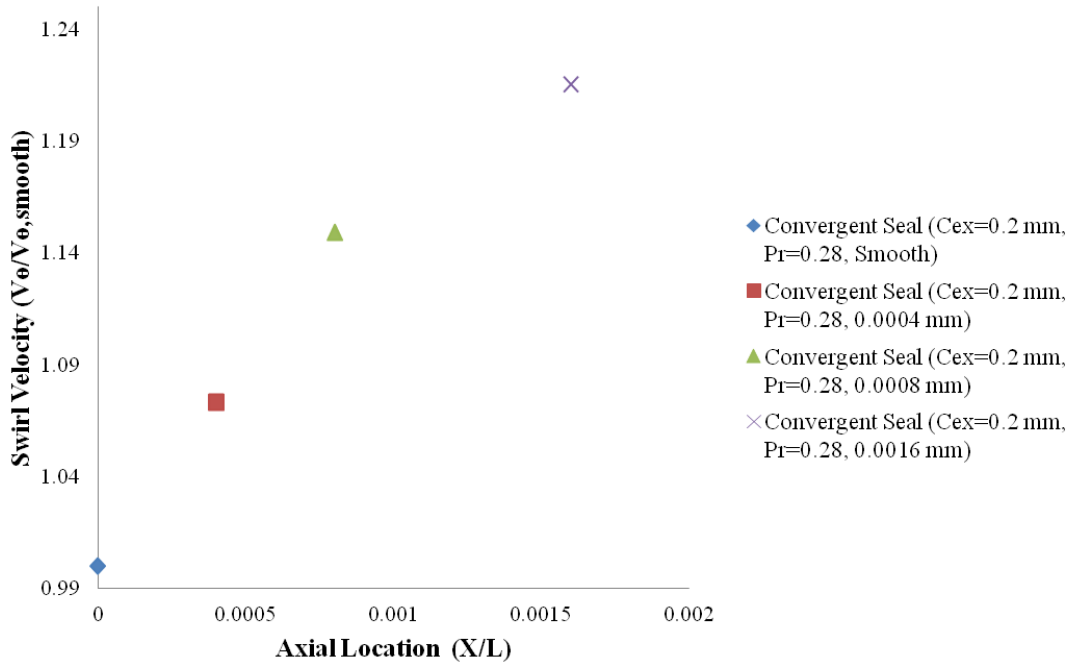

Fig. 85 Average swirl velocity distributions for the convergent seal configurations (C_{ex}=0.2 mm, air flow, 20,200 rpm, X/L=1, Pr=0.28, roughness=0-0.0004-0.0008-0.0016 mm)

In figure 85, average swirl velocity distributions along the axial direction with respect to the different surface roughness heights for the convergent seal configurations with 0.2 mm exit seal clearances, and 0.28 pressure ratios are presented. Shaft speeds are set at 20,200 rpm. Results show that there is about 21 % increase in the swirl velocity with the increase of the surface roughness height. The difference between the average swirl velocity distributions of the straight annular, and convergent seal configurations is

resulted from the seal clearance, which affects the non-dimensional boundary layer thickness.

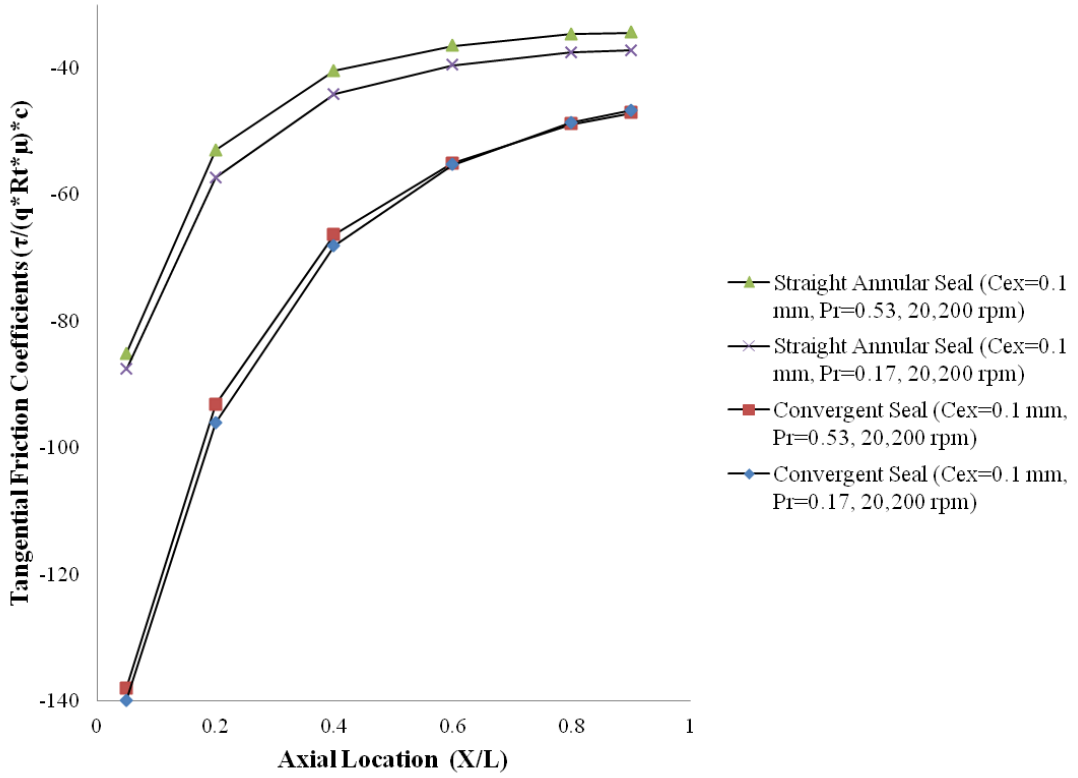

Fig. 86 Tangential friction coefficients on the rotor wall for the convergent and straight annular seal (C_{ex}=0.1 mm, 20,200 rpm, Pr=0.17-0.53)

In figure 86, the tangential friction coefficients on the rotor wall for the convergent, and straight annular seal configurations with 0.1 mm exit seal clearances are shown. Six data points are specified along the rotor wall for these seal configurations. Dynamic viscosities at these data points are found based upon the temperature at these points. Local clearances are calculated for convergent seal configurations, and then swirl

shear stresses are made non-dimensional. Figure 86 shows the effects of the seal clearances, and pressure ratios on the friction coefficients. Results show that convergent seal configurations give greater friction coefficients on the rotor wall compared to the straight annular seal configurations. Additionally, pressure ratio does not have a considerable effects on friction coefficient distributions on the rotor wall. Slight increase is observed with the decrease of the pressure ratio.

Convergent seal configurations cause the increase of the flow acceleration, which suppresses the boundary layer. Therefore, surface roughness heights protrude further into the flow, which makes non-dimensional boundary layer thickness larger. Due to this reason, convergent seal configurations give higher non-dimensional boundary layer thicknesses. Same analyses are also performed for the water flow, and convergent seal configurations exhibit same flow characteristics as in the air flow case.

In the following section, tangential friction coefficients on the rotor wall for both the straight annular and convergent seal configurations at 20,200 rpm shaft speed will be analyzed. As clearly seen in previous section, convergent seal configurations with 0.1 mm exit seal clearances exhibit greater tangential friction coefficients than straight annular seal configurations.

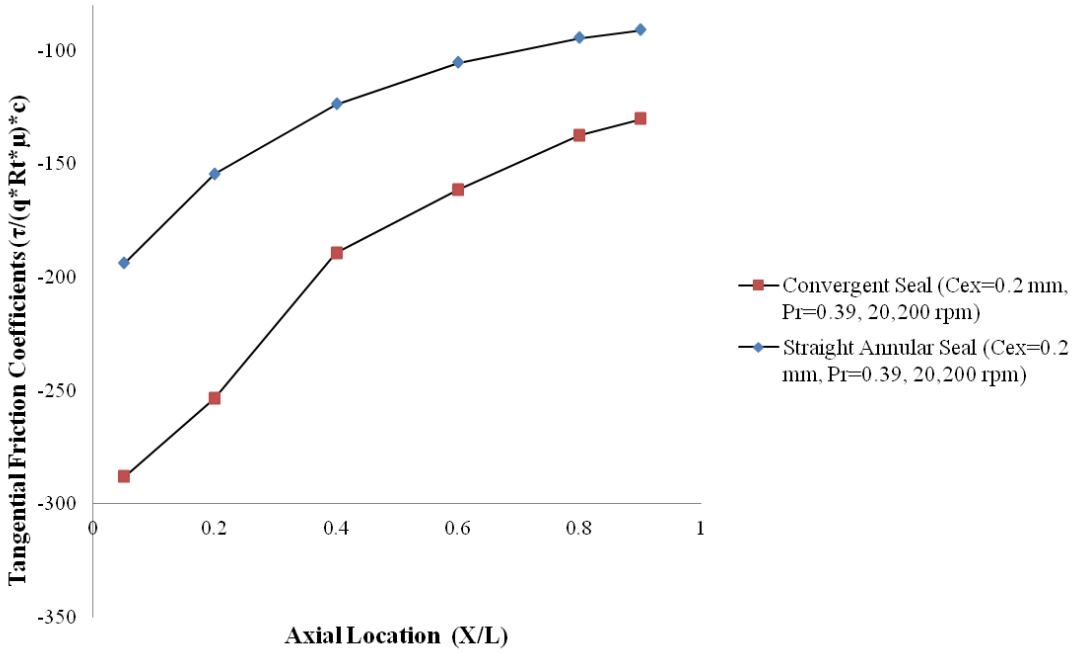

Fig. 87 Tangential friction coefficients on the rotor wall for the convergent and straight annular seals (C_{ex}=0.2 mm, air flow, 20,200 rpm, Pr=0.39)

In figure 87, the tangential friction coefficients on the rotor wall for the convergent, and straight annular seal configurations with 0.2 mm exit seal clearances are presented. Results show that the convergent seal configuration exhibits greater friction coefficient formation on the rotor wall, and friction coefficients continuously increase up to the exit plane. Variation of the tangential friction coefficients with respect to the shaft speeds will be analyzed in following section. Results show that the tangential friction coefficient distributions for the convergent seal configurations are in same trend with figure 86 but magnitudes are about 2 times larger, which is resulted from the higher seal clearance.

In figure 88, the tangential friction coefficients on the rotor wall for the straight annular seal configurations with 0.1 mm exit seal clearances, and 0.53 pressure ratios. Results show that the tangential friction coefficients decrease in magnitude with the increase of the shaft speed, and there is about 7 % change.

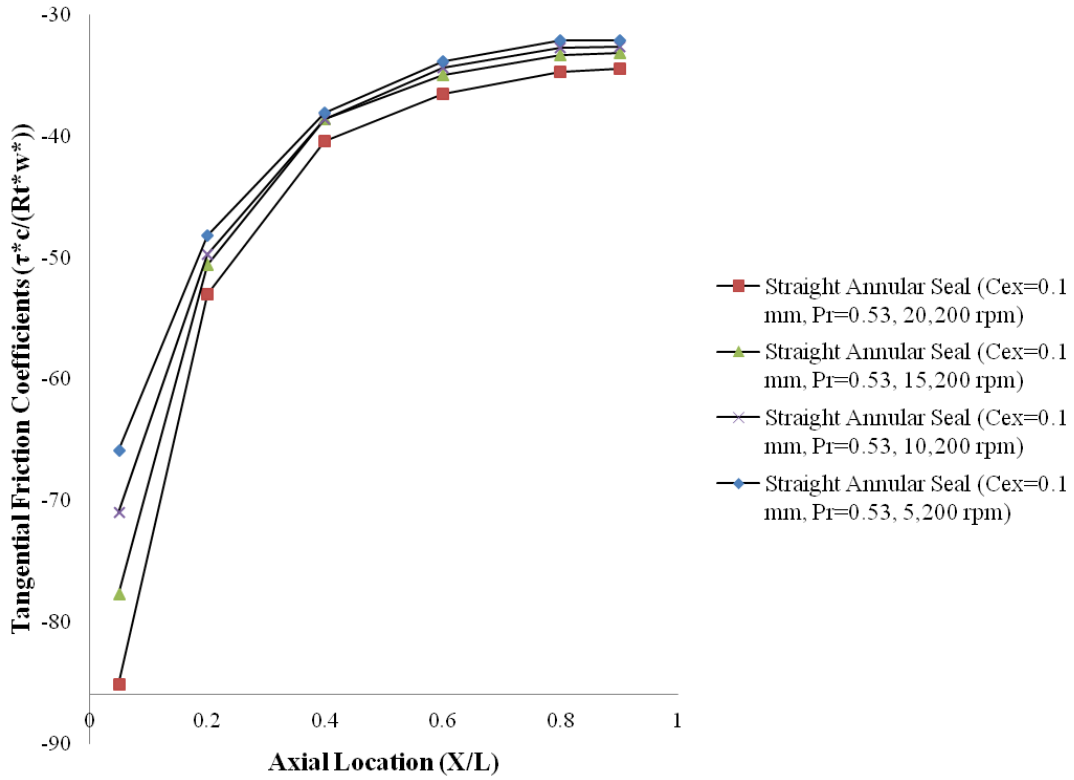

Fig. 88 Tangential friction coefficients on the rotor wall for the straight annular seals (C_{ex}=0.1 mm, air flow, 20,200 rpm, Pr=0.53)

In figure 89, the tangential friction coefficients on the rotor wall for the convergent seal configurations with 0.1 mm exit seal clearances, and 0.53 pressure ratios. Results show that the tangential friction coefficients increase with the increase of

the shaft speed, and there is about 2 % change. Additionally, convergent seal configurations produce 37 % higher tangential friction coefficients than the straight annular seal configurations.

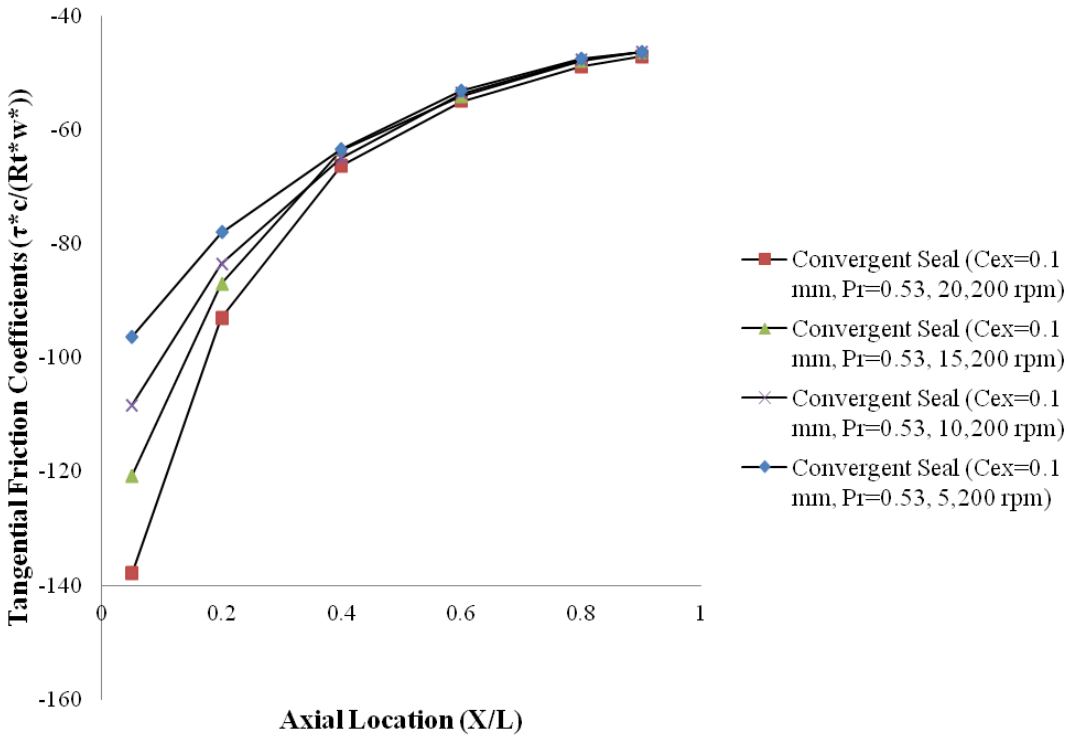

Fig. 89 Tangential friction coefficients on the rotor wall for the convergent seals (C_{ex}=0.1 mm, air flow, 20,200 rpm, Pr=0.53)

In figure 90, the tangential friction coefficients on the rotor wall for the straight annular seal configurations with 0.2 mm exit seal clearances, and 0.48 pressure ratios. Results show that the tangential friction coefficients decrease in magnitude with the increase of the shaft speed, and there is about 3 % change.

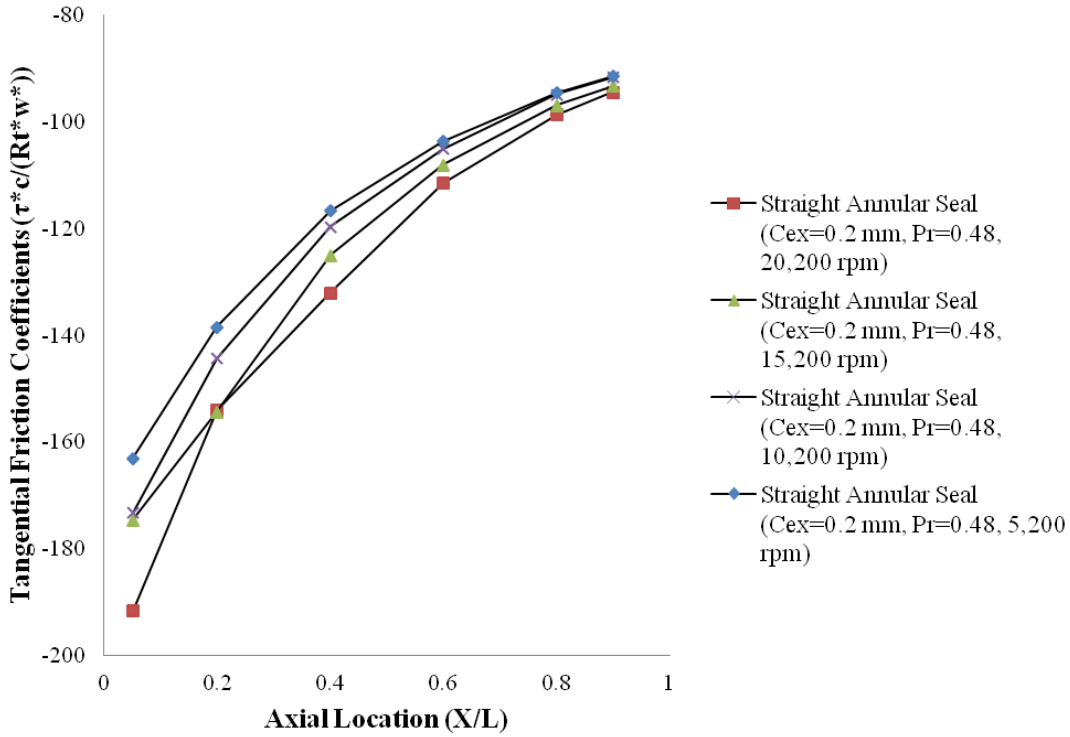

Fig. 90 Tangential friction coefficients on the rotor wall for the straight annular seals (C_{ex}=0.2 mm, air flow, 20,200 rpm, Pr=0.48)

In figure 91, the tangential friction coefficients on the rotor wall for the convergent seal configurations with 0.2 mm exit seal clearances, and 0.48 pressure ratios. Results show that the tangential friction coefficients decrease in magnitude with the increase of the shaft speed, and there is about 4 % change.

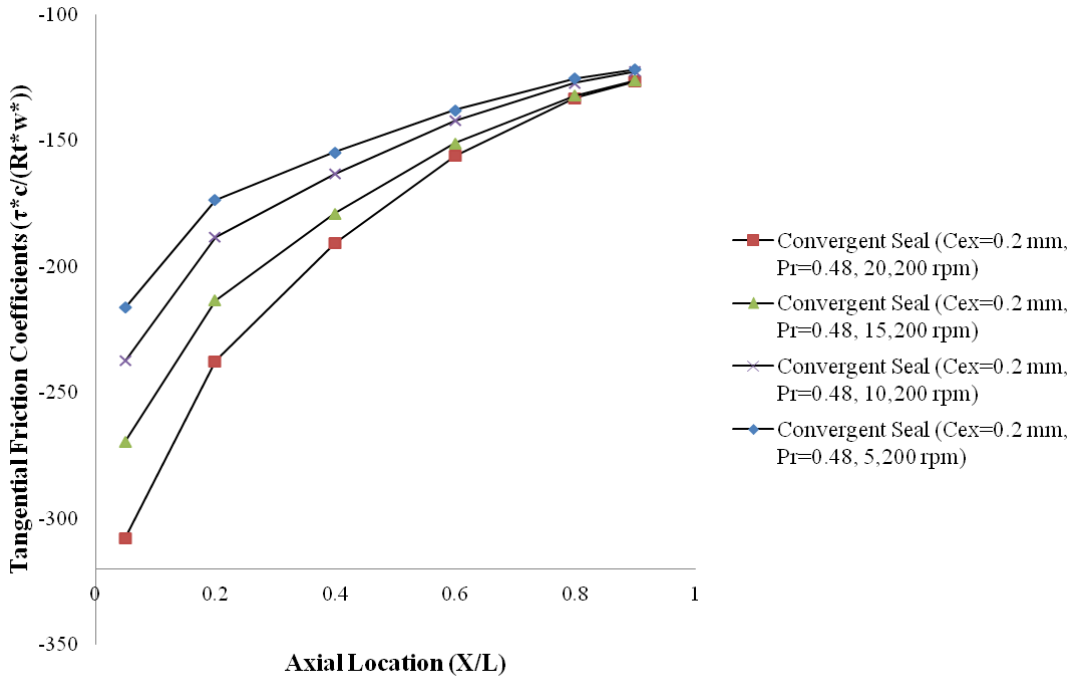

Fig. 91 Tangential friction coefficients on the rotor wall for the convergent seals (C_{ex}=0.2 mm, air flow, 0-20,200 rpm, Pr=0.48)

In addition to that, convergent seal configurations exhibits larger tangential frictional coefficients than straight annular seal configurations, and the increase of the seal clearance causes an increase of the tangential frictional coefficients in magnitude. Tangential friction coefficients at the exit plane at different shaft speeds for the convergent seal configurations are almost equal.

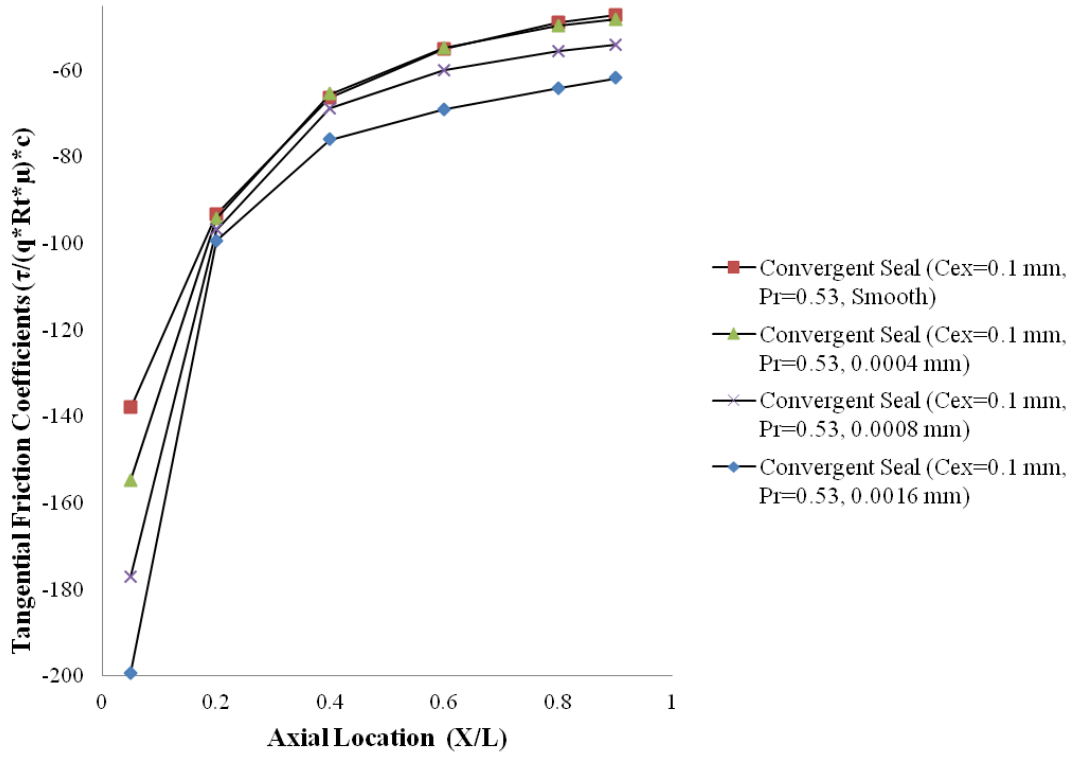

Fig. 92 Tangential friction coefficients on the rotor wall for the convergent seals (C_{ex}=0.1 mm, air flow, 20,200 rpm, Pr=0.53)

In figure 92, the tangential friction coefficients on the rotor wall for the convergent seal configurations with 0.1 mm exit seal clearances, and 0.53 pressure ratios are presented. Results show that the increase of the surface roughness causes an increase of the tangential friction coefficients magnitude along the rotor wall. Higher roughness height provides higher friction effects on the flow, which decrease the linear inertia of the flow. Due to the increase of circumferential stresses on the flow, dissipation rate of the flow kinetic energy also increases.

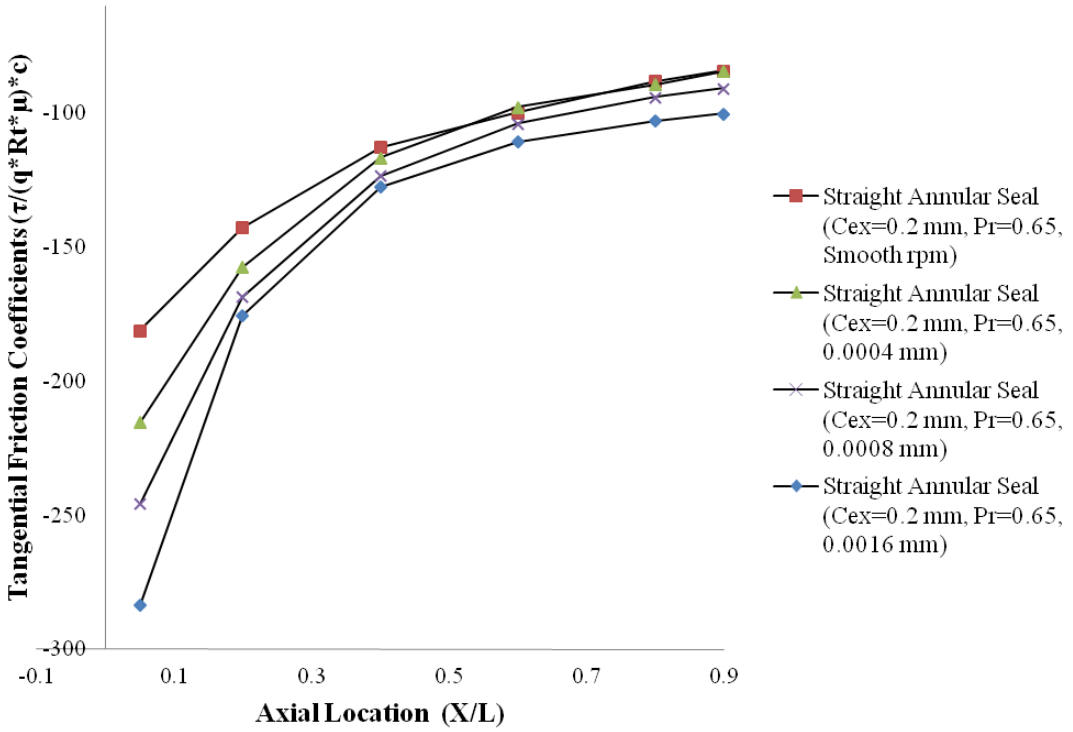

Fig. 93 Tangential friction coefficients on the rotor wall for the straight annular seals (C_{ex}=0.2 mm, air flow, 20,200 rpm, Pr=0.65)

In figure 93, the tangential friction coefficients on the rotor wall for the straight annular seal configurations with 0.2 mm exit seal clearances, and 0.65 pressure ratios are presented. Shaft speeds are set at 20,200 rpm for all cases. Results show that the increase of the surface roughness causes an increase of the tangential friction coefficients magnitude along the rotor wall. Higher roughness height provides higher friction effects on the axial flow, which decrease the linear inertia of the flow. Due to the increase of circumferential stresses on the flow, dissipation rate of the flow kinetic energy also increases.

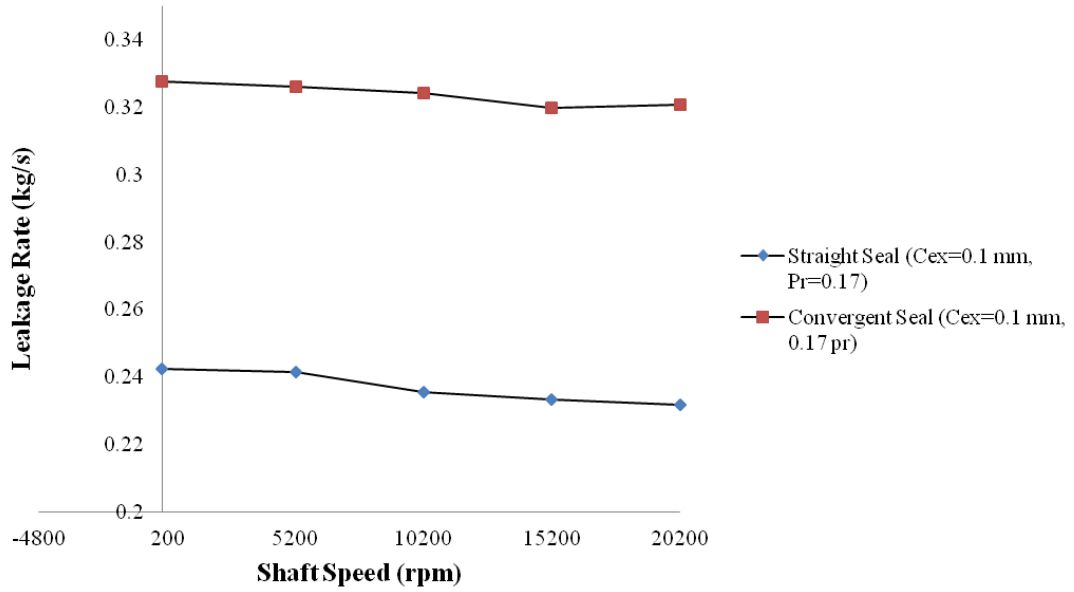

Fig. 94 Leakage rates for the straight annular and convergent seals (C_{ex}=0.1 mm, air flow, 0-20,200 rpm, Pr=0.17)

In figure 94, the leakage rates for the straight annular, and convergent seal configurations with 0.1 mm exit seal clearances, and 0.17 pressure ratios are presented. Results show that the leakage flow rate decreases with the decrease of the average seal clearances. As specified in the previous section, Rhode [27] also performed same analyses to investigate leakage characteristics of the annular and staggered labyrinth seal configurations. He applied two different seal clearances for performing the analyses. He suggested by his study that the increase of the seal clearances causes the increase of the linear inertia of the flow, which decrease effects of the circumferential stresses on the flow. Due to that reason, flow kinetic energy transferred along the seal increases. Figure 94 also shows the effects of the shaft speeds on the leakage rate. It can be deduced from this figure that shaft speeds do have not a significant impact on the leakage rate. Results

show that there is about 25 % decrease in the leakage flow rate with the decrease of the seal leakage. Additionally, there is about 4-5 % decrease in the leakage flow rate for both cases with the increase of the shaft speed.

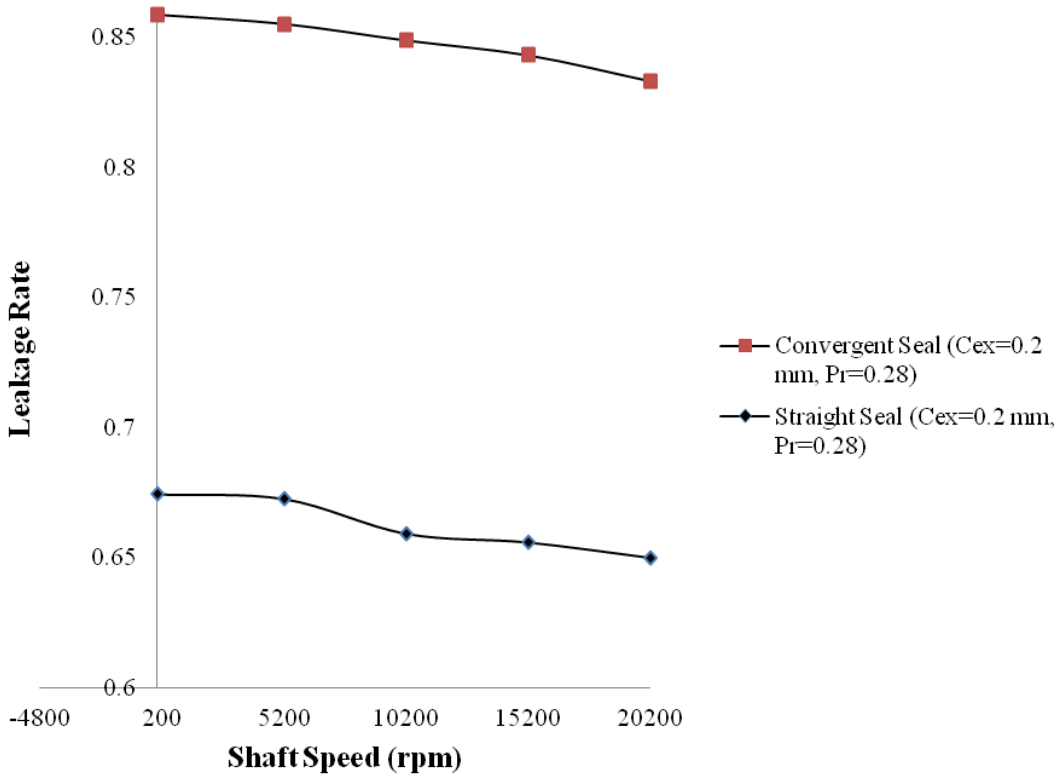

Fig. 95 Leakage rates for the straight annular and convergent seals (C_{ex}=0.2 mm, air flow, 0-20,200 rpm, Pr=0.28)

In figure 95, leakage rates for the straight annular, and convergent seal configurations with 0.2 mm exit seal clearances, and 0.28 pressure ratios are presented. Results show that the leakage flow rate decreases with the decrease of the seal clearances as in the previous case. Straight annular seal configurations give lower

leakage rates. There is about 21 % decrease in the leakage flow rate with the decrease of the seal clearance. In addition, the increase of the shaft speed causes about 5 % decrease in the leakage for both cases.

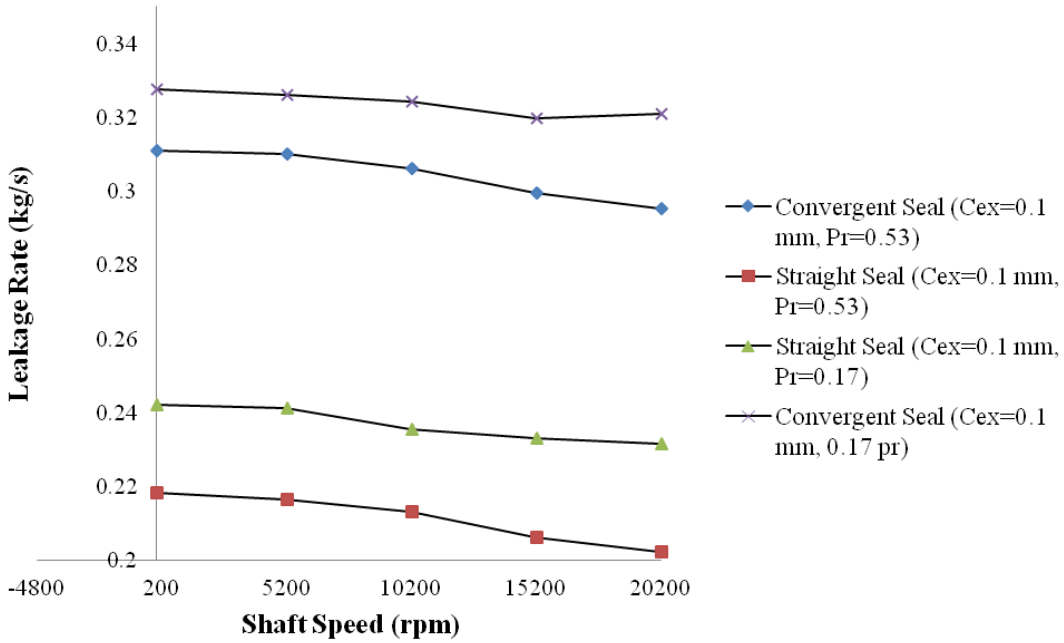

Fig. 96 Leakage rates for the straight annular and convergent seals (C_{ex}=0.1 mm, air flow, 0-20,200 rpm, Pr=0.17-0.53)

In figure 96, the leakage rates for the straight annular, and convergent seal configurations with 0.1 mm exit seal clearances, and 0.17-0.53 pressure ratios are presented. Results show that the increase of the pressure ratio gives lower leakage rates, and straight annular seal configurations exhibits better leakage characteristics compared to the convergent seal configurations. In figure 96, effects of the shaft speed on the

leakage are also presented. Results show that the increase of the shaft speed causes 8-5 % decrease in the leakage flow rate.

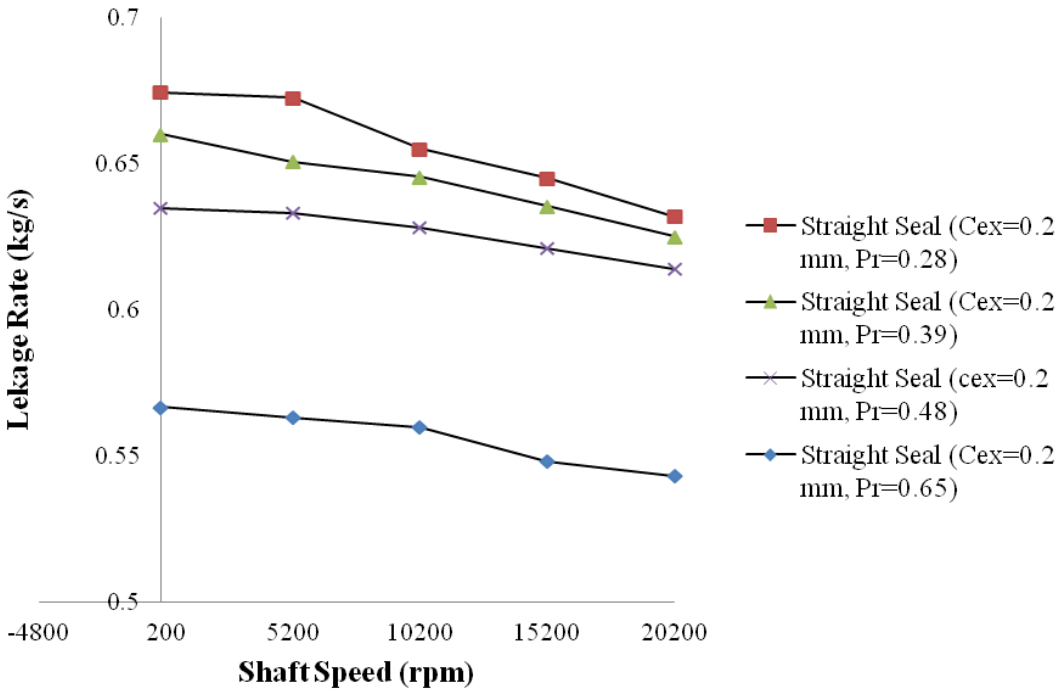

Fig. 97 Leakage rates for the straight annular seals (C_{ex}=0.2 mm, air flow, 0-20,200 rpm, Pr=0.28-0.39-0.48-0.65)

In figure 97, the leakage rates for the straight annular seal configurations with 0.2 mm exit seal clearances, and 0.28-0.39-0.48-0.65 pressure ratios are presented. Results show that the decrease of the pressure ratio gives lower leakage rates as is happened in the same seal configurations with 0.1 mm exit seal clearances. There is about 14 % decrease in the leakage flow rate with the decrease of the pressure ratio. The same analyses are also performed for the convergent seal configurations with 0.2 mm exit seal

clearances, and results do not change. In following section, variation of the leakage rates with respect to the different surface roughness heights will be analyzed, and results will be discussed. Additionally, it can be deduced from figure 97 that the there is about 7-4 % decrease in the leakage rate with the increase of the shaft speed.

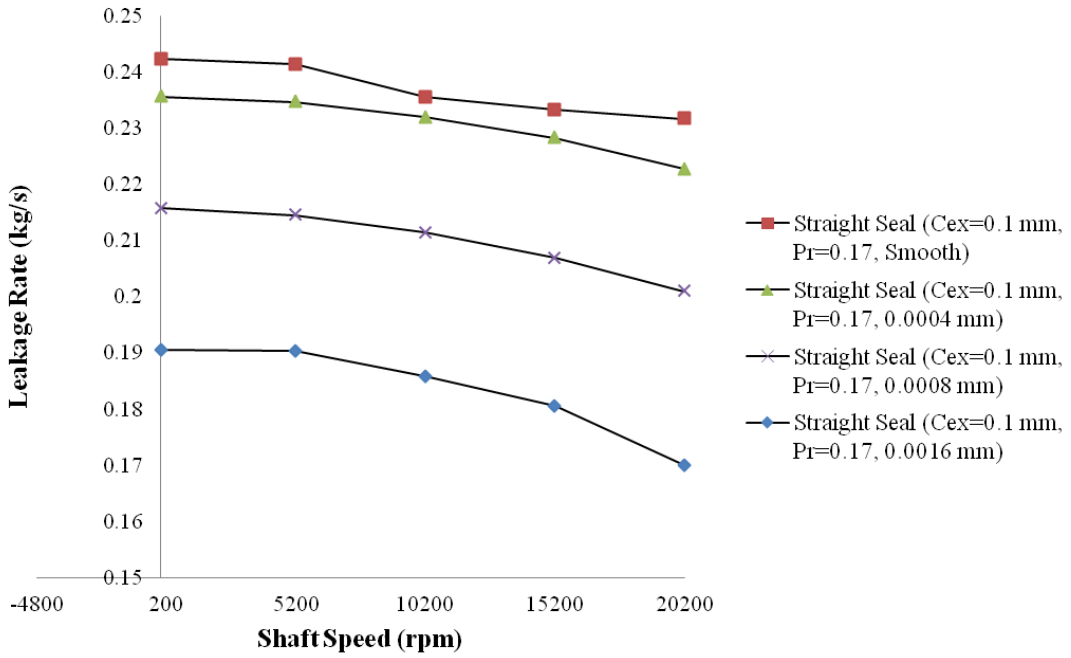

Fig. 98 Leakage rates for the straight annular seals (C_{ex}=0.1 mm, air flow, 0-20,200 rpm, Pr=0.17, roughness=0-0.0004-0.0008-0.0016 mm)

In figure 98, the leakage rates for the straight annular seal configurations with 0.1 mm exit seal clearances, and 0.17 pressure ratios are presented. Results show that the increase of the surface roughness heights gives lower leakage rates. The increase of the surface roughness on the wall causes the increase of the effects of viscous shear stresses along the free shear layers. Due to that reason, the effects of the circumferential stresses

dominate the linear inertia of the flow. As a consequence of that, the flow kinetic energy transferred along the seal length is decreases, an secondary flow rate decreases. In addition to that the increase of the shaft speed causes 10 % decrease in the leakage flow rate.

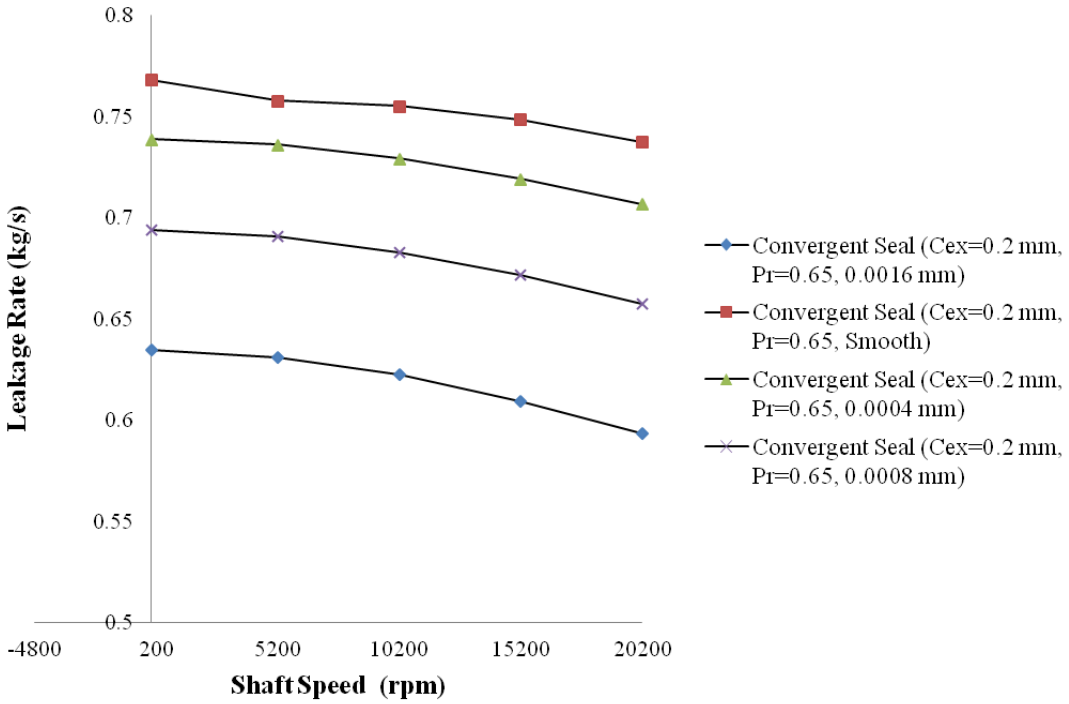

Fig. 99 Leakage rates for the convergent seals (C_{ex}=0.2 mm, air flow, 0-20,200 rpm, Pr=0.65, Roughness=0-0.0004-0.0008-0.0016 mm)

In figure 99, the leakage rates for convergent seal configurations with 0.2 mm exit seal clearances, and 0.65 pressure ratios are presented. Results show that the increase of the surface roughness heights gives lower leakage rates as in the previous section, and the decrease in the leakage flow rate is about 20 %. The increase of the

surface roughness on the wall causes the increase of the effects of viscous shear stresses along the free shear layers. Due to that reason, the effects of the circumferential stresses dominate the linear inertia of the flow. As a consequence of that, the flow kinetic energy transferred along the seal length is decreases, an secondary flow rate decreases. In addition, there is about 6 % decrease in the leakage flow rate with the increase of the shaft speed.

In terms of rotordynamic aspect, keeping the swirl velocity as low as possible is a very important point. In this study, effects of the seal clearance, surface roughness, and pressure ratio on the swirl formation are analyzed for both air, and water flow. Results show that straight annular seal configurations exhibit higher swirl velocity formations than convergent seal configurations under same working conditions, which is resulted from the lower seal clearance. In addition, the increase of the surface roughness causes small increases of the swirl velocity for both water, and air cases. Effects of the pressure ratio are also analyzed, and results show that the decrease of the pressure ratio causes an increase of the swirl velocity. As a consequence of these analyses, it can be said that keeping the surface roughness height, and pressure ratio low, and average seal clearance as high as possible provides better seal characteristics in the rotordynamic aspect.

These analyses also show that leakage flow rate decreases considerably with the increase of the roughness height on both rotor, and stator walls. Additionally, higher seal clearance causes an increase of the leakage flow rate, and convergent seal configurations produce higher leakage flow rate than straight annular ones. Table 24 includes the maximum, and minimum leakage flow rates for the convergent, and straight annular seal

configurations. Table 24 shows that maximum leakage flow rate for the convergent seal configurations with smaller clearance is about 0.3 kg/s. There is a slight difference between the straight annular, and convergent seal configurations. Straight annular sea configurations exhibits better leakage characteristics than convergent seal configurations under same working conditions. In addition, table 24 also shows that increase of the shaft speed causes an increase in the leakage flow rate, which decreases the efficiency of the system.

Table 24 Maximum, and minimum leakage rates for the convergent and straight annular seals (Pr=0.53-0.17, Pr=0.28-0.65)

Clearance	Convergent	Straight
0.1	0.311	0.242
0.1	0.224	0.148
0.2	0.859	0.674
0.2	0.594	0.417

7.SUMMARY AND CONCLUSIONS

7.1. Comparison of the Standard k-ε Model, and Enhanced Wall Treatment Model

Flow simulations are performed by applying both the standard k-ε model, and the enhanced wall treatment models. In order to understand the flow behavior under the effects of the surface roughness, the standard wall function model is used. It is concluded from the simulations performed with these two turbulent models that the leakage rates do not change significantly with the variation of the turbulent model. The enhanced wall treatment model cannot be used to perform the flow simulations with surface roughness.

7.2. Effects of the Seal Clearance

In this study, effects of seal clearances on water and air flow through the convergent, and straight annular seal configurations are investigated. Two different seal clearances are applied to both the convergent, and straight annular seal configurations. Static pressure distributions, axial velocity, and swirl velocity distributions with respect to the different exit seal clearances are analyzed. It is observed that straight annular seal configurations exhibit linear pressure distributions as a main difference from the convergent seal configurations. In order to understand the main reason, the pressure gradient variations based upon different seal clearances are analyzed. The pressure gradient-to-axial wall shear stress ratios are calculated for all seal configurations. After these analyses, a coefficient, which provides us with modeling the axial wall shear stress distributions based upon the pressure distributions.

The decrease of the seal clearances causes the slight decrease in the axial velocity formations. In addition, the greater swirl velocity formation is given by the seal configurations, which have lower exit seal clearances, which is caused by the low residence time. As a consequence, the decrease of the seal clearance causes the increase of the circumferential stresses affecting the flow. The linear inertia of the flow is dominated by the effects of the tangential stresses along the shear layer. Therefore, the flow leakage decreases with the decrease of the seal clearances, and is less for the straight annular seal configurations.

7.3. Effects of the Shaft Speed

Effects of the shaft speeds on the leakage flow through the convergent, and straight annular seal configurations are investigated as well. Five different shaft speeds are applied. Average swirl velocity distributions are analyzed with respect to the different shaft speeds, and a considerable increase in the swirl velocity is observed when the high shaft speeds are applied. Additionally, greater friction coefficients, which cause the increase of the dissipation rate of the flow kinetic energy, are obtained at the high shaft speeds. When the shaft speed is less than 15,000 rpm, effects of the shaft speed are not apparent because of rotational dependency. On the other hand, shaft speeds higher than 15,000 rpm, the flow linear inertia is dominated by the effects of tangential stresses, which affects along the free shear layers. As a result of this, the leakage rate decreases for all seal configurations at the highest shaft speed.

7.4. Effects of the Pressure Ratios, Gas Flow

Two different pressure ratios for the seal configurations with 0.1 mm exit seal clearances, and four different pressure ratios for the seal configurations with 0.2 mm exit seal clearances are analyzed. Effects of the pressure ratios are investigated just for the air flow. Average axial, and swirl velocity distributions with respect to the different pressure ratios are analyzed. Greater swirl formation is obtained at high pressure ratios. When pressure ratios is increased, it is observed that pressure drop along the axial direction decreases. As a consequence of this, effects of the shear stresses along the walls on the flow increases, and dissipation rate of the flow kinetic energy increases.

7.5. Effects of the Surface Roughness

Four different surface roughness heights are applied to both the stator, and rotor walls. It is observed that the increase of the surface roughness heights causes the increase of the effects of the friction forces on the flow. The effects of the surface roughness on the water flow are not apparent. In terms of air flow, higher surface roughness causes a significant decrease in the flow leakage. This is due to the thinner boundary layer for the gas flow compared to the liquid resulting in the surface roughness penetrating the flow more for the gas flow.

REFERENCES

[1] Ha, T., and Childs, D., 1994, "Annular Honeycomb Turbulent-Stator Turbulent Gas Seal Analysis Using New Friction-Factor Model Based on Flat Plate Tests," ASME J. Tribol., **116**, pp. 352-360.

[2] Kleyhans, G., and Childs, D., 1997, "The Acoustic Influence of Cell Depth on the Rotor Dynamic Characteristics of Smooth Rotor/Honeycomb Stator Annular Gas Seals," ASME J. Eng. Gas Turbines Power, **19**, pp. 949-957.

[3] Benckert, H., and Wachter, J., 1980, ‘‘Flow Induced Spring Coefficients of Labyrinth Seals for Application in Rotor Dynamics,’’ *Proceedings of the Annual Workshop on Rotordynamic Instability Problems in High-Performance Turbomachinery*, Texas A&M University, NASA cp 2133, pp. 189–212.

[4] Childs, D., Nelson, C., Scharrer, J., Elrod, D., and Hale, K., 1986, "Theory Versus Experiments for Rotor Dynamic Coefficients of Annular Gas Seals: Part 1-Test Facility and Apparatus," ASME J. Tribol., **108**, pp. 426-432.

[5] Kerr, B. G., 2004, "Experimental and Theoretical Rotordynamic Coefficients and Leakage of Straight Smooth Annular Gas Seals," M.S Thesis, Department of Mechanical Engineering, Texas A&M University, College Station, TX

[6] Nelson, C. C., and Nguyen, D. T., 1987, "Comparison of Hirs' Equation with Moody's Equation For Determining Rotordynamic Coefficients of Annular Pressure Seals," ASME J. Tribol., **109**, pp. 144-148.

[7] Childs, D., and Chang-Ho, Kim., 1985, "Analysis and Testing for Rotordynamic Coefficients of Turbulent Annular Seals with Different, Directionally-Homogeneous Surface Roughness Treatment for Rotor and Stator Elements," ASME J. Tribol., **107**, pp. 296-306.

[8] Hirs, G. G., 1973, "A bulk Flow Theory for Turbulence in Lubricant Films," ASME J. Lubrication Technology, **95**, pp. 137-146.

[9] Lucas, V., Danaila, S., Bonneau, O., and Frene, J., 1994, "Roughness Influence on Turbulent Flow through Annular Seals," ASME J. Tribol., **116**, pp. 321-329.

[10] Fleming, P., 1979, "Stiffness of Straight and Tapered Annular Gas Seals," ASME J. Lubrication Technology, **101**, No. 3, pp. 349-355.

[11] Fleming, P., 1980, "Damping in Ring Seals for Compressible Fluids", *Proceedings from a Workshop on Rotordynamic Instability Problems in High Performance TurboMachinery*, Texas A&M University, College Station TX, NASA CP2133, pp.169-188.

[12] Nelson, C. C., 1985, "Rotordynamic Coefficients for Compressible Flow in Tapered Annular Seals," ASME J. Tribol., **107,** pp. 318-325.

[13] Nelson, C., 1984, " Analysis for Leakage and Rotordynamic Coefficients of Surface Roughened Tapered Annular Gas Seals," ASME Trans. Engineering for Power, **106**, pp. 927-934.

[14] Childs, D., 1983, "Dynamic Analysis of Turbulent Annular Seals Based on Hirs' Lubrication Equations," ASME J. Lubrication Technology, **105**, pp. 429-436.

[15] Childs, D., 1983, "Finite-Length Solutions for the Rotordynamic Coefficients Turbulent Annular Seals," ASME J. Lubrication Technology, **105**, pp. 437-444.

[16] Black, H. F., 1969, "Effects of Hydraulic Forces in Annular Pressure Seals on the Vibrations of Centrifugal Pump Rotors," J. Mech. Engr. Sci., **11**, No. 2, pp. 206-213.

[17] Jenssen, D. N., 1970, "Dynamics of Rotor Systems Embodying High Pressure Ring Seals," PhD. Dissertation, Heriot-Watt University, Edinburgh, Scotland.

[18] Jenssen, D. N., and Black, H. F., 1970, "Dynamic Hybrid Properties of Annular Pressure Seals," Proc. J. Mech. Engr., **184**, pp. 92-100.

[19] Jenssen, D. N., and Black, H. F., 1971, "Effects of High-Pressure Ring Seals on Pump Rotor Vibrations," ASME Paper, No.71-WA/FF-38.

[20] Allaire, P. E., Gunter, E. J., Lee, C. P., and Barrett, L. E., 1976, "The Dynamic Analysis of the Space Shuttle Main Engine High Pressure Fuel Turbopump Final Report, Part II, Load Capacity and Hybrid Coefficients for Turbulent Interstage Seals," University of Virginia, Report UVA/528140/ME76/103.

[21] Ustinov, D. E., "Influence of Radial Seals on Dynamics of High Speed Rotors Supported by Fluid-Film Bearings with Cryogenic Lubrication, PhD. Dissertation, Orel State Technical University, Russia.

[22] Smalley, A.J., Camatti, M., Childs, D.W., Hollingsworth, J.R., Vannini, G., and Carter, J.J., 2006, "Dynamic Characteristics of the Diverging Taper Honeycomb-Stator Seal," ASME J. TurboMachinery, **128**, pp. 717-724.

[23] Marquette, O.R., Childs, D. W., and San Andres, L., 1997, "Eccentricity Effects on the Rotordynamic Coefficients of Plain Annular Seals; Theory Versus Experiment," ASME J. Tribol., **119**, pp. 443-448.

[24] Morrison, G. L., and Al-Ghasem, A., 2007, "Experimental and Computational Analysis of a Gas Compressor Windback Seal," *Proceeding of ASME Turbo Expo*, Montreal, Canada, GT2007-27986.

[25] Chupp, R. E., Hendrilciks, R. C., Lattime S. B., Steinetz, B. M., 2006, "Sealing in TurboMachinery," J. Propul.Power, **22**, pp. 313-349.

[26] Willenborg, K., Schramm, V., Kim, S., and Witting, S., 2002, "Influence of a Honeycomb Facing on the Heat Transfer in a Stepped Labyrinth Seal," ASME J. Eng. Gas Turbine Power, **124**, pp. 133-139.

[27] Rhode D. L., 1993, "Clearance Effects on Corresponding Annular and Labyrinth Seal Flow Leakage Characteristics," ASME J. Tribol., **115,** pp. 699-704.

[28] Childs, D. W., Dressman, J. B., 1985, "Convergent-Tapered Annular Seals: Analysis and Testing for Rotordyanmic Coefficients," ASME J. Tribol., **107**, pp. 307-316.

[29] Matsuzaki, Y., and Kazamaki, T, 1988, "Effect of Surface Roughness on Compressive Stress of Static Seals," JSME International J., **31**, pp. 103.

APPENDIX

Standard k – ε Turbulence Model

Reynolds Averaged version of the Navier Stokes equations (RANS) is commonly used in turboMachinery design. In order to simulate the flow accurately, the most suitable turbulence model has to be applied. In this model, the velocity is separated into mean, and fluctuating components. When the mean flow is steady, the RANS equation has the following form.

$$\overline{U_k}\frac{\partial\overline{\rho U_i}}{\partial x_k} = -\frac{\partial\overline{P}}{\partial x_i} + \mu\frac{\partial^2\overline{U_i}}{\partial x_k\,\partial x_k} - \frac{\partial\,(\overline{\rho u_i' u_k'})}{\partial x_k} \tag{9}$$

The Reynolds stress tensor ($\overline{\rho u_i' u_k'}$) can be modeled by using a 'turbulent viscosity (μ_t)' to arrive equation 10.

$$\overline{U_k}\frac{\partial\overline{\rho U_i}}{\partial x_k} = -\frac{\partial\overline{P}}{\partial x_i} + (\mu + \mu_t)\frac{\partial^2\overline{U_i}}{\partial x_k\,\partial x_k} \tag{10}$$

The k-ε model cannot be used to model the turbulence flow near the wall. In Fluent, wall functions are employed for near-wall region.

VITA

Name:	Serafettin Ustun
Address:	Petroleum Pipeline Corporation (BOTAS), Bilkent Plaza A - II Blok, Bilkent / 06800 ANKARA, TURKEY
Email Address:	seref_ustun@yahoo.com.tr
Education:	B.E., Mechanical Engineering, Gazi University, Turkey, 2009 M.S., Mechanical Engineering, Texas A&M University, 2012